AD NUMBER
AD617181
CLASSIFICATION CHANGES
TO: **UNCLASSIFIED**
FROM: **CONFIDENTIAL**
LIMITATION CHANGES
TO: **Approved for public release; distribution is unlimited. Document partially illegible.**
FROM: **Distribution authorized to U.S. Gov't. agencies only; Test and Evaluation; MAR 1958. Other requests shall be referred to Armed Forces Special Weapons Project, Albuquerque, NM. Document partially illegible.**
AUTHORITY
DASA Hr dtd 8 Jun 1959, per document marking; DNA per document marking

WT-1106

This document consists of 120 pages

No. 184 of 210 copies, Series A

Operation TEAPOT

NEVADA TEST SITE

February – May 1955

Project 1.7

UNDERGROUND EXPLOSION EFFECTS

Issuance Date: March 3, 1958

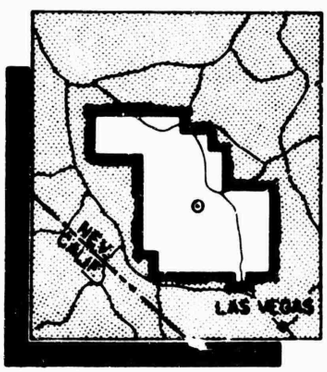

HEADQUARTERS FIELD COMMAND, ARMED FORCES SPECIAL WEAPONS PROJECT
SANDIA BASE, ALBUQUERQUE, NEW MEXICO

DISCLAIMER NOTICE

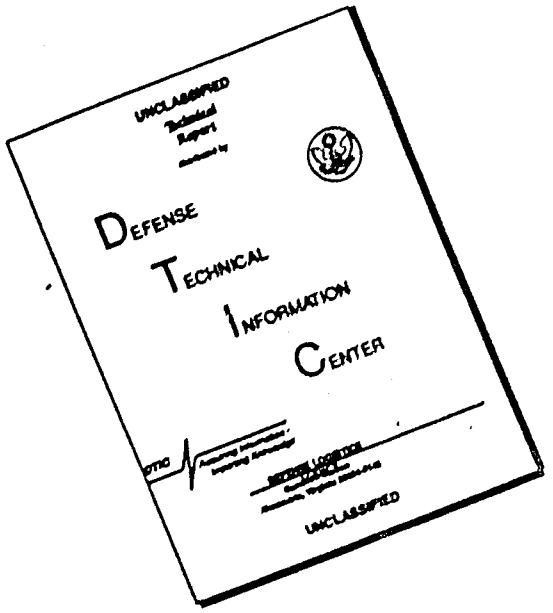

THIS DOCUMENT IS BEST QUALITY AVAILABLE. THE COPY FURNISHED TO DTIC CONTAINED A SIGNIFICANT NUMBER OF PAGES WHICH DO NOT REPRODUCE LEGIBLY.

WT—1106

OPERATION TEAPOT—PROJECT 1.7

Report to the Test Director

UNDERGROUND EXPLOSION EFFECTS

D. C. Sachs
L. M. Swift

Stanford Research Institute
Menlo Park, California

SUMMARY OF SHOT DATA, OPERATION TEAPOT

Shot	Code Name	Date	Time*	Area	Type	Latitude and Longitude of Zero Point
1	Wasp	18 February	1200	T–7–4†	762-ft Air	37° 05' 11.6856" 116° 01' 18.7366"
2	Moth	22 February	0545	T–3	300-ft Tower	37° 02' 52.2854" 116° 01' 15.6967"
3	Tesla	1 March	0530	T–9b	300–ft Tower	37° 07' 31.5737" 116° 02' 51.0077"
4	Turk	7 March	0520	T–2	500-ft Tower	37° 08' 18.4944" 116° 07' 03.3579"
5	Hornet	12 March	0520	T–3a	300-ft Tower	37° 02' 25.4043" 116° 01' 31.3674"
6	Bee	22 March	0505	T–7–1a	500-ft Tower	37° 05' 41.3889" 116° 01' 25.5474"
7	ESS	23 March	1230	T–10a	67-ft Underground	37° 10' 06.1283" 116° 02' 37.7010"
8	Apple	29 March	0455	T–4	500-ft Tower	37° 05' 43.9200" 116° 06' 09.9040"
9	Wasp'	29 March	1000	T–7–4‡	740-ft Air	37° 05' 11.6856" 116° 01' 18.7366"
10	HA	6 April	1000	T–5§	36,620-ft MSL Air	37° 01' 43.3842" 116° 03' 28.2624"
11	Post	9 April	0430	T–9c	300-ft Tower	37° 07' 19.6965" 116° 02' 03.8860"
12	MET	15 April	1115	FF	400-ft Tower	36° 47' 52.6887" 115° 55' 44.1086"
13	Apple 2	5 May	0510	T–1	500-ft Tower	36° 03' 11.1095" 115° 06' 09.4937"
14	Zucchini	15 May	0500	T–7–1a	500-ft Tower	37° 05' 41.3880" 116° 01' 25.5474"

* Approximate local time, PST prior to 24 April, PDT after 24 April.
† Actual zero point 36 feet north, 426 feet west of T–7–4.
‡ Actual zero point 94 feet north, 62 feet west of T–7–4.
§ Actual zero point 36 feet south, 397 feet west of T–5.

ABSTRACT

Project 1.7 of Operation TEAPOT was concerned with the measurement of surface and subsurface effects of an underground explosion of a 1.2-kt nuclear burst (Shot 7). The measurements included free-field earth and air-blast effects, as well as loading on underground structural devices. This report deals with the presentation and analysis of the free-field data only; the structural data have been transmitted to the appropriate agencies for their analysis.

From the 76 channels installed on TEAPOT Shot 7, 75 usable records were obtained. The free-field quantities measured include air-blast pressure, earth acceleration, earth stress and strain, and permanent earth displacement.

The results are discussed by phenomenon and, in each case, the TEAPOT data are compared with pretest predictions. Also, where data are available, comparisons are made with previous underground nuclear test results. Some aspects of seismology and soil mechanics as applied to underground explosion phenomena are presented and, finally, the most pertinent high explosives results from subsequent tests conducted at the TEAPOT location are summarized.

FOREWORD

This report presents the final results of one of the 56 projects comprising the Military Effects Program of Operation Teapot, which included 14 test detonations at the Nevada Test Site in 1955.

For overall Teapot military-effects information, the reader is referred to "Summary Report of the Technical Director, Military Effects Program," WT-1153, which includes the following: (1) a description of each detonation including yield, zero-point environment, type of device, ambient atmospheric conditions, etc.; (2) a discussion of project results; (3) a summary of the objectives and results of each project; and (4) a listing of project reports for the Military Effects Program.

PREFACE

The planning and execution of Project 1.7 were under the direction of L. M. Swift, with L. H. Inman serving as Field Party Chief, D. C. Sachs being responsible for data reduction and analysis, and S. C. Ashton handling logistics problems. Other members of the field party included C. M. Westbrook, C. T. Vincent, R. V. Chler, V. E. Krakow, D. L. Knirck, and C. C. Hughes.

The excellent cooperation of CDR W. M. McLellan, USN, and MJR. H. T. Bingham, USAF, and their staff is gratefully acknowledged.

The authors wish to express gratitude to Dr. S. Katz of Stanford Research Institute for his analysis of the travel-time curves and for many stimulating discussions concerning the seismological aspects of the data.

CONTENTS

TABLES

Chapter 1
INTRODUCTION

1.1 OBJECTIVE

The primary objective was to obtain data on the free-field underground effects of an underground nuclear explosion (1.2 kt, 67 feet burial depth) for a correlation with similar measurements made on small-charge high explosives tests, particularly those of Project Mole, and the Operation JANGLE underground shot (1.2 kt, 17 feet burial depth). Such correlation, if established, would contribute to the prediction of free-field effects from larger nuclear charges fired underground under various conditions.

A second objective was to furnish instrumentation for two projects concerned with loading on structural devices from an underground nuclear explosion. On these projects, the responsibility of Project 1.7 was limited to obtaining and reporting data.

Crater measurements and analysis, although a portion of Stanford Research Institute Project Mole, were assigned to another agency for Operation TEAPOT (Project 1.6) and do not form a portion of Project 1.7. However, since crater predictions form an important part of the prediction technique, a certain amount of attention is paid in this report to the prediction of crater radii and to crater formation mechanisms.

1.2 HISTORY

Before 1939, essentially the only systematic investigation of the effect of underground explosions was a study of the remote effects of quarry blasts, which had been undertaken by some explosive manufacturers and the U. S. Bureau of Mines (Reference 1) to establish the limit of distance for certain varieties of superficial damage to dwellings. These investigations have little bearing on the problems of military damage.

Table 1.1 presents a summary of the significant work that has been done since 1940 on the effects of surface and underground explosions. In 1940, the problem of underground damage became of immediate interest to the British, who initiated the program of experiment to determine crater radii, earth movements, acceleration, and damage radii from bombs (Reference 2). By 1941, the British had collected a wealth of information on damage to structures from actual bombing incidents, but the complexity

of these results, together with lack of knowledge as to the exact position, point of impact, and size of bomb, made correlation difficult, if not impossible.

It became evident in 1941, during the course of U. S. bombing experiments, that considerable damage to a fortification might be caused by a near miss penetrating into the earth adjacent to the structure and exploding there. The results were sometimes quite unexpected and led to the conclusion that a systematic study of the underground phenomena caused by a buried bomb was necessary. After some preliminary work with buried dynamite charges, it became clear that the phenomena were indeed complicated and that only a long-term program which followed the principle of investigating one variable at a time while holding the others constant would yield the kind of data that would permit a quantitative evaluation of the influence of the various parameters. A large program was organized at the Princeton Station of the National Defense Research Council (NDRC) (Division 2), and the field work began in 1943 (see Table 1.1).

The NDRC project involved detonation of about 100,000 pounds of explosives, in units ranging from 8 to 3,200 pounds per shot, and construction of over 50 target structures (Reference 3). The tests were conducted in three different soil types, and the final report on the work (Reference 4) appeared in 1946.

The Corps of Engineers, seeking more complete information on underground explosion effects, began in 1948 its Underground Explosion Test (UET) program. The purpose of the program was to establish criteria for the design of subsurface structures and tunnels that would resist the effects of underground explosions of then-current and projected types of bombs and guided missiles. The tests were conducted principally at Dugway Proving Grounds, Utah, using a series of charges of TNT which varied in weight from 8 pounds to 320,000 pounds and which were detonated in several soils. The smaller charges were detonated at different depths to determine the effect of charge depth and relation to gage depth. Some free-field earth pressure and earth acceleration measurements were made in the UET program by Engineering Research Association, Inc. (ERA) (Reference 5). For this work, ERA used 320-pound charges buried in silty clay. They obtained data on four rounds.

In 1951, to assist in the planning of a possible future underground nuclear explosion test, the Armed Forces Special Weapons Project (AFSWP) added the Stanford Research Institute (SRI) Surface Structure Program (Reference 6) to the UET series at Dugway. This supplementary program was designed to study the effects on surface structures of three buried TNT charges (2560, 40,000, and 320,000 pounds). Some free-field earth measurements were made by SRI on the same shots, supplementing those made by ERA. It was decided to test the validity of the simple model laws for air blast, motion of soil, and response of surface structures.

When the Nevada Test Site was chosen as the site of the Operation JANGLE underground nuclear test (U shot), several differences were anticipated between U shot results and those from previous underground explosion tests. Important differences were considered to be the type of explosive, the relatively shallow depth (scaled) of charge burial,

TABLE 1.1 SUMMARY OF UNDERGROUND EXPLOSION TEST PROGRAMS

Program and Agency	General Description	Date of Experiment
British (World War II) Ministry of Home Security	Measurement of craters and permanent displacements from approx. 250-pound TNT explosions. Buried and in open trenches, various soils	1940 to 1941
United States (World War II) NDRC (Princeton)	Measurement of pressure, particle velocity, acceleration, and displacement of the medium as a function of distance, size of charge, depth of burial of both charge and gage, and soil type. Charge sizes: 8 to 3,200 pounds of TNT	June 1943 to August 1945
Underground Effects Tests (UET) - Dugway ERA	Principally to measure effects of underground explosions on subsurface structures; a few free-field earth measurements using 8 to 320,000-pound TNT charges; also included investigations of effect of soil type	1948 to 1951
Underground Effects Tests (UET) - Dugway SRI	Principally to measure effects of underground explosions (2,560 to 320,000 pounds of TNT) on surface structures; some free-field earth measurements of pressure and acceleration	May 1951
Operation JANGLE HE Tests - Nevada SRI, BRL, NOL, OCE	Series of 4 TNT explosions - 3 underground and one surface. Detailed measurement of earth pressure, earth acceleration, and airblast. Charges were 2,560 to 40,000 pounds	August September 1951
Operation JANGLE U and S Shots - Nevada Various Agencies	Measurement of free-field earth effects and structure damage due to detonation of a shallow-buried underground weapon and a surface nuclear weapon (both 1.2 kt)[1]	October to November 1951
Project Mole Utah Nevada California SRI	Measurement of free-field earth effects from underground and near-surface aboveground explosions of a 256-pound TNT charge. These measurements included earth stress, strain, pressure, acceleration, and airblast pressure. Permanent displacements and crater profiles were also determined. The program of explosions extended over four different soil sites, two of which corresponded to sites of large-scale tests.	100 series - Utah dry clay - July, August 1952 200 series - Nevada sand-gravel mix - September, October 1952 300 series - California wet sand, moist clay - September, October 1953 400 series - Nevada sand-gravel mix - October, November 1954
Operation TEAPOT Shot 7 - Nevada SRI, OCE	Measurement of free-field earth effects (techniques similar to Mole) and subsurface structure damage due to a "deep" (67 feet) buried nuclear charge (1.2 kt). Detailed crater profile and permanent displacement measurements.	March 1955

1. It should be pointed out that the 1.2-kt radiochemical yields assigned to the JANGLE U and TEAPOT Shot 7 detonations are only estimated values. Specifically, there is no known mechanism for determining the radiochemical yield of an underground nuclear burst, but the same kind of nuclear gadget had been tested sufficiently in air-burst configuration to permit its yield to be estimated with reasonable confidence.

and the soil characteristics. To establish a better basis for prediction of corresponding phenomena from larger explosions at the same site, the JANGLE HE (high explosive) test program was undertaken (Reference 7). The part of this program executed by Stanford Research Institute (see Table 1.1) included four TNT explosion tests, three 2,560-pound size charges and one 40,000-pound charge. The surface-detonated HE-4 shot (2,560-pound) was included to provide predictions for the surface nuclear test (S shot).

In the fall of 1951, JANGLE U and S nuclear charges (1.2 kt) were detonated at the Nevada site (Reference 8). One of the objectives of the nuclear tests was to determine the physical laws governing shock wave propagation (in air and earth) and those governing scaling between conventional high explosives (TNT) and nuclear detonations, so that HE test results could be used to predict the effects of nuclear explosions under varying conditions on a wide variety of targets. However, since the JANGLE test weapons were considerably lower in yield than present operational weapons and since the test programs were carried out in only one environment, only marginal basic data on the effects of surface and underground detonations were obtained.

Project Mole field work, which employed 256-pound spherical TNT charges detonated both underground and aboveground, was begun in the summer of 1952 (see Table 1.1). The Mole program was designed to investigate, using a single-size TNT charge, the effects of charge and gage burial depths, soil characteristics, and air-earth energy partition from underground and near-surface aboveground explosions (Reference 9). The field work associated with this program continued through the fall of 1954, when a series of rounds was fired at the Nevada Test Site adjacent to the site designated for Shot 7 of Operation TEAPOT, which occurred in March 1955.

Shot 7, a 1.2-kt nuclear device buried 67 feet below the surface, was included in the 1955 TEAPOT series in an effort to facilitate the correlation of TNT and nuclear underground data. Prior to this test, since the JANGLE U charge was shallow-burial, there were no data available on a "deep"-buried underground nuclear explosion. It was hoped that the TEAPOT underground detonation would resolve many of the uncertainties inherent in current prediction methods. It is with that shot that this report is primarily concerned.

Chapter 2
THEORY and ANALYSIS

2.1 SCALE EXPERIMENTS AND MODELING

2.1.1 Model Laws. A simplified discussion of the model laws as normally applied to explosion phenomena is presented here principally to familiarize the reader with the nomenclature used in the main body of this report. If all dimensions of an experiment are increased by factor S, where S is designated as the scale factor, and if it is assumed that all times associated with the experiment are increased by this same factor S, the model law or scaled relations for the various phenomena concerned can be derived by simple dimensional analysis. The model law is known to be invalid under some conditions, such as when the velocity of propagation is a function of the rate of application of stress, when viscosity effects exist, and when the effects of gravity are important. However, extensive scale tests using small TNT charges (References 3, 4) have indicated fair model law behavior for underground explosion phenomena, particularly for deep-buried charges, where the effects of explosive products venting into a completely different medium are reduced or eliminated.

For cube-root scaling, if all dimensions of an explosive charge (same explosive type) are changed by factor S, this factor is then equal to $(W_2/W_1)^{1/3}$, the cube root of the ratio between the explosive charge weights. As a consequence, the cube root of the charge weight in pounds is a convenient quantity to use in describing the scale of an experiment, and the ratio of the cube root of the weights of the two charges is generally considered to be the scale factor between the two tests. It is convenient to use the symbol λ in describing the dimensions of an experiment, wherein λ is designated as follows: $\lambda = R/W^{1/3}$, where R is a length in feet and W is the charge weight in pounds of TNT of equivalent energy release. In this report, λ refers specifically to horizontal ground distances measured from ground zero. The term λ_c describes the charge depth and the term λ_g describes the gage depth. To obtain distances in feet, λ is multiplied by the cube root of the explosive charge weight in pounds of TNT or equivalent.

When the dimensional analysis referred to above is applied to the various phenomena of interest, it is found that at scaled distances (corresponding values of λ) and scaled times the pressure and particle velocity are independent of charge size or scale factor, S; impulse and particle displacement are proportional to S; particle acceleration is inversely proportional to S. The model law tells nothing of how the

quantities themselves vary with distance, so that the error should not be made of trying to predict magnitudes at a distance other than the scaled distances.

When the statement is made that a certain phenomenon follows the scaling laws, it must be noted that this refers to the total phenomenon, and not merely to selected aspects of it. Thus, if the earth acceleration is known to be a function of time and position, in true scaling the acceleration function for a similarly scaled experiment can be predicted directly; but if the scale factor for amplitude and the time differ from each other or are markedly different from the known value (S), then confidence in extrapolation must decrease. If empirical scaling laws are derived, then the test of their validity is the universality of their application to all aspects of the phenomena in the charge weight range from which they were derived.

2.1.2 Limitations on Modeling. Earth or soil as a transmission medium for mechanical effects is characterized as a nonelastic or plastic medium. Its transmission properties vary with moisture content, with type (as distinguished by grain size and shape), compaction, and possibly other factors. These effects combine to make the properties with respect to location and position variable with depth, location, and weather. For small charges, a slightly changing irregularity, such as increase of seismic velocity with depth, has little effect. This is because in the region of military interest the transmission of earth motion is along a near-surface path with practically constant velocity. For large charges, however, the path embraces a considerable variation in seismic velocity, with consequent change of transmission properties, direction of arrival, and the like. This variation could definitely be even more pronounced in the presence of faults, reflecting layers, hard-rock boundaries, and water tables at distances comparable to those used for describing the experiments.

The moisture in the soil is probably the most important variable and the one which produces the greatest effect on the transmission of the pressure. Moisture content can change rapidly with depth, as for example at the boundary of the subsurface water table. The consequent rapid variation of velocity produces refraction effects and possibly reflection effects, although these cannot be definitely separated in most cases. The velocity of transmission in a water-soaked soil may be appreciably higher than the velocity through dry soil, which produces a resultant high transmission of pressure for wet soils. This high transmissibility appears in the data as a very high soil constant for wet soils.

A direct application of the model laws to high explosive tests and nuclear tests having yields described in equivalent pounds of TNT must assume an explosive configuration equivalent to that of TNT. It is at once obvious that the explosive source characteristics of a nuclear charge are not equivalent to those of a TNT charge. In other words, in a direct sense, the dimensions of the experiment do not obey the assumed model law relationship. The hydrodynamics and thermodynamics of the early-stage gas bubbles are obviously different for the two types of explosives (References 10, 11, 12, 13). It is suspected that the effect

of these differences is even more pronounced for the relatively shallow charge depths, since the energy relationships in the venting processes can readily be affected by the thermodynamic conditions in the gas bubbles. Furthermore, there is no reason to assume that all physical output characteristics of a nuclear explosion can be described by a single equivalent energy release. It is well understood that the equivalent yield of a nuclear explosion is a function of the phenomenon that is used to judge this yield; for instance, the equivalent yield for thermal and radiation effects will obviously be different from the equivalent yield for such mechanical effects as earth pressure, earth acceleration, or cratering.

To summarize, the TNT efficiency of a nuclear detonation must be defined for the particular parameter being considered. If a nuclear detonation of known total yield, W_{NU} kt, at a depth, D, produces an apparent crater of radius, R, and if it is estimated that W_{HE} kt of TNT at the same depth, D, would produce the same crater radius, R, the TNT efficiency is defined as 100 W_{HE}/W_{NU} in per cent. Since extremely large TNT tests are not practical, some scaling relationship must be assumed to calculate the TNT efficiency of a nuclear test; it is worth noting that TNT efficiency and scaling relationships are inextricably related and that one cannot be determined without assuming a value for the other, unless absurdly large TNT tests are conducted. There is little reason to suggest that the nuclear TNT efficiency for a particular phenomenon should be exactly 100 per cent; in fact, for peak airblast overpressure, in the region of principal interest from a free air burst, the TNT efficiency of a nuclear explosion has been well documented at slightly below 50 per cent, whereas the TNT efficiency of a nuclear detonation for gamma radiation would normally be much greater than 100 per cent.

2.2 UNDERGROUND EXPLOSION PHENOMENA

The broad objective of all the studies in the field of underground explosion phenomena has been to formulate a detailed theory of the mechanism of propagation of explosive waves in a semiplastic medium, taking account of the three-dimensional nature of the problem and the presence of a boundary. This theory would include consideration of such factors as the nature of the explosive, the characteristics of the medium (soil), the effect of the depth of the explosives below the surface of the medium, and the energy partition of the detonation.

The problem is to calculate the time variation of the stresses and earth movements near the explosion of a spherical charge. The charge may be detonated at various depths below the ground level (possibly near the surface), so the problem cannot be treated as one of spherical symmetry. The transmission of elastic waves to great distances has been thoroughly examined for its seismological application; however, the main interest is in what happens in the plastic region comparatively close to the center of the explosion, where the earth's movements are great and the strains are largely permanent. The assumption is usually made that

in the plastic region one can neglect the elastic compressibility. As for the criterion of yielding, the plastic behavior of soil under combined stresses is not known with sufficient certainty to make any detailed theory worthwhile, and it is usually assumed that the soil has a definite yield point not depending on the hydrostatic component of the applied stress. The stress system at any point in a problem of spherical symmetry is just a hydrostatic stress superimposed on pure uniaxial compression, so the maximum stress difference in the plastic region is equal to the ordinary compressive yield stress. However, for an underground explosion close to the earth's surface, the spherical symmetry condition is not satisfied and it is necessary to know the general relations between plastic strain and combined stress.

The above general considerations of underground explosion phenomena have led to many theoretical attempts at organizing the concepts into a coherent and consistent theory (References 10, 12, 14). However, it has not been possible with the use of these theoretical approaches to explain the experimental results obtained from underground explosions in which different weights of TNT were buried in different soils at various depths below the ground surface.

It is convenient in estimating energy released by an explosion to simplify the picture by assuming that (1) the detonation takes place instantaneously, filling the cavity originally occupied by the explosive with the final gaseous combustion byproducts so that the amount of energy released per unit weight is the energy density of the detonation and (2) as the gas in the cavity expands, it does so adiabatically (without heat transfer between the gas and the confining medium).

While the energy is being transferred inelastically, the particle velocity necessary to accomplish this far exceeds that of a shock wave. Hence such a wave, if it may be said to exist, lags behind the detonation front at which energy is transferred to as yet inactive material; however, once the material collisions become less energetic and more elastic there is no more interpenetration, and a shock wave develops. In the earth, which is nonlinear, plastic, absorptive, dispersive, anisotropic, and inhomogeneous, only the general features of the pressure wave are known at present. While the pressure wave is traveling in the earth, any obstacles it encounters are moved, accelerated, or subjected to pressure and impulsive forces. In particular, close to the charge the shock strength-distance gradient is expected to be large enough to loosen the cohesive forces in the soil to an extent depending on the type of soil, pressure of the overburden, moisture, aeration, etc. At large distances from the charge, the shock rapidly reaches a seismic and acoustic regime for which much information is already available; however, it is unlikely that any effects of military importance occur in this region.

The shock wave, arising from elastic collisions, leaves behind it a gas bubble with considerable expansion energy remaining. The overburden directly above the charge has been more or less shattered by the shock wave, while the earth below the charge suffers less decohesion, because the static pressure is greater. Thus, the gas bubble tends to escape

upward, since the shock wave suffers less attenuation in traveling the short distance from the top of the gas bubble directly to the surface of the earth than in traveling the longer distance at elevation angles removed from the vertical. The gases tend to escape directly upward; hence, something akin to a broad conical jet of hot gases emerges, carrying with it the immediate overburden.

Since it is possible to associate an energy density with conventional types of explosives, it is a fairly simple matter to compute the total energy release for a particular charge weight. However, the energy density concept can lead to some of the difficulties of correlating HE and nuclear explosions, since their respective initial energy densities can differ by a factor of as much as 10^7. A nuclear air burst loses a large percentage of its total energy in radiation effects, whereas only a small percentage of a low-temperature, nonradioactive HE burst goes into radiation. A nuclear air burst is found to have a blast (mechanical) efficiency of about 45 per cent relative to TNT. This mechanical efficiency is more difficult to define when energy travels from one medium into another (e.g., ground to air). It is likely that the energy partition of both TNT and nuclear detonations is dependent upon such factors as charge depth and soil properties.

Fortunately, the earth lends itself to one form of measurement which such media as air and water do not, namely cratering. The earth, when ruptured by an explosion, leaves behind a record in the form of rearranged, pulverized, and sheared earth. Experimental measurements using conventional explosives such as TNT led to some optimism that craters produced by such explosion could be predicted with an accuracy adequate for military purposes, even though it is clear that some properties of the earth medium in which the explosive is fired are very sensitive parameters in affecting the crater. The situation regarding craters produced by nuclear explosives is less satisfactory. First, the evidence is meager; second, the existing evidence leads to the conclusion that the TNT efficiency (assuming cube-root scaling) for cratering is a function of soil type, charge depth, etc. Although there is some evidence that the proper scaling relationship is greater than cube-root, i.e., fourth root or greater, cube-root scaling of crater linear dimensions is assumed for this report.

The effect of charge depth or height is fairly well established for TNT. If scaled crater diameter is plotted against scaled charge depth, it is clear from both experiments and physical reasoning that the curve will be concave downward, since no surface crater is produced if the charge is sufficiently high above the surface or sufficiently deep below it. For TNT, the maximum of this curve is rather broad, and occurs in the range of $1 < \lambda_c < 3$.

The effect of the medium has been shown to be as large as a factor of 2 in the field experiments with TNT. Unfortunately, the specific properties of the medium which affect the crater are not yet established. It is postulated that strength, either shear or tension, and density are sensitive parameters. It is possible that the elastic moduli are also

important. In regard to strength, it is, of course, the strength under shock load conditions that is important. It is difficult to make laboratory test under shock load conditions, and the heterogeneous character of earth makes the extrapolation from laboratory to field conditions uncertain. Thus, although appropriate values for strength under shock

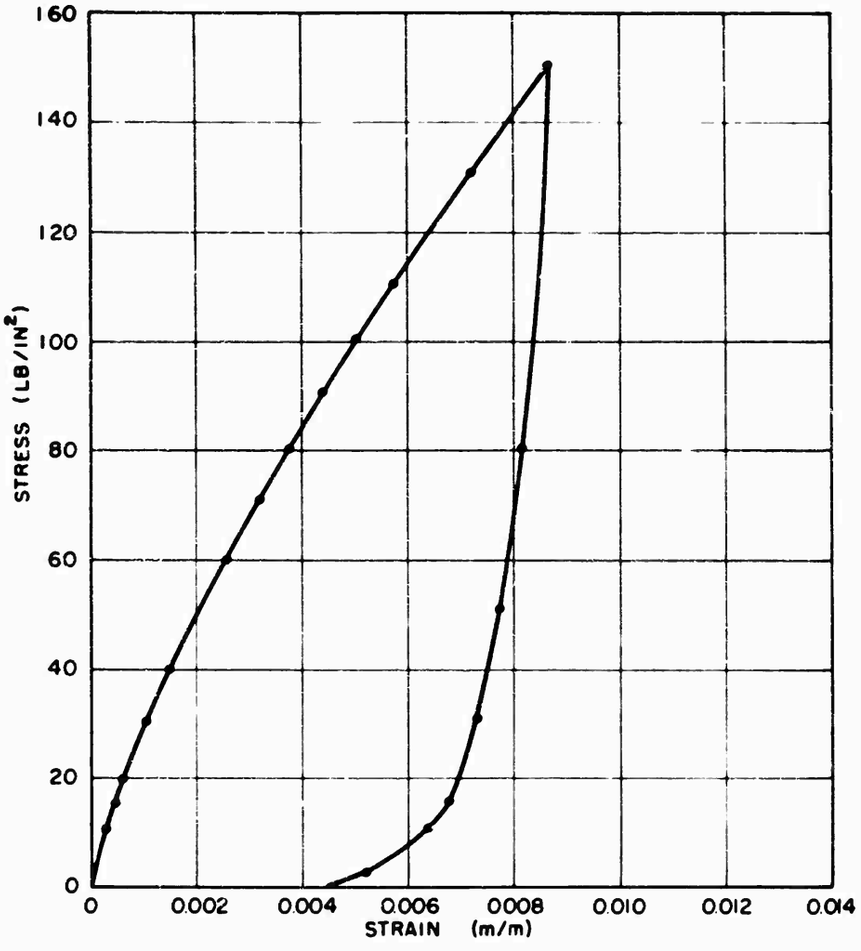

2.1 Typical experimental dynamic stress-strain curve for free earth (silty clay) corrected for spherical spreading.

load are not known, it appears clear that strength under such conditions may differ widely from strength under static load.

2.3 SOIL CONSIDERATIONS

2.3.1 Stress-Strain for Soil. The plastic nature of earth as a transmission medium is most readily realized by an examination of the stress-strain curves for a typical silty clay soil (Reference 4). This stress-strain curve, which is shown in Figure 2.1, was determined from dynamic measurements obtained in earth. Figure 2.1 shows the slope of the loading part of the stress-strain curve decreases with an increase of pressure (in other words, the loading part of the curve is concave

downward), whereas the slope of the unloading part of the curve decreases with decreasing pressure (is concave upward).

The result of such a stress-strain curve is to produce dispersion in the transmitted compressional wave in such a way as to prohibit transmission of a shock wave. This comes about through the decrease of the slope of the loading curve with an increase of stress, which causes the higher pressure levels of the waves to be propagated more slowly, just the opposite of the case of a shock wave in air. This effect of variation of propagation velocity as a function of pressure is shown by the equation:

$$V\ (\sigma) = \sqrt{\frac{1}{\rho}\ \frac{d\sigma}{d\delta}} \qquad (2.1)$$

where ρ = density
σ = stress
δ = strain
V = velocity of transmission of the pressure level.

The net result is that the peak of the wave travels more slowly than does the initial part, so that the wave continually stretches out in space and time. The unloading portion of the curve has a steeper slope than does the loading part except at low pressures, where it is less steep. The result of this property of the stress-strain curve is that the wave suffers a continual change of shape from the rear as well as in the front. The peak tends to be eaten away by the rarefaction or unloading curve; in addition, the slow speed of the low pressures associated with the unloading curve results in an over-all increase in the space length of the wave. This feature points up a basic difference between pressures measured in the earth and those measured in air. In air, when a shock wave is disturbed in some way by mechanical or thermal conditions, it seeks an equilibrium or classical shock configuration again when the disturbance decays. That is, when the "shocked-up" condition of the wave in air is disturbed it will "return" to the classical shock front condition, because the velocity of propagation of the higher pressure levels is greater than for lower pressure levels. However, quite the opposite is true for a pressure wave in earth. Any deviation of a wave in earth from the pure compression type will be maintained (and even enhanced) as the wave progresses out to larger ground ranges. Consequently, the inhomogeneities or nonisotropic characteristics of the medium, which give rise to these deviations suffered by the waves in earth, assume greater importance in any analysis of underground explosion phenomena.

Referring again to Figure 2.1, the area between the loading and unloading parts of the curve represents an energy loss per unit volume of the soil passed over by the wave. This must cause an attenuation of the amplitude and energy of the wave as it progresses away from the source. The rate of propagation of the initial part of the wave or of waves of very small amplitude is determined by the slope of the stress-strain curve near zero pressure. This is the propagation rate determined by seismic refraction shooting.

It has been found in laboratory tests on soils (Reference 15) that the rate of application of strain can be an important variable ("strain-

rate" effect) in determining the dynamic stress-strain relationship for a soil. The stress-strain curves obtained using transient strains differ appreciably from those obtained on static tests. By way of example, the curve shown in Figure 2.2 is typical of the strain-rate characteristic for soils which have been laboratory tested. The factor usually used to define strain-rate characteristic is the ordinate of Figure 2.2, i.e., the ratio of transient and static strengths corresponding to a specific loading time.

In confined soil sample tests upon plastic or slightly nonplastic soils, the strain-rate effect is probably due to viscous resistance to deformation. However, in confined tests upon very brittle and stiff soils, the strain-rate effect is believed to be a result of time lag

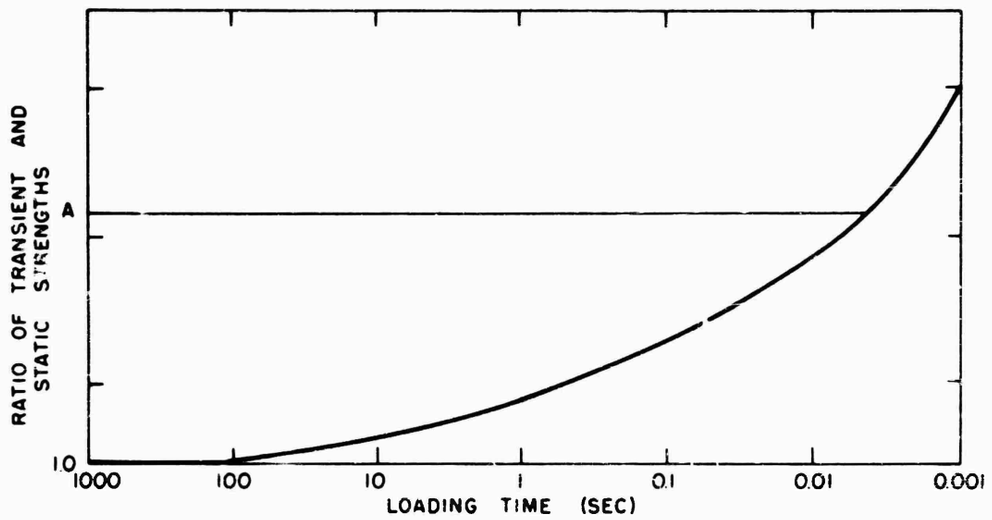

2.2 Typical strain-rate curve.

phenomena. This time lag is, in some manner, related to the effort required to overcome the bonds existing between the soil particles and the bonded water. The Dugway dry clay soil seems to fall in this latter classification.

2.3.2 Soil Mechanics. In considering soil structure, it is noteworthy that the fluid filling the pore spaces of the soil may be air or water or a combination of the two. When the transmission of pressure waves from an explosion is considered, it is important to separate two effects.

Primarily, there is the transmission of the pressures directly from the explosive source through the interstitial spaces, which may lead to the transmission of pressures over great distances. This effect is clearly present when the pore spaces are completely filled with water. However, when the pore fluid is air, the transmission is severely attenuated and does not occur over great distances.

The second effect, important only when the pore fluid is water, is the generation of pore pressures as the soil mass distorts under the

effect of the explosion. If a mass of soil whose voids are completely filled with water is compressed, a substantial portion of the compressing pressure is induced in the pore water, and large amounts of energy may be stored there. Also, if the saturated soil mass is sheared, changes occur in the pore water pressure. It is practically impossible to separate these effects by observation, because both occur simultaneously. However, it is possible to predict, in an approximate manner, which of these effects might be most significant for a particular soil.

Another aspect of soil mechanics application can be seen when radial stresses and strains are considered. In stiff soils (e.g., dry clay), the lateral strains necessary to retain continuity cannot readily occur. Thus, radial splits occur, whereupon the explosion pressures may vent along the splits and penetrate into the soil mass. This process leads to soil breakup into large clods and to subsequent throwout of the material. In soft, plastic soils (e.g., moist clay) the soil tends to retain continuity. Hence, a ring of soil unable to resist increased radial pressure may move outward but still be fairly well intact. This movement continues until this ring has expanded against a mass of soil capable of containing it. This suggests that the material of the walls of soft soil craters should exhibit large radial strains, the magnitudes of which approach the maximum strain the soil can sustain.

For permanent displacement measurements taken at the ground surface, it is to be expected that sand sites would yield displacements much larger than those at clay sites. This is because a sand soil at ground surface has no resistance to deformation, whereas a clay may possess considerable resistance. Displacements at greater depths in sandy soils would be considerably less, whereas for clay the decrease of movement with depth is expected to be small. This again is the relative behavior which one should expect of cohesionless and cohesive soils.

The foregoing examples help to illustrate how the basic principles of soil mechanics can be profitably applied to the analyses of underground explosion phenomena. Attempts will be made throughout this report to explain the experimental results in terms of these principles.

2.3.3 Seismology. Many attempts have been made to correlate some physical property of the soil with the various parameters that influence the earth stress, acceleration, and damage, but to date no field test has yielded useful information on this score. However, some useful information is obtained from the measurement of the velocity of propagation of seismic waves. The seismic velocity is obtained by means of shallow refraction shooting in a manner familiar to geophysicists.

A relationship exists between the soil constant, k, and the velocity of propagation of a seismic wave in the material. This velocity is that of a low amplitude wave corresponding to a sound wave in air and is to be distinguished from the velocity of the peak of a finite wave. The slope of a stress-strain curve near the origin would be associated with the velocity of very low amplitude waves. The seismic velocity of these low amplitude waves can be obtained by shallow refraction shooting, using

small charges. Such explorations can be carried out easily and cheaply compared with the direct method of measuring explosion pressures. The soil constant is defined by the relation

$$k = \frac{1}{2} \rho V^2 \qquad (2.2)$$

where k = soil constant (pounds per square foot)

ρ = density of the soil (slugs per cubic foot)

V = velocity of propagation (feet per second).

It is noteworthy that some underground explosion phenomena seem to correlate with the concept of soil constant given above (Reference 4). In other words, there is evidence that the propagation velocity of large-magnitude stress waves is comparable with the velocity of seismic (infinitesimal amplitudes) waves in the same medium (see Section 5.6.1). This evidence leads to some hope that seismic exploration will prove useful in predicting effects from underground nuclear detonations.

An impulsive disturbance in soil generates waves which decay with distance and propagate outward with characteristic velocities. If the soil behaved as a semi-infinite, homogeneous, elastic medium, three waves would be observed: (1) the compressional wave with velocity

$$V_P = \sqrt{\frac{K - \frac{4}{3} G}{\rho}} \qquad (2.3)$$

where K, G, and ρ are the compressibility, rigidity, and density, respectively: (2) the distortional wave with velocity

$$V_S = \sqrt{\frac{G}{\rho}} \qquad (2.4)$$

(3) the Rayleigh surface wave with a velocity

$$V_R \cong 0.9\, V_S \qquad (2.5)$$

The compressional and distortional waves are body waves related through Poisson's ratio γ, by

$$\left(\frac{V_P}{V_S}\right)^2 = \frac{2(1-\gamma)}{1 - 2\gamma} \qquad (2.6)$$

or

$$\gamma = \frac{\frac{1}{2}\left(\frac{V_P}{V_S}\right)^2 - 1}{\left(\frac{V_P}{V_S}\right)^2 - 1} \qquad (2.6)$$

Thus, measurement of V_P and V_S would lead to a determination of γ, or to any of the other elastic constants of the soil. In general, the surface wave predominates at long ranges, since its amplitude decays as $R^{-1/2}$, compared with R^{-1} decay for the body waves.

An actual soil may differ from the above described solid in three respects: (1) its structure may vary with depth, resulting in either a continuous or discontinuous depth variation of elastic constants and wave velocities; (2) its structure may change over relatively short ranges, resulting in nonuniform horizontal propagation; and (3) it may exhibit an elastic response over only a small range of stresses. In particular,

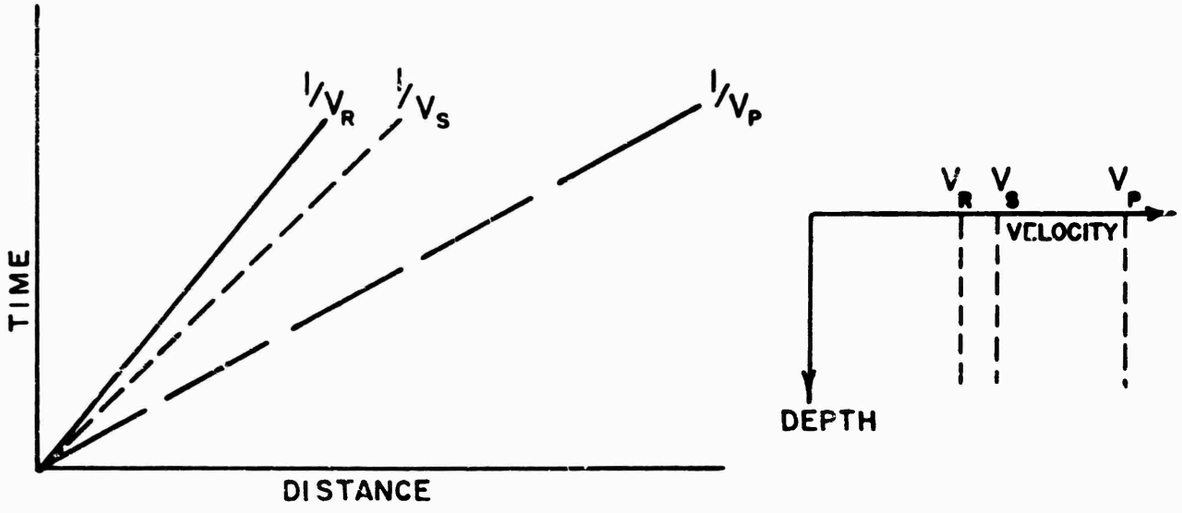

2.3 Travel-time curve for surface shot in homogeneous, semi-infinite, elastic solid.

soil has a porous structure which is compressible and which can be destroyed by sufficiently large stresses. In such a solid, propagation of waves other than those described above may be expected.

In the study of blast effects, the variation with radius from the detonation point of stress, strain, impulse, and particle velocity and acceleration is usually of primary importance. However, such data may give no direct information on the type of deformation or wave propagation involved. An important adjunct to these parameters of ground motion is a study of the propagation velocities of identifiable waves. By plotting the travel time (T) of the prominent waves as a function of charge-to-gage distance (X), the travel-time curve familiar in seismology is obtained. The curve in Figure 2.3 would result from a surface shot on a homogeneous, semi-infinite, elastic solid having velocities defined above. Travel-time curves for the compressional wave in more complicated distributions appear in Figures 2.4 and 2.5 (the air wave has been omitted). Conversely, the observed travel-time curves may be used to derive the velocity structure and the mode of propagation of the observed waves. However, this derivation is not always unambiguous. For example, a small velocity gradient may give an apparent linear travel-time curve.

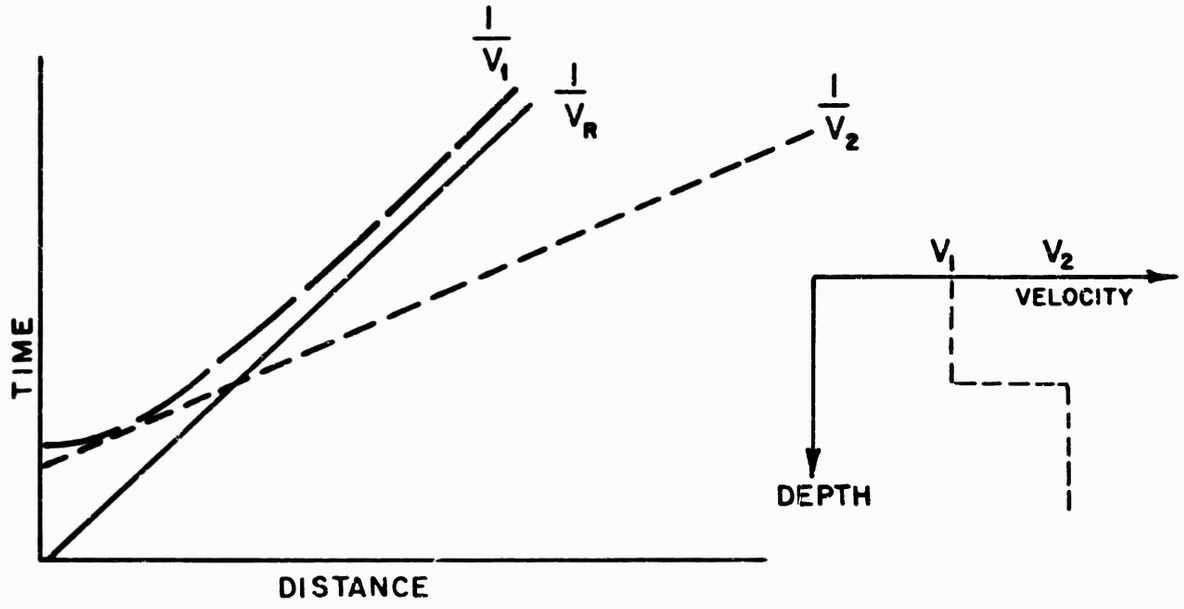

2.4 Travel-time curve for surface shot in two-layer solid.

For the charge sizes and gage distances of interest here, the departure from elastic response may be considerable. Terzaghi and Peck (Reference 16) report typical response of soils in a confined compression test. Taking e_o and ρ_o as the void ratio and density at atmospheric pressure of the undeformed soil, ρ_s as the density of solid constituents, and e and ρ as the corresponding quantities at pressure P, Terzaghi's curves may be transformed from P-e to P-ρ coordinates. The P-ρ curves are more useful in the following considerations:

Using

$$\rho_o = \frac{\rho_s}{1-e_o} \quad \text{and} \tag{2.7}$$

$$\rho = \frac{\rho_s}{1-e} \quad , \tag{2.8}$$

it follows that

$$1 - \frac{\rho_o}{\rho} = \frac{e_o - e}{1-e_o} = \frac{\Delta e}{1-e_o} \tag{2.9}$$

The transformed curves appear in Figure 2.6. From these curves it is clear that above approximately 70 psi

$$\frac{d^2P}{d\rho^2} > 0, \tag{2.10}$$

which means that with increasing pressure the soil becomes increasingly "harder." Therefore, the condition for the formation of a shock wave

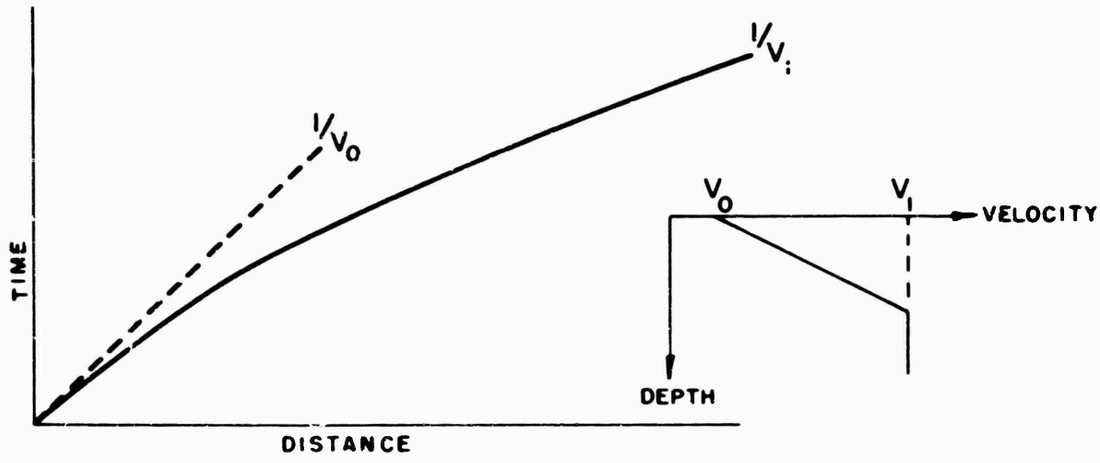

2.5 Travel-time curve for surface shot in solid having linear velocity gradient layer above constant velocity layer.

(Reference 17) is fulfilled. Although no comparable data are available for the soil at the Nevada Test Site, similar relationships are expected to hold.

A brief analysis of the conservation laws for plane shock waves indicates what may be expected in soils with the properties shown in

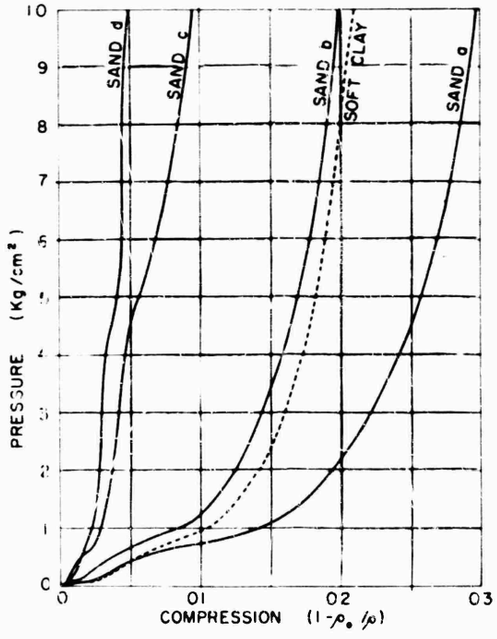

2.6 ypical response curves of soils in confined sample compression est.

Figure 2.6. Of course, an analysis of the spherical shock wave would be more pertinent, but the plane wave case is far simpler and should indicate the general features. Consider a plane uniform shock of pressure p, traveling with shock velocity U_s into undisturbed material with density ρ_o and with an equation of state derived from Equation 2.6. Assume in

addition that the entropy change across the shock front is small. This is equivalent to assuming that the correction required to convert Equation 2.6 to the Hugoniot equation of state is small compared with the uncertainty in Equation 2.6. Behind the shock the soil density is ρ and

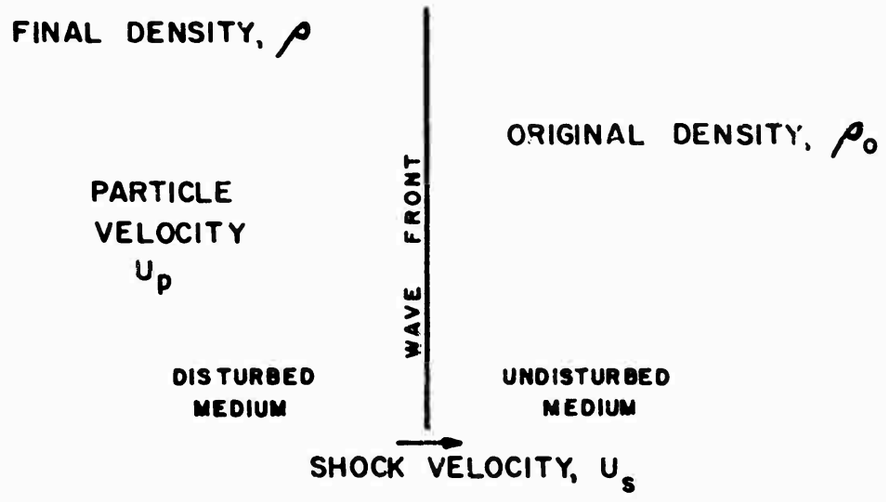

2.7 Schematic diagram of plane shock wave.

the particle velocity U_p, as shown in Figure 2.7. Conservation of mass and momentum across the shock front gives

$$(a)\quad \rho_o U_s = \rho(U_s - U_p), \text{ and} \tag{2.11}$$

$$(b)\quad P = \rho_o U_s U_p \tag{2.12}$$

Solved for U_s and U_p, (a) and (b) give

$$U_s = \sqrt{\frac{P}{\rho_o(1-\rho_o/\rho)}}, \text{ and} \tag{2.13}$$

$$U_p = \sqrt{\frac{P}{\rho_o}\,(1-\rho_o/\rho)}. \tag{2.14}$$

From the data of Figure 2.6 and Equation 2.13, the shock velocity as a function of pressure was computed and is shown in Figure 2.8. The ordinate is in units of $U_s\sqrt{\rho_o}$; to obtain the shock velocity in feet per second, divide the scale by the square root of specific gravity of the soil. The range of velocities predicted for shocks in soil ($\rho_o \simeq 1.6$) is from about 360 ft/sec for P = 145 psi to 75 ft/sec for 15 psi. For higher pressure, and less compressible soils, the velocity would be greater. The variations in slope of the curves of Figure 2.6 are reflected in the velocity curves of Figure 2.8 as ranges of pressure over which the velocity varies slowly or is at a minimum. Two of Terzaghi's soils (Sand c and Sand d) have such a constant velocity region at about 73 psi and four of the soils from about 1.5 to 15 psi. Of course, these

curves have little significance in the pressure range from zero to the level at which the soil can support the stress without permanent deformation (e.g., elastic regime). The data indicate that this level is of the order of several pounds per square inch. However, above this stress level this analysis predicts one or more waves propagating with a velocity in the range of several hundred feet per second and an amplitude large compared with the initial disturbance.

A word should be interjected here concerning the manner in which the airblast may influence effects measured by underground gages. This can best be explained by reference to the time of arrival considerations as pictured in Figure 2.9.

As the air-blast wave sweeps over the surface of the earth, the disturbance originates at the surface is transmitted through the earth. The travel time, T_y, to depth y may be expressed as

$$T_y = \frac{1}{a} \frac{y^{1-1/n}}{1 - 1/n} \qquad (2.15)$$

where a and n are constants. In addition, it can be demonstrated that

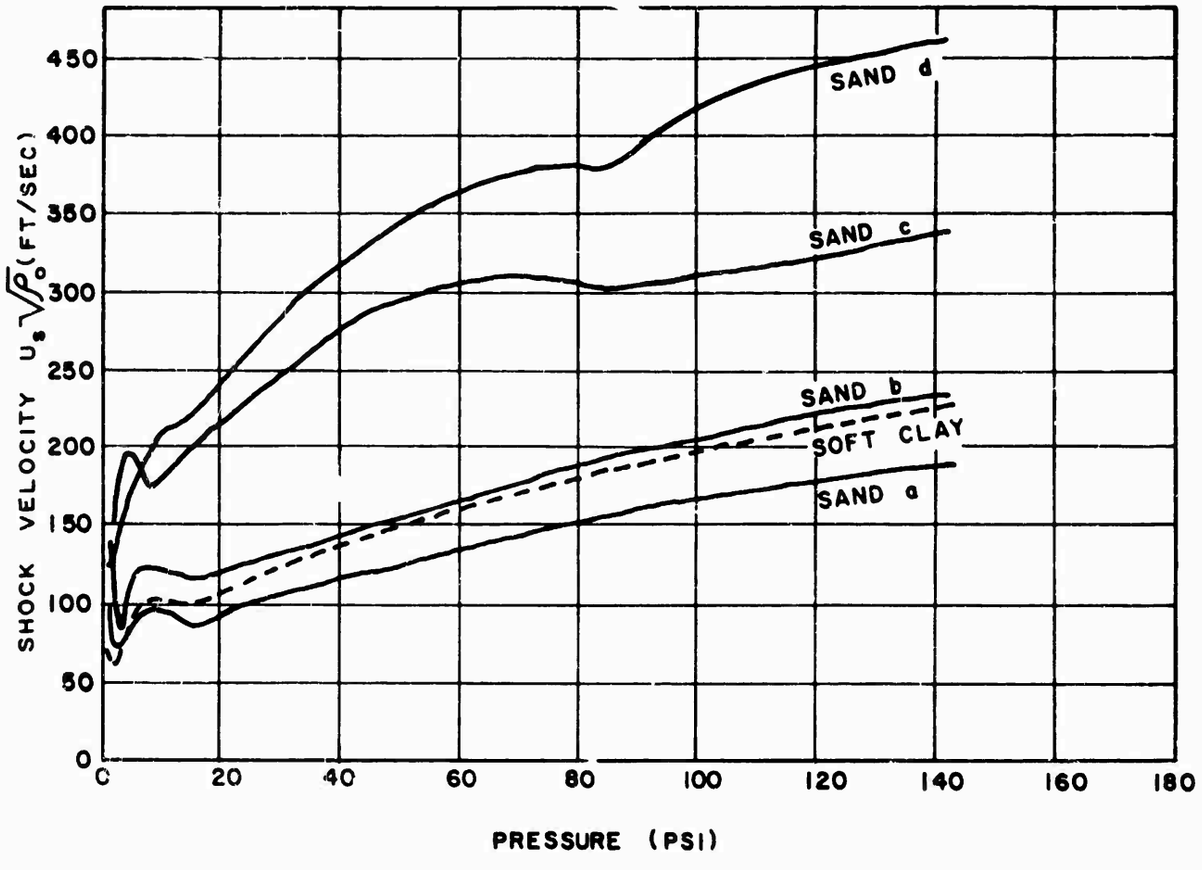

2.8 Representative shock velocity vs pressure curves for various soils.

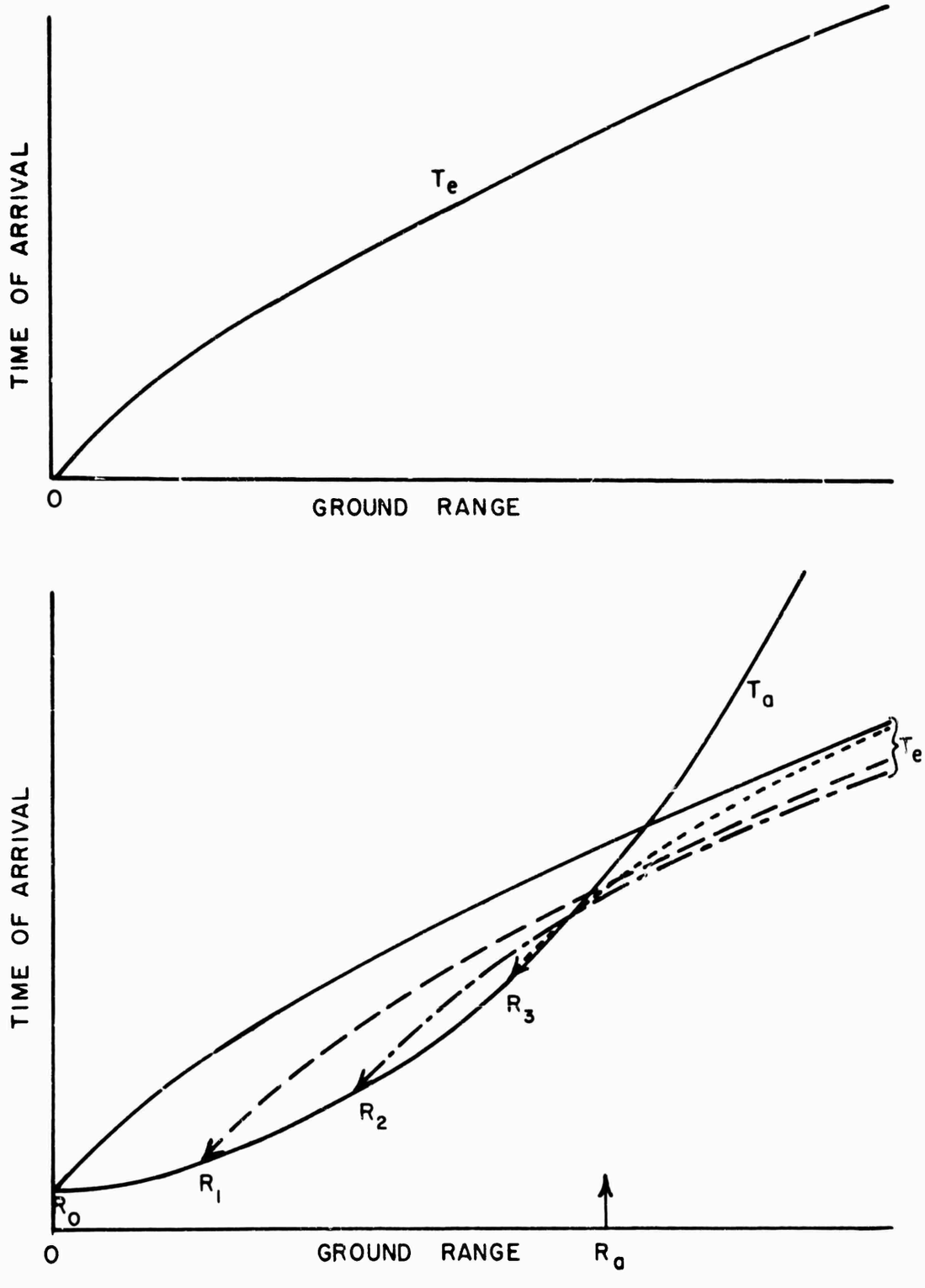

2.9 Incident and reflected wave fronts for airblast and time of arrival diagram for information received by surface gage.

the refracted travel time, T_x, from a disturbance on the surface, distance x from the disturbance, is given by

$$T_x = \frac{x}{(1 - 1/n)\, V_x} \qquad (2.16)$$

where V_x is the apparent horizontal velocity at distance x.

The upper graph of Figure 2.9 is a plot of Equation 2.16; as the blast wave progresses from ground zero, a series of refracted seismic waves originate at the blast front at each instant of time. Each of these signals follows the time-distance curve shown in the figure, with the starting point (origin) at the blast front. The lower graph of Figure 2.9 shows the air-blast arrival time-distance curve (T_a) in addition to some earth-transmitted time-distance curves (T_e) originating at various arbitrary ranges (R_o, R, etc.). It becomes obvious from the figure that at ground ranges beyond R_a, the "breakaway" range, the first information received by a near surface gage will be from the earth-transmitted refracted wave.

Consider what happens in an amplitude sense at ground range beyond R_a (Reference 18). The disturbance received at some time intermediate between earth and air arrivals will have suffered attenuation in both earth and air paths. Because of the much smaller attenuation in the air path, the largest air-coupled amplitudes will occur when the earth path is minimal. This corresponds to the airblast passing over the buried gages. This direct local effect of the airblast is termed the "slap" because of the sudden increase in earth motion which is observed. Another consequence of the smaller attenuation in the air path is the observed increased relative importance of the air-coupled slap at the larger ground range gage stations.

2.4 PREDICTIONS AND REPORT SCOPE

If the model laws of similitude were satisfied for underground explosions of all types, it would be a fairly straightforward matter to construct a prediction method for underground nuclear detonations, applicable to any yield. The procedure would include small charge tests to determine the effects of scaled charge depth and soil characteristics upon the important underground wave parameters. Thereafter, predictions of effects due to nuclear detonations could be computed using model law rules, and military operational decisions could be confidently based upon these results. However, it has long been realized that the basic assumptions necessary to model behavior are violated when effects from HE and nuclear underground explosions are considered. This fact has required the analyst to attack the problem piecemeal to build up a prediction method of even reasonable reliability.

The available pertinent underground and near-surface data fall into the following five main groups:

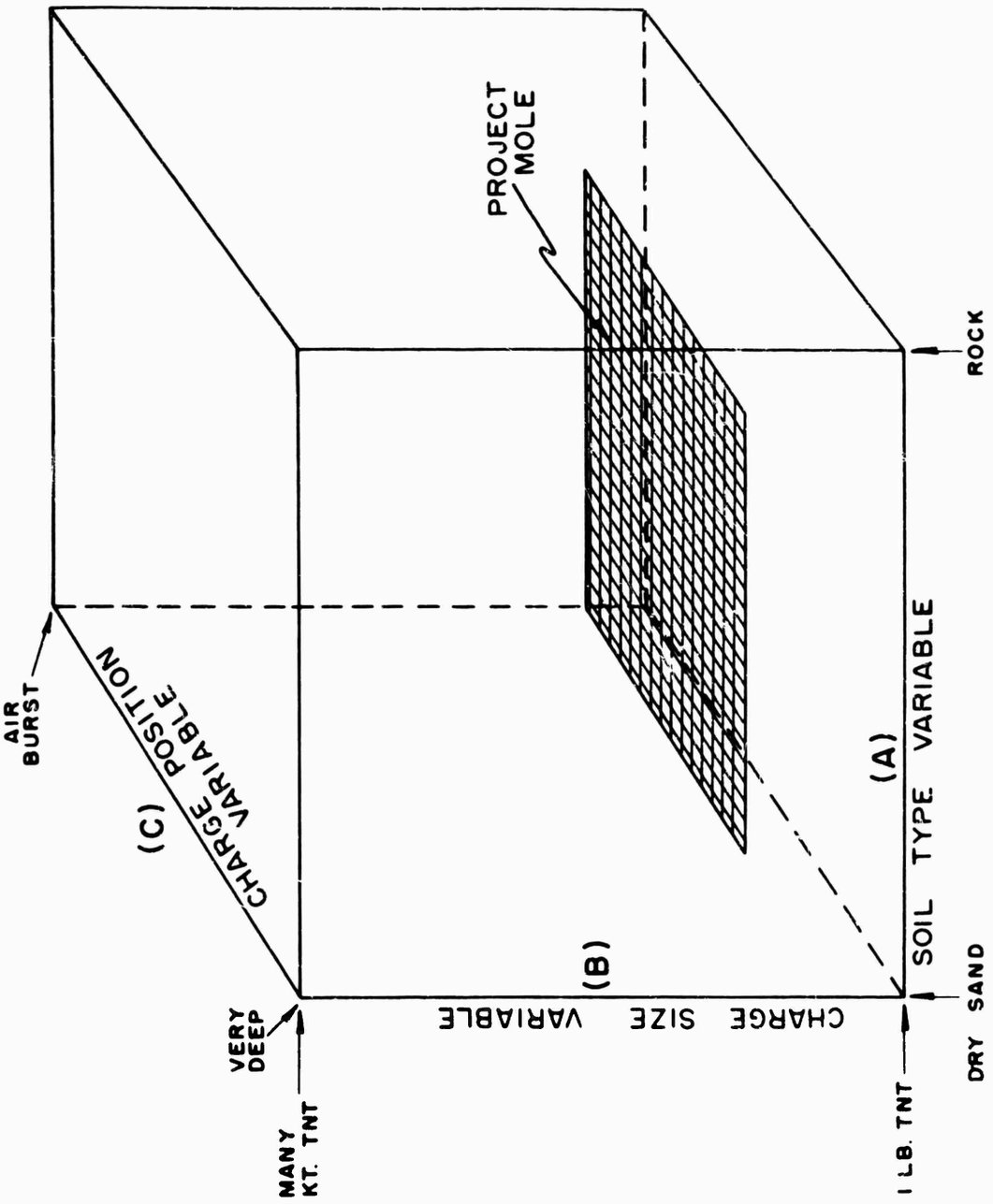

2.10 Schematic diagram of method of approach to prediction of weapon effects.

1. JANGLE U and S (nuclear, 1.2 kt radiochemical) in Nevada sand-gravel mix.

2. TEAPOT Shot 7 (nuclear, 1.2 kt radiochemical) in Nevada sand-gravel mix.

3. UET Program (8 pounds to 320,000 pounds of TNT) in Dugway dry clay.

4. JANGLE HE (2560 pounds of TNT, 40,000 pounds of TNT) in Nevada sand-gravel mix.

5. Project Mole (256 pounds of TNT) in Dugway dry clay, Nevada sand-gravel mix, California wet sand and moist clay.

The various approaches to the final result of obtaining a prediction method for operational nuclear underground detonations can be illustrated by a three-dimensional plot, as in Figure 2.10. The three variables associated with the plot are soil characteristics, charge size (W), and charge depth or height. The approaches may be identified with reference to the figure as:

(A) Horizontal: variable soils, constant charge size and charge depth.

Example: Project Mole

(B) Vertical: variable charge size, constant soil and charge depth.

Example: Dugway UET Program.

(C) Transverse: variable charge depth, constant soil and charge size.

Example: Project Mole or Nevada nuclear shots.

A first look at the above breakdown indicates an optimistic picture; that is, the available HE data serve to tie down the horizontal and vertical ramifications of the prediction procedure and then the transverse considerations are used to predict effects from nuclear weapons. However, this conclusion only holds provided consistent and meaningful relations can be established when applying the "horizontal," "vertical," and "transverse" analyses. If the measured physical quantities such as earth stress, earth acceleration, etc., obeyed the laws of similitude, then the optimism referred to above would be wholly justified. But it has been explained why nuclear test effects do not agree (and indeed should not be expected to agree) with effects predicted from model-law scaling of HE test results. Such considerations influence the scope of this report.

Chapter 3
EXPERIMENT DESIGN and PROCEDURES

The explosion with which this report is concerned was Shot 7, a nuclear device having a radiochemical yield of 1.2 kt buried at a depth of 67 feet in Area 10 of the Nevada Test Site (NTS). The location of this shot was chosen to be as near as possible to the JANGLE U ground zero location to minimize possible ambiguity in correlation due to soil variations. The shot point chosen was 650 feet southwest of the JANGLE U shot point, a distance considered to be adequate to avoid asymmetry due to the proximity of the JANGLE U crater.

3.1 TYPE OF MEASUREMENT

The prior underground (and surface) explosions affecting this study which have been conducted at the Nevada Test Site are shown in Table 3.1. The data from these shots constituted essentially the sole available material for preshot prediction of Shot 7 effects, except that certain similarities have been noted between effects of these shots and those conducted in the dry clay area of the Dugway Proving Grounds in the Underground Explosion Tests (Table 3.2). Since the effect of depth of charge is quite pronounced, the results of the surface shots, JANGLE S, HE-4, and Mole surface shots, were not particularly applicable. Likewise, the results of JANGLE U, HE-1, HE-2, and Mole shots, with similar charge depth were useful largely in predicting the trend of scaling over a wide range of charge sizes. The most useful shots for the present purposes were HE-3 and the Mole shots at depths

$$0.5 \leq \lambda_c \leq 1.0.$$

In establishing the instrument plans for Project 1.7, it was naturally desirable, for the maximum possibility for correlation, to make measurements similar to those made in previous applicable tests. At the same time it was considered desirable to use improved instrumentation wherever possible. Several measurement techniques were used on the earlier tests and found to be unreliable, and substitutes for these techniques were desired. To assist in meeting both types of requirement, it was decided to schedule a series of Project Mole tests in Area 10 prior to Operation TEAPOT; that is, in October and November 1954 (Reference 9). In these tests measurement techniques previously found most promising were applied in addition to a few new techniques not previously attempted. The location of the tests was chosen to be as close as possible to the planned ground zero for the nuclear detonation. The shots were located within 2,000 feet of ground zero. The types of dynamic measurements

TABLE 3.1 - PREVIOUS UNDERGROUND AND SURFACE SHOTS AT NEVADA TEST SITE

Shot	Date	Location	Yield	λ_c
JANGLE S	11/19/51	Area 9	1.2 KT[1]	-0.027[2]
JANGLE U	11/29/51	Area 10	1.2 KT[1]	0.13[2]
HE-2	9/ 3/51	Area 9 and 10	40,000 lb - TNT	0.15
HE-4	9/ 9/51	Area 9 and 10	2,560 lb	-0.15
HE-1	8/25/51	Area 9 and 10	2,560 lb	0.15
HE-3	9/15/51	Area 9 and 10	2,560 lb	0.5
MOLE 206	10/11/52	Area 9 and 10	256 lb	0.0
MOLE 205	10/ 8/52	Area 9 and 10	256 lb	0.13
MOLE 204	10/ 4/52	Area 9 and 10	256 lb	0.26
MOLE 203	9/19/52	Area 9 and 10	256 lb	0.5
MOLE 202	9/14/52	Area 9 and 10	256 lb	1.0
MOLE 403	10/28/54	Area 10	256 lb	0.13
MOLE 405	11/ 2/54	Area 10	256 lb	0.26
MOLE 401	10/23/54	Area 10	256 lb	0.5
MOLE 406	11/ 4/54	Area 10	256 lb	0.5
MOLE 402	10/26/54	Area 10	256 lb	0.75
MOLE 404	10/30/54	Area 10	256 lb	1.0

1. Radiochemical yield; mechanical yield indeterminate.

2. Based on radiochemical yield; effective figures greater.

used on previous tests and considered for Shot 7 are discussed in the following sections.

3.1.1 Acceleration. Measurements of horizontal (radial) and vertical acceleration were conducted on all previous underground tests at NTS. Tangential acceleration was measured in only a few instances. Horizontal acceleration is considered to be an important phenomenon in underground explosions, although its scaling over wide ranges of charge sizes is complicated by several effects. Wave forms are relatively complex and are influenced by changes in the effects of variations of soil

TABLE 3.2 - LARGE UNDERGROUND TNT SHOTS, DUGWAY PROVING GROUND, UTAH

Shot	Date	Yield	λ_c
UET-318	5/22/51	320,000 lb	0.50
UET-315	5/10/51	40,000 lb	0.50
UET-312	5/ 5/51	2,560 lb	0.50

characteristics. In shallower shots, confusion is introduced by the different scaling factors of acceleration due to airblast, compared with directly-induced acceleration, but this is not an important consideration at the Shot 7 depth of burial. Acceleration versus time records can also be integrated to provide data on particle velocity and displacement versus time, although the accuracy of such integration is subject to question, except in the early phases of the transients involved. Acceleration, per se, is considered to be of considerable importance in structural effects on certain types of structures and components.

Vertical acceleration measurements, although conducted on all previous tests, have not proved as internally consistent or as subject to scaling as horizontal acceleration measurements. Their magnitude is usually one-half of the horizontal accelerations, and the wave forms are more complex. They are affected more by the incident airblast than is the horizontal acceleration. Vertical acceleration is probably not as important in structural effects since most structures and components are normally designed to be stronger in the vertical direction.

Tangential acceleration has been shown to be almost completely unpredictable since it is apparently primarily a function of the asymmetry of the medium. It is almost invariably small compared with the other components.

In view of the above considerations and of the limited number of channels available, acceleration measurements on Project 1.7 were limited to horizontal (radial) acceleration, except for one isolated case in which vertical acceleration was considered of interest to another project.

3.1.2 Air-blast Pressure. Air-blast pressure at several radii has been measured on all previous shots. It has been shown to be subject to scaling quite satisfactorily and is an important effect of underground explosions at shallower depths of burial. Its importance at the projected depth of Shot 7 is questionable with regard to its effects on structures, but such measurements are useful for establishment of yield and partition of energy. As a consequence, a limited number of measurements of air blast were included in the experiment plan.

3.1.3 Earth Stress and Pressure. In the earlier underground tests efforts were made to measure earth pressure by pressure gages immersed in fluid-filled holes of various depths. The results of these measurements were found to be questionable, and these measurements were omitted in later tests. An earth stress gage, based on gages developed by Roy W. Carlson, was used to a limited degree on HE-1 and extensively on Project Mole, particularly on Phase II-B (the series of tests immediately prior to TEAPOT). Similar gages were used by Sandia Corporation on Operations TUMBLER-SNAPPER and UPSHOT-KNOTHOLE in the measurement of underground effects due to an air burst.

These gages measure directional stress; and to describe the stress tensor completely at any point, it is necessary to install a number of such gages. From previous relatively deep underground tests, however,

it was found that the horizontal component of stress is from two to eleven times greater than any other component and may be considered to be a good representation of the major component of stress. The dynamic records from these measurements are usually relatively simple in wave form, particularly at radii of major interest, but little information is available on the scaling of such measurements. Since earth stress is considered to be an important factor in the effects on structures, a number of these measurements were included in the experiment plan.

3.1.4 Earth Strain. Earth strain was previously measured at NTS only in Project Mole (Reference 9), Phase II-B. A limited number of experimental earth strain measurements were taken in Project Mole, Phase I, at the Dugway Proving Grounds, using short span gages of the differential transformer type. In Mole, Phase II, at Camp Cooke, California, several measurements were taken of earth strain using long-span surface gages, with promising results. As a consequence, these measurements were incorporated in the Phase II-B tests. A high degree of internal consistency was observed. Although strain measurements integrated against radius were found to correlate well with dynamic displacement measurements, they correlated only moderately well with final values of permanent displacement as measured by survey.

The wave forms of the strain records were surprisingly different from those of the stress measurements, being of much longer time duration and simpler wave form. This is in contrast with comparisons of measurements made on air bursts, where the wave forms of stress and strain records were very similar. It is particularly pertinent to note that the ratio of maximum strain to maximum stress from underground shots was from 30 to 100 times greater than the equivalent ratio from air bursts, indicating that different mechanisms govern stress-strain relationships in the two cases, probably due to the proximity of the surface and the different direction of wave propagation. Since these measurements appear to give such consistent results and since earth strain could be a very important factor in effects upon certain types of structures, a number of these measurements were included in the experiment plan. The strain measurements were limited, however, to measurement of horizontal component, since vertical strain appeared to be of minor importance and since no background of data was available. Two types of gages were used: long-span gages at the surface and short-span gages at a depth of 10 feet.

3.1.5 Displacement. Dynamic measurements of radial particle displacements have been limited in all early tests to results obtained from doubly integrated acceleration records. In many such efforts minor base line shifts, etc., have introduced serious errors in the integrated results after the first several milliseconds of the record. Since the accelerations most important in producing major displacements are the low amplitude, low-frequency disturbances (occurring after the high amplitude peaks) and since these later accelerations are subject to considerable error due to their small magnitude, the double integration method to obtain dynamic displacement yields only approximate results.

On Mole Phase II-B, experiments were conducted for the measurement of displacement by determination of tangential strain. Assuming symmetry,

the particle displacement at a given radius is equal to the product of the tangential strain and the radius. It is recognized that the assumption of symmetry introduces an important unknown, but a number of measurements on Project Mole indicate good correlation between displacement as determined from tangential strain and as measured by other means (consecutive long-span measurements of horizontal strain.) In a project of the magnitude of Shot 7, the long-span measurements are not feasible; therefore, a few measurements of displacement by tangential strain were included in the experimental plan.

3.2 GAGE DEPTH AND LAYOUT

On previous HE and nuclear tests, measurements were made of free-field effects at a variety of (relatively shallow) depths. The majority of acceleration measurements were made at a depth of 5 feet regardless of the size of charge. Practically all earth stress measurements were made at a depth of 2-1/2 feet. The experimental short-span earth strain measurements were made at a depth of 2-1/2 feet, whereas all long-span measurements were, of necessity, made at the surface. Air-blast measurements have historically been made at the surface, although a few have been made at heights of a few feet above the surface.

In planning an experiment on a large explosion, the question naturally arises as to the proper scaling of depth of measurement. The soil at NTS, Area 10, varies inconsistently and quite widely with depth in the first 10 or 20 feet; therefore, there is no assurance of similarity in using scaled depth of measurements. There is some reason, on the other hand, to favor the uniform depth of gage, regardless of the scale size of charge. In any case, fully scaled measurements are impracticable, since they would require planting gages at unreasonable depths. Since no clear choice existed, it was decided that for this experiment acceleration and earth stress would be measured at depths most useful to the structural program. This was decided upon as 10 feet. Strain measurements by long-span strain gages are restricted to the surface, however, so a few channels of horizontal acceleration were included at a depth of 1 foot for correlation with the surface strain measurements. Air-blast measurements were made at the surface.

A total of 28 free-field channels were available for Project 1.7.1. In accordance with the principles outlined above, these channels were divided among the various types of measurements and gages distributed over a range of radii considered to be important. The final gage layout is shown in Figure 3.1 and Table 3.3 In addition to the 28 channels of Project 1.7.1, Project 1.7.2 included two free-field channels for horizontal earth stress measurement at a depth of 15 feet at a radius of 300 feet from ground zero (see Figure 3.2). These measurements were included to determine the extent of asymmetry, if any, at that radius for Project 3.3.1.

The location of the structures and test devices involved in Project 3.3.1 and 3.3.2 is shown in Figure 3.2. A total of 46 channels of

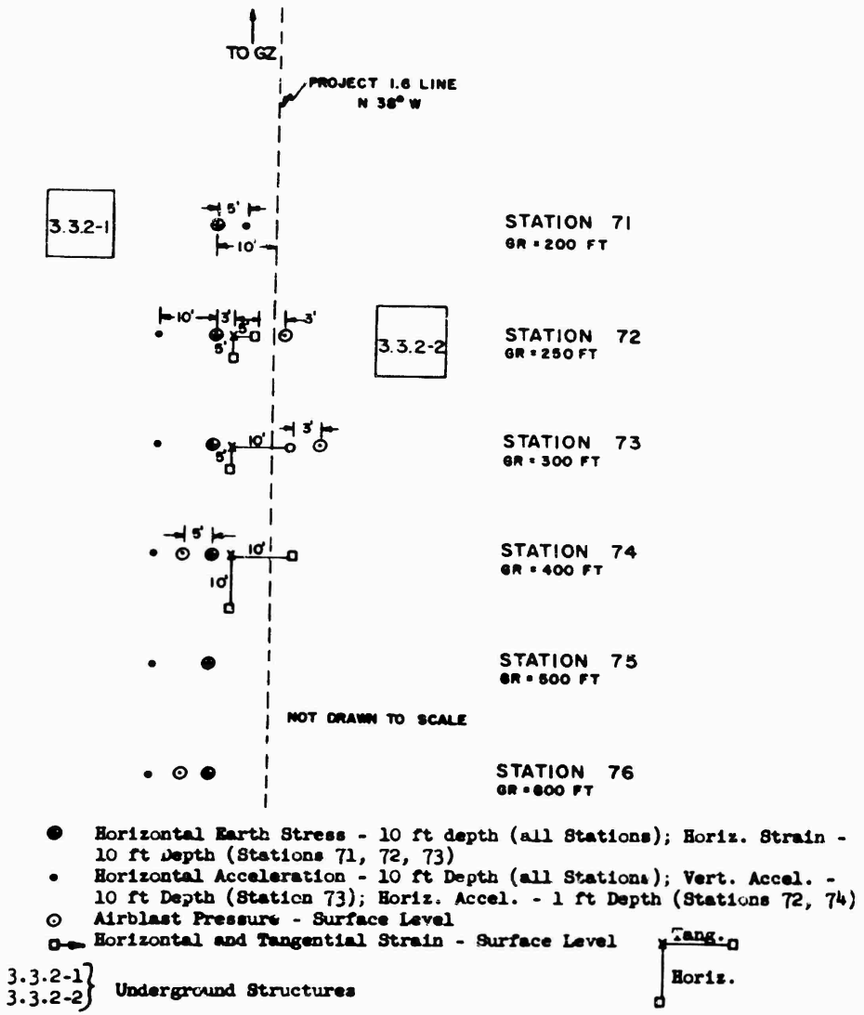

3.1 Free-field gage layout (Project 1.7.1).

TABLE 3.3 - FREE-FIELD GAGE LAYOUT

Station	Range (ft)	Gage Code[1]	Galvano-meter Std.	Type A[2]	Predicted Peak[3]	Actual Peak
71	200	71H10	300	200	7.2 g	9.9
71	200	71CH10	300	300	90 psi	126
72	250	72H10	300	200	5.3 g	2.2
72	250	72H1	300	200	4.0 g	1.9
72	250	72CH10	300	300	53 psi	44
72	250	72SH	300	300	136 ppk[4]	156
72	250	72SH10	300	200	68 ppk	19
72	250	72ST	300	300	60 ppk (15-ft displacement)	15.2
72	250	72B	300	—	2.5 psi	14.4
73	300	73H10	300	200	3.75 g	-1.50
73	300	73V10	300	200	1.9 g	0.5
73	300	73CH10	300	300	30 psi	40.1
73	300	73SH	300	300	88 ppk	11
73	300	73SH10	300	200	44 ppk	12
73	300	73ST	300	300	30 ppk (9-ft displacement)	2.4
73	300	73B	300	—	2.3 psi	14.1
74	400	74H10	300	200	2.2 g	-0.9
74	400	74H1	300	200	1.6 g	-1.3
74	400	74CH10	300	300	13 psi	22
74	400	74SH	300	300	37 ppk	2.6
74	400	74SH10	300	200	19 ppk	2.0
74	400	74ST	300	300	7.5 ppk (3-ft displacement)	0.4
74	400	74B	300	—	2.05 psi	11.3
75	500	75H10	300	200	1.5 g	1.0
75	500	75CH10	300	300	9.5 psi	6.1
76	600	76H10	300	200	1.0 g	1.1
76	600	76CH10	300	300	7.3 psi	3.8
76	600	76B	300	—	1.75 psi	6.1

1. See Sec. 3.6
2. See Sec. 3.7 and 3.7.2
3. See Sec. 3.5
4. ppk = strain measured in parts per thousand

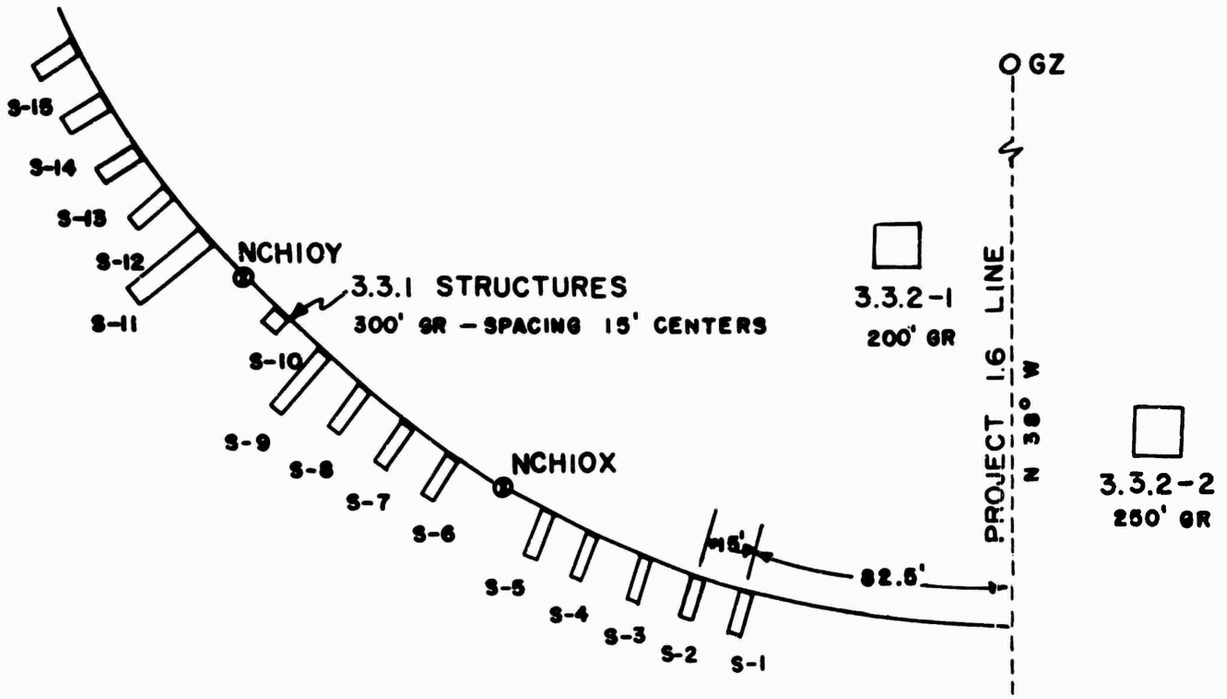

3.2 Structure layout (Project 1.7.2).

instrumentation was applied to these devices, which, including the two free-field gages mentioned above, brings the total channels of Project 1.7.2 to 48.

In addition to the dynamic measurements of displacement, provisions were included for the measurement of permanent displacement. An array of 40 monuments was installed, consisting of 10 monuments on each of four mutually perpendicular lines, at ranges from 180 to 500 feet. The preshot location and elevation of each monument were determined by survey.

3.3 PREDICTIONS

In planning an experiment of this type, it is necessary to predict the values of the functions to be measured to an accuracy sufficient to allow the sensitivity of each channel to be set closely enough that satisfactory deflection may be obtained. For best results these should be within a factor of 2 of the true values, but a factor of 3 is acceptable. A greater range is acceptable on channels where dual sensitivity galvanometers are used. Predictions are also important in the selection of gage ratings, to ensure that gages are not overranged, introducing nonlinearities. Predictions discussed herein were, in general, not used in calculating predictions for the structural measurements of Project 1.7.2; the project officers of 3.3.1 and 3.3.2 provided their own predictions. However, by discussion, an effort was made to bring the several sets of predictions to compatibility.

Predictions for a shot of this type are complicated by a number of factors. Full-scale data are meager, and scaling from smaller charges

is not as simple as in the case of air bursts. It is influenced greatly by uncontrollable differences in the medium, since variations of soil characteristics with depth do not scale. This causes an uncertainty as to the effects of charge depth, partial resolution of which was one of the prime reasons for the establishment of Shot 7. This uncertainty is increased by a lack of knowledge of the variation of mechanical TNT efficiency with depth of a nuclear device.

For this experiment, it was decided to tie effects predictions to crater predictions wherever possible. When small-charge data (other than airblast) are plotted against crater radius, the scaled depth of burial becomes less important because a closely grouped family of curves is usually obtained for depths of burial from $\lambda_c = 0.25$ to $\lambda_c = 1.0$. This permits the use of more data than if other techniques were used.

Crater predictions were made prior to Shot 7 by several agencies, using many techniques. Early predictions of apparent crater radius ranged from 155 to 275 feet. These variations, based largely on different estimates of yield variation and on different approaches to the relations between true and apparent craters, eventually were narrowed considerably. New crater data from Mole Phase II-B, tended to increase slightly the slope of the curve for radius-versus-charge depth obtained from HE data, and the majority of estimates tended to center around 188 feet (Reference 19); therefore this figure was chosen as the design reference for Project 1.7 predictions.

Free-field effects data from HE charges were plotted against crater radius, and the best curve was drawn through the scatter of data, with slight modifications of slope in some cases, based on JANGLE U experience. The resultant curves were used in the prediction of peak values to be expected (Reference 20). In most cases, this results in predicted values lower than would be obtained from direct $W^{1/3}$ scaling of HE results, assigning 100 per cent TNT efficiency to the nuclear charge. No predictions were made of time relationships, since these were unimportant for the primary purpose of these studies (range setting). The predictions used are shown in Table 3.3; also shown on this table are the actual peak values recorded on Shot 7. The accuracy of the predictions and the scaling method employed will be discussed in detail in Chapter 5.

3.4 GAGE CODING

For identification of channels and recorded traces with their proper gages a systematic coding was adopted. For Project 1.7.1 a station number was assigned to each gage station, as shown in Figure 3.1. These numbers were used as the first part of the gage code. The second part of the gage code was a letter indicating the nature of the measurement. In this project, B, for airblast, measured by surface baffle-mounted gages; H, for horizontal acceleration; V, for vertical acceleration; CH, for horizontal stress; SH, for horizontal strain; and ST, for tangential strain (displacement) were used. A third part of the code, where necessary, indicated the depth of the gage below the surface in feet. Typical

gage code numbers would then be 72CH10 (horizontal stress at 10 feet depth, Station 72), 73ST (tangential strain at surface, Station 73), and 76B (airblast at surface, Station 76). The two free-field stress measurements made near the Project 3.3.1 structures (Figure 3.2) are designated NCH10X and NCH10Y.

3.5 INSTRUMENTATION

All channels of instrumentation for measurement of acceleration and pressure were essentially identical to those described in previous reports (Reference 9). Wiancko balanced variable-reluctance transducers were connected through modified Wiancko station equipment to William Miller Corporation oscillograph recorders. The basic earth stress gage used in these tests was a modification of the one originally designed by R. W. Carlson for the measurement of static stress in foundations and grades. The gage consists of two flat, stiff, circular plates with thin, flexible edges attached together at the edges so as to be separated by a narrow space filled with oil. A Wiancko pressure gage is arranged to measure the pressure in this oil as a measure of the actual component of the stress in the medium in which the gage is buried. The Wiancko gage protruding from the center of one of the circular plates was protected by a housing designed to occupy a volume as small as possible and to provide an air-tight seal to the back of the gage, permitting easy calibration.

The short-span strain gages used were supplied by Sandia Corporation and consisted of two discs so arranged that relative motion between the discs actuates the moving element of a linear differential transformer, creating an unbalance in a previously balanced inductive bridge. Electrically, then, it is equivalent to a Wiancko gage. The long-span strain gages used at the surface were of a type designed by and manufactured for the Ballistic Research Laboratories and were identical to those used for measurements of relative displacement between two parts of a test structure. These gages essentially consist of a potentiometer whose shaft is arranged to be rotated by a powerful coil spring. A sheave on the end of this shaft carries a length of piano wire approximately 0.025 inch in diameter. When the end of this piano wire is anchored at one point and the gage itself at another point and when the spring is wound so as to create a heavy tension in the piano wire, the position of the potentiometer then indicates any change in the relative location of the two points. This potentiometer is connected as a resistive half-bridge in the normal Wiancko circuitry.

The structural strain measurements made in Project 1.7.2 consisted of SR-4 strain gages in a balanced full-bridge connected through Consolidated Type DII carrier amplifiers to the Miller recorders. Provisions were included for applying, automatically, a synthetic calibrating signal to each channel immediately prior to zero time for purposes of comparison of the final deflection on the record with the deflection produced by the same signal at the time of calibration. A highly accurate timing signal of 100 and 1,000 cps was also applied to all recorders simultaneously from a single source having a time accuracy of better than 10 parts per million. This provided means for time correlation of records to a high

degree of accuracy. The prime power supply for all instruments during actual shots was a bank of storage batteries. Suitable converters were used to produce 115 volts of alternating current for components requiring this type of source. An individual converter was used for each rectifier power supply, thus minimizing the probability of gross failure due to converter failures.

Of the 76 gage channels available on this project, 55 used dual recordings with one galvanometer on each of two recorders. This provision was included as a protection against recorder failure. On 20 of these 55 channels, one of the galvanometers used was of 200 cps natural frequency, whereas the remaining galvanometers were of 300 cps natural frequency. The channels incorporating one 200-cps galvanometer were used on gages where the uncertainty of the predicted peak was greatest and where the expected signal was such as not to be worsened appreciably by the reduced frequency response of the lower frequency galvanometer. Since there was an appreciable difference in the sensitivity of the two galvanometers thus used on a single channel, a wider range of input signal could be accommodated without loss of data (provided both recorders operated properly).

Instruments were powered at suitable times before zero time by EG&G relay circuits with lock-in relays controlled by time delay relay to continue operation for approximately 1 minute after zero time, in spite of the fact that the EG&G relays dropped out sooner. Utmost attention was paid to circuitry and procedures to ensure maximum reliability of operation. Dual relay contacts or dual relays were used wherever feasible. A separate recording was made of the output voltage of each power oscillator supplying the carrier power to a group of 12 gages, so that correction might be made in the final data reduction for any change in output voltage due to cables which became shorted during the shot or to any other such cause. A multipen recorder was connected to provide a record of operating time and sequence of various elements so that any failure might be traced to its source in a post-test study.

All terminal instruments and recorders were mounted in a single shelter, 3.28 g, located about 1,300 feet from ground zero. The recording shelter was covered with earth to a sufficient depth to reduce the integrated radiation dosage within the shelter to below 10 r. This figure had been determined previously to represent an acceptable figure to avoid fogging of the recording paper by radiation.

3.5.1 Gage Mounting. Air-blast pressure gages were mounted with the inlets at the center of a 17-inch diameter cast aluminum baffle. This baffle was cemented flush with the earth surface and held in place with a buried anchor. These installations were identical to those used in blast measurements of air bursts (see Figure 3.3). Accelerometers were mounted in a canister for planting in the earth. The basic canister structure was a stiff brass cylinder with an internal mount for the accelerometer. Internal damping of the accelerometer mount was provided by an "O" ring near the bottom contacting the interior of the enclosing cylinder. One of these canisters is shown in Figure 3.4. In installa-

3.3 Airblast gage installation.

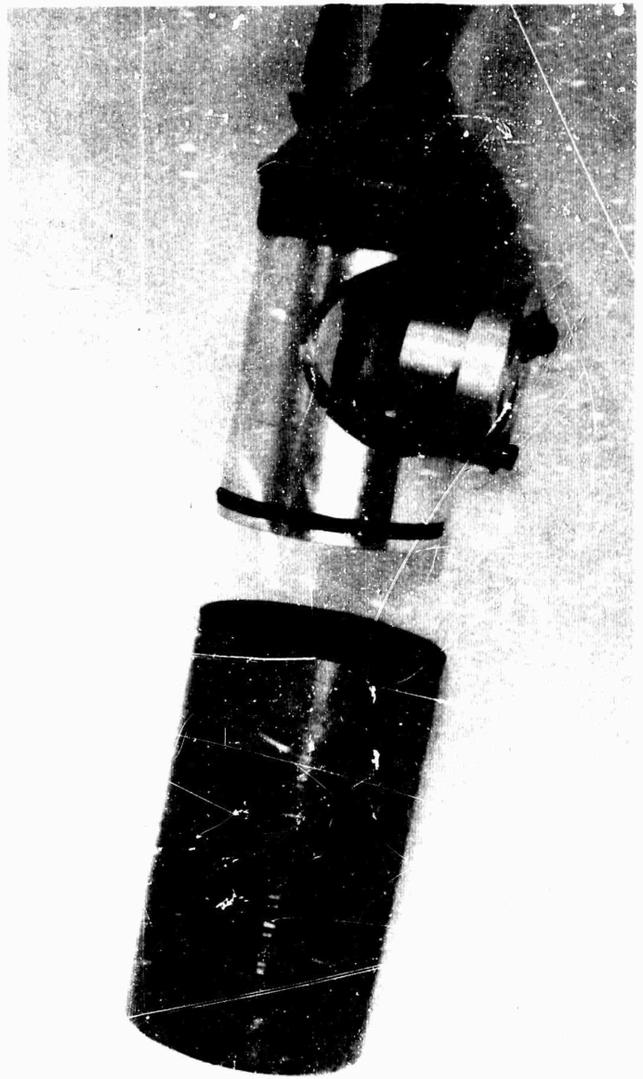

3.4 Accelerometer gage and canister.

tion, after calibration, the canisters were placed in the bottom of an 8-inch hole in the proper orientation and sealed in place with Cal-Seal, a quick-setting plaster.

Earth stress gages and short-span earth strain gages were mounted at the bottom of a 10-foot deep, 30-inch diameter hole. Moistened, screened, surface material was carefully tamped around the gages by hand to a depth of approximately one foot; the remaining hole was tamped by mechanical tampers with attention being paid to a uniform tamping procedure throughout.

The long-span strain gages at the surface were installed in two parts. The span of these gages was determined by the deflections expected, a minimum of 60 inches and a maximum of 50 feet being used. The gage proper was mounted in a wooden box, which was secured in turn to a concrete monument flush with the surface of the earth. The end of the measuring wire was then attached to a second monument 5 to 50 feet from the box. The layout of these gages is shown in Figure 3.1.

Displacement (deflection) gages used on structures were similarly mounted to show the relative displacement between the center of a wall and its supports. Carlson (stress) gages, used on structures, were set flush with the surfaces of the structures and cemented in place after calibration. Structural strain gages used for Project 3.3.1 were installed by personnel of that project on the torque arms of the compliant member of their devices in such a fashion as to measure shear stress or torque in these arms. Eight of these gages (16 single elements) were used on each structure and connected in a four-arm bridge to a single channel to indicate the total average force applicable.

3.5.2 Instrument Response. The response time of the pressure gage recording system was determined by the characteristics of the recording galvanometers used. The 300 cps galvanometers had an undamped natural frequency of 315 to 340 cps and were damped to have an overshoot of approximately 7-1/2 per cent. This corresponds to a damping factor of approximately 0.65 and provides a nominal rise time (to 90 per cent of final amplitude) of 1.3 millisecond. The 200-cps galvanometers had an actual undamped natural frequency of 200 to 230 cycles per second and were similarly damped, giving a rated rise time of approximately 1.8 msec. Since the rise time of the Wiancko gages when properly adjusted was appreciably smaller than either of these figures, it does not enter into the characteristics of the final records. The frequency response of the Wiancko gage and associated recording system is basically flat down to steady-state conditions. To avoid drift due to temperature changes or to changes in ambient pressure, the lower range gages, however, are provided with a bleed plug in the case of the gage so that any pressure difference between the inside and outside of the case will be equalized over a period of time. The time constant of this bleed plug was adjusted to a minimum of 30 seconds, so that it would have no effect on the recording of a blast wave of normal duration. As a consequence, the low-frequency response of the gage system may be considered as completely flat.

The response time of the acceleration recording system was determined, in general, by the characteristics of the accelerometers. Since

the peak accelerations encountered in a shot if this magnitude are relatively low, accelerometers rated at 5 G maximum were used, having an undamped natural frequency of 85 cps. Some of the accelerometers on structures, however, were connected through the Consolidated recording systems having higher gain and thus permitting the use of a higher rating accelerometer having a natural frequency of 450 cps. In this case, the response time of the system was chiefly determined by the characteristics of the recording galvanometers.

The frequency response characteristics of the Carlson stress gages are difficult to determine explicitly since they are affected greatly by the loading of the earth on the gages; however, the basic gage is known to have a response similar to that of the pressure gage alone (it had been used satisfactorily to measure airblast and provided a good record of a shock wave). Similarly, the response time of the earth strain gages is difficult to describe explicitly, but measurements indicate that they have a response time far shorter than the rise times indicated on the final records; therefore, no distortion from this cause is attributed to the gages.

3.5.3 Calibration. Each gage was calibrated in the field after the gage had been connected to its associated cable and recording equipment for the shot and immediately prior to its final installation in the earth. Air-blast gages and Carlson stress gages were calibrated by the direct application of air pressure. Accelerometers were calibrated by placing them in several orientations with respect to the earth field in a jig designed for the purpose or, where necessary, on a spin table. Earth strain gages were calibrated by the introduction of directly measured deflection on the gages themselves. The structural strain gages were precalibrated by personnel of Project 3.3.1 to show the gage constants of the strain gages used. These checked quite acceptably with the manufacturer's gage constants. The conventional technique of introducing a known unbalance to the bridge and observing the deflection caused thereby was used in the final calibration of these gages.

In the calibration procedures, several deflections ranging from zero to well above the expected peak were applied to each gage in sequence. Each galvanometer deflection was noted and recorded. In addition the deflection caused by an artificial signal injected into the gage circuit was recorded. From the former deflection a calibration curve of deflection versus the function of interest was constructed; the latter deflection served to correct for any changes of sensitivity of the recording system between calibration and the final tests, since an identical signal was injected on the final record about 4 sec before zero time.

3.6 OPERATIONS

Owing to the scheduling of TEAPOT, the operations involved in Project 1.7 were not conducted under optimum conditions. Field operations commenced on 20 January 1955, with a scheduled completion date of 15 February 1955. During this period there was severe cold weather including

snow at times followed by slush. Frozen earth extended 12 to 20 inches below the surface, impeding excavation and particularly grading. Also, melting snow on occasion flooded portions of the cable trenches causing instances of leakage to ground greater than is normally tolerated.

In addition, there was a series of unavoidable operational problems and delays which, though resulting in no known errors, nevertheless tend to reduce somewhat the normal confidence in the accuracy and reliability of the gage calibrations used. Since all gages had to be calibrated prior to burial, it was necessary to commence calibration procedures on 27 January. Contrary to desired procedure, for constructional reasons, many of the gages were disconnected after calibration and reconnected after placement. Owing to the scheduling of other shots, it was also necessary to transfer the recorders to Area F after gage calibration and installation were completed. Later, the recorders were returned, and Shot 7 was fired on 23 March, some 55 days after the first calibration.

3.7 PERFORMANCE OF INSTRUMENTATION

Of a total of 76 channels connected, records were obtained on all but one channel. This one channel, a Project 3.3.1 measurement, suffered an electrical failure after installation and before the shot.

Owing to a large overprediction of structural effects, the deflections of several records, Project 3.2.2 channels in particular, were so small as to give negligible data. On the other hand, unexpectedly large air-blast pressures resulted in three of the four air-pressure traces leaving the paper, making it necessary to estimate maximum air-blast pressures by extrapolation of the pressure decay curve. Also, in several instances cable breaks occurred at 0.6 to 1.0 seconds after zero time, preventing determination of positive phase durations but not affecting the important early phases of the records and the determination of peak values.

3.8 RECORD READING AND DATA REDUCTION

The raw data on this project appear as recorded traces on 12-inch wide oscillograph paper. Each record includes approximately twenty channels of instrumentation; therefore, the initial task was the indentification of the traces with the proper gage channel. The records were then read (inches deflection of trace versus time) using an electro-mechanical reader (Benson-Lehner Oscar) which fed into an IBM card punch. The data cards so obtained, along with the appropriate calibration cards for each gage, were processed by the IBM Card-Programmed Calculator (CPC). The final reduced data came out in the form of listings of acceleration versus time, air blast pressure versus time, etc., corresponding to each gage record. The integrations of the acceleration records to obtain velocity and displacement versus time were done on the computer, using the trapezoidal rule.

Tracings of the Project 1.7.1 original gage records (reduced photographically) are presented in Figures 4.4 through 4.8 of this report.

Air-blast records (Figure 4.6) were replotted to a smaller scale, since the original records have very high amplitude peaks.

In the absence of excessively high temperature, it is believed that the calibration procedure assures that the Wiancko gage measurements are reliable to within ± 5 per cent. Small magnitude measurements, far below nominal gage rating, may be somewhat less accurate. The measurements of time should be accurate to ± 0.5 msec between events, with a slightly larger uncertainty of time from zero time (i.e., time of detonation). Durations are necessarily subject to greater reading errors, due to the difficulty of determining true crossover times; this error is of the order of ± 10 msec.

The above statements concerning accuracy are not intended to intimate that the representative values of the measured functions involved are known to that degree of accuracy. In most of the gage types used, the mounting and planting procedures introduce perturbations in the medium whose effects cannot be calculated. Where statistical information is available (e.g., earth stress measurements), it appears that a reliable figure for standard deviation is approximately 16 per cent. The standard deviation for strain measurements is probably similar. Of course, to the effects due to the medium must be added effects due to explosion asymmetry, which are totally unknown.

Chapter 4
RESULTS

4.1 FREE-FIELD DATA (PROJECT 1.7.1)

Tables 4.1 through 4.6 present the tabulated free-field data (Project 1.7.1). To supplement the tabulations, Figures 4.1 through 4.3 present some typical gage records which have been labeled appropriately to correspond with the table headings. Reductions of tracings of the

TABLE 4.1 EARTH ACCELERATION TEAPOT SHOT 7

Gage Code	Ground Range (ft)	Gage Depth (ft)	Arrival Time (sec)	First Positive Peak (G)	Time of First Positive Peak (sec)	Maximum Positive Peak (G)	Time of Maximum Positive Peak (sec)	Maximum Negative Peak (G)	Time of Maximum Negative Peak (sec)
HORIZONTAL									
71H10	200	10	0.050	9.90	0.159	9.90	0.159	-1.40	0.270
72H10	250	10	0.065	2.23	0.193	2.23	0.193	-1.38	0.335
73H10	300	10	0.076	0.81	0.200	0.81	0.200	-1.48	0.325
74H10	400	10	0.103	0.47	0.125	0.797	0.445	-0.92	0.360
75H10	500	10	0.130	0.36	0.173	1.04	0.470	-0.72	0.340
76H10	600	10	0.161	0.30	0.210	1.07	0.500	-0.66	0.350
72H1	250	1	0.070	1.92	0.205	1.92	0.205	-1.08	0.355
74H1	400	1	0.110	0.55	0.155	1.08	0.470	-1.32	0.355
VERTICAL									
73V10	300	10	0.076	0.477	0.197	0.542	0.315	-0.262	0.271

interesting portions of all usable gage records are presented in Figures 4.4 through 4.8. The records are arranged in the order earth acceleration, airblast pressure, earth stress, and earth strain.

4.2 STRUCTURAL DATA (PROJECT 1.7.2)

The reduced data obtained on Project 1.7.2 have been transmitted to the proper agencies for their reporting and analysis. (See References 21 and 22). Preliminary data reduction of the measurements taken on the underground structures of Project 3.3.2 showed that the forces, accelerations, and relative displacements on these structures deviated markedly from the predictions based upon HE data. Following Operation TEAPOT, it was decided to conduct a series of tests on the 3.3.2 structures using HE charges at such a time as the radiation level in the area permitted. These tests were conducted in October 1955, and the data report which was submitted to Office, Chief of Engineers, is included in the Appendix to this report.

TABLE 4.2 EARTH VELOCITY AND DISPLACEMENT, TEAPOT SHOT 7

Gage Code	Ground Range (ft)	Gage Depth (ft)	Arrival Time (sec)	Maximum Positive Velocity (ft/sec)	Rise Time to Maximum Positive Velocity (sec)	Maximum Peak-to-Peak Velocity (ft/sec)	Peak-to-Peak Time Interval (sec)	Maximum Positive Displacement (in.)	Time of Maximum Positive Displacement (sec)
HORIZONTAL									
71H10	200	10	0.050	10.8	0.140	a	a	a(> 34)	a(>0.590)
72H10	250	10	0.065	5.2	0.165	7.8	0.375	9.8	0.390
73H10	300	10	0.076	3.1	0.179	5.1	0.200	5.6	0.355
74H10	400	10	0.103	1.51	0.142	3.21	0.160	2.33	0.330
75H10	500	10	0.130	0.97	0.135	2.20	0.135	1.32	0.330
76H10	600	10	0.161	0.76	0.130	2.28	0.160	0.96	0.350
72H1	250	1	0.070	6.0	0.190	6.2	0.50	23	1.0
74H1	400	1	0.110	1.68	0.190	3.98	0.165	2.6	0.345
VERTICAL									
73V10	300	10	0.076	1.75	0.294	1.79	0.172	4.2	0.500

a-data uncertain

TABLE 4.3 HORIZONTAL EARTH STRESS, TEAPOT SHOT 7

Gage Code	Ground Range (ft)	Gage Depth (ft)	Arrival Time (sec)	First Positive Peak (psi)	Time of First Positive Peak (sec)	Maximum Positive Peak (psi)	Time of Maximum Positive Peak (sec)	Positive Phase Duration (sec)
71CH10	200	10	0.055	126	0.180	126	0.180	a
72CH10	250	10	0.066	37	0.220	44	0.350	a
73CH10	300	10	0.077	27.5	0.260	40.1	0.337	0.58
74CH10	400	10	0.102	8.9	0.230	22	0.355	0.49
75CH10	500	10	0.130	4.4	0.260	6.1	0.320	0.48
76CH10	600	10	0.162	3.1	0.285	3.8	0.525	0.25

a-data uncertain

TABLE 4.4 EARTH STRAIN, TEAPOT SHOT 7

Gage Code	Ground Range (ft)	Gage Depth (ft)	Arrival Time (sec)	First Peak (ppk)	Time of First Peak (sec)	Second Peak (ppk)	Time of Second Peak (sec)	Residual Strain (ppk)
(HORIZONTAL)								
72SH	250	0	0.095	156	0.81	156	1.077	152
73SH	300	0	0.188	11.0	0.57	11.0	0.98	10.7
74SH	400	0	0.138	2.4	0.35	2.6	1.04	1.6
72SH10	250	10	0.085	19	0.62	—	—	16.7
73SH10	300	10	0.105	12	0.42	—	—	6.5
74SH10	400	10	0.178	2.0	0.36	—	—	0.9
(TANGENTIAL)								
72ST	250	0	0.200	9.2	0.47	15.2	0.81	12.9
73ST	300	0	0.200	2.4	0.42	—	—	0.8
74ST	400	0	0.265	0.36	0.34	-0.64	0.80	-0.64

TABLE 4.5 PERMANENT HORIZONTAL AND VERTICAL EARTH DISPLACEMENT, TEAPOT SHOT 7

Monument	Ground Range (ft)	N52° E Line		S52° W Line		N38° W Line		S38° E Line	
		Vert. (in.)	Horiz. (in.)	Vert. (in.)	Horiz. (in.)	Vert. (in.)	Horiz. (in.)	Vert. (in.)	Horiz. (in.)
1	180	---	---	57.6	174.6	---	---	55.6	97.2
2	200	---	---	---	---	39.5	72.2	24.7	52.8
3.	225	8.5	34.6	8.5	50.5	12.5	34.2	6.24	28.2
4	250	-2.9	19.0	12.7	37.1	3.2	13.8	6.6	18.2
5	275	0.8	8.9	1.7	30.0	-1.4	8.0	-0.1	4.2
6	300	-2.3	2.8	---	---	-2.0	2.5	0.2	3.6
7	350	0.8	0.1	-0.2	1.1	-2.0	1.4	-0.9	2.6
8	400	-1.0	-0.2	-0.4	0.5	---	-0.4	-1.0	0.8
9	450	-1.4	-0.2	-0.4	0.3	-0.4	-0.1	-0.8	0
10	500	-1.3	0	0.1	0	-0.5	0	-0.5	0

TABLE 4.6 AIRBLAST PRESSURE, TEAPOT SHOT 7

Gage Code	Ground Range (ft)	Gage Height (ft)	"Front Porch"		Main Shock		Positive Phase Impulse (psi-sec)	Positive Phase Duration (sec)
			Arrival Time (sec)	Peak Press. (psi)	Arrival Time (sec)	Peak Press. (psi)		
72B	250	0	0.202	0.70	0.225	14.4	1.20	0.297
73B	300	0	0.243	0.52	0.255	14.1	0.93	0.278
74B	400	0	---	---	0.318	11.3	0.77	0.273
76B	600	0	---	---	0.458	6.14	0.58	0.286

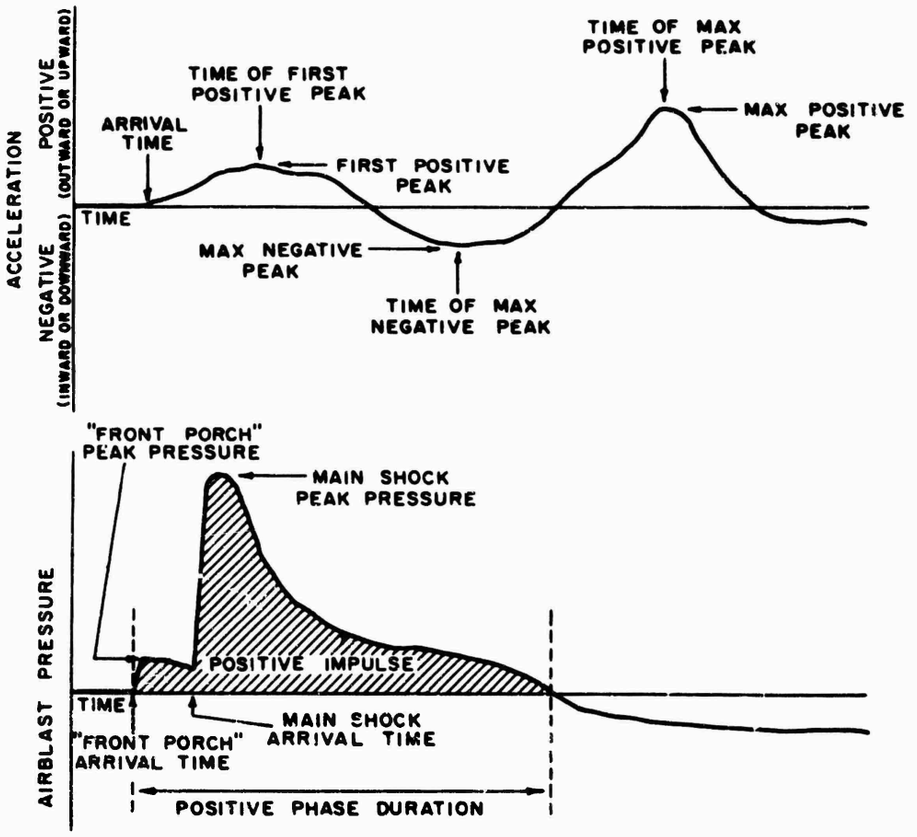

4.1 Diagram of tabulated quantities; acceleration and airblast.

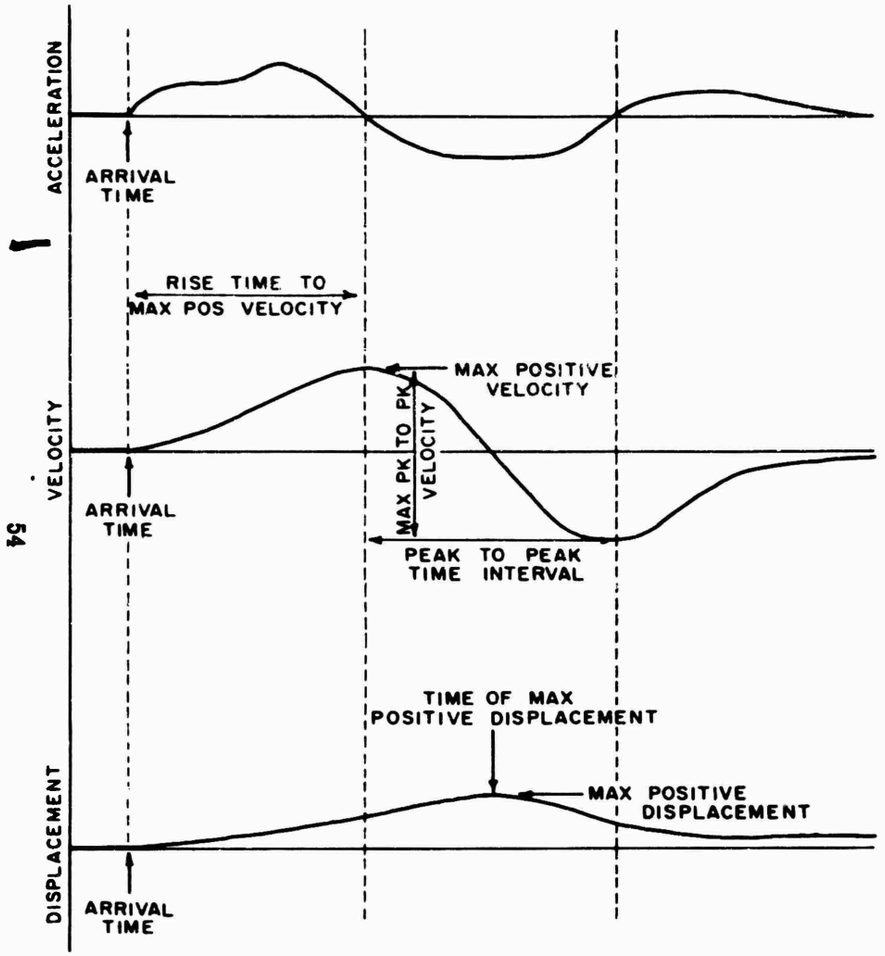

4.2 Diagram of tabulated quantities; velocity and displacement.

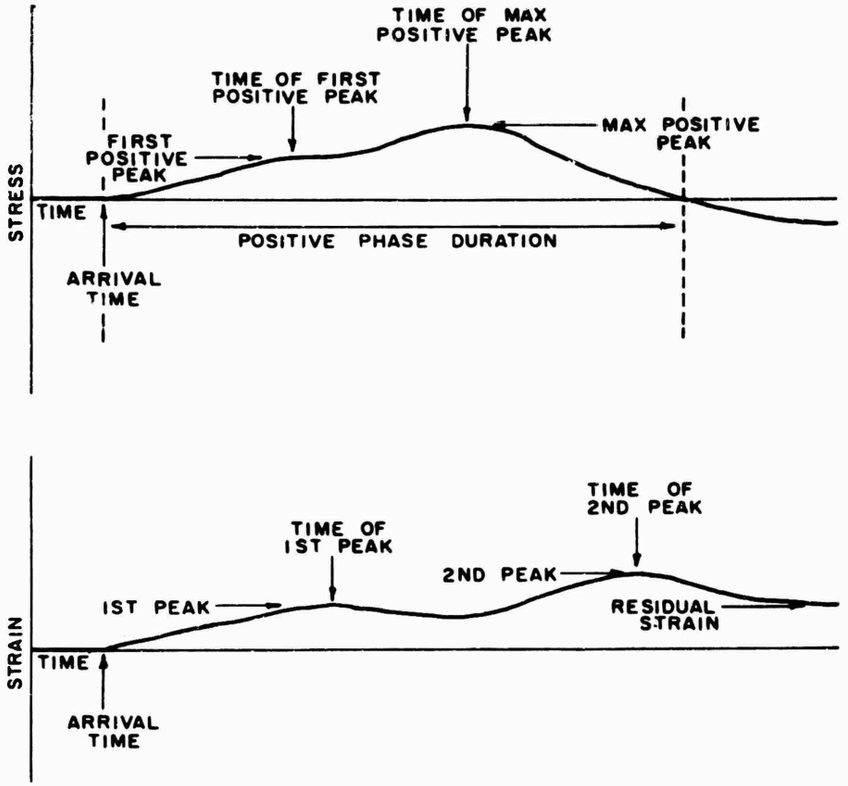

4.3 Diagram of tabulated quantities; stress and strain.

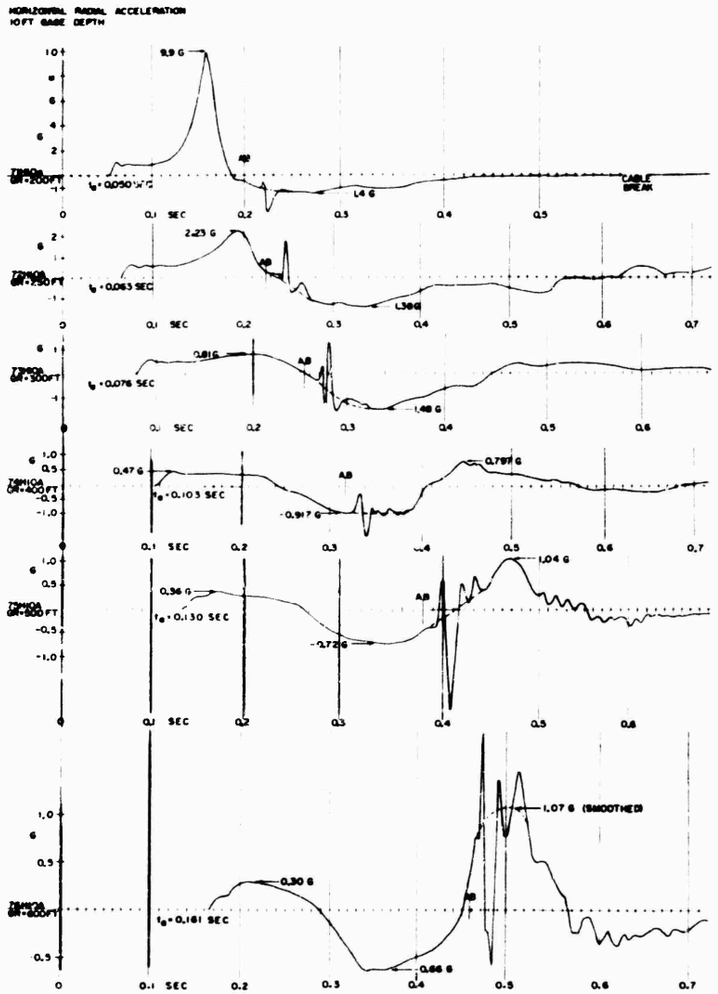

4.4 Gage record tracings, horizontal acceleration 10 feet deep.

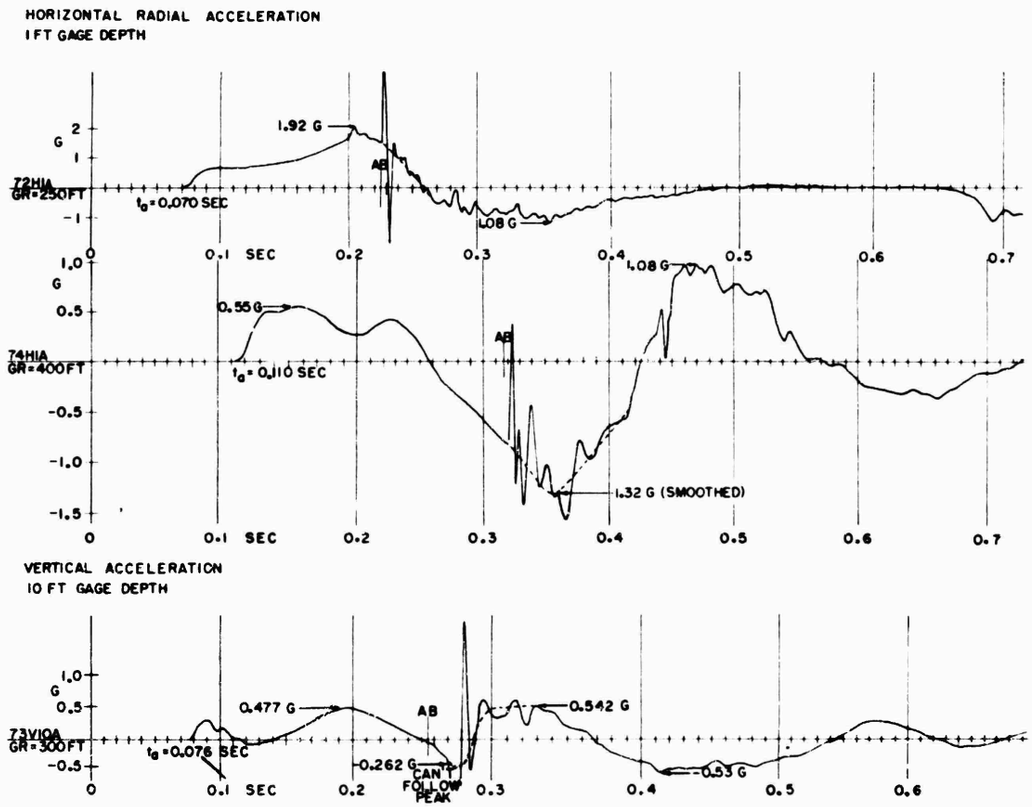

4.5 Gage record tracings, horizontal acceleration 1 foot deep and vertical acceleration 10 feet deep.

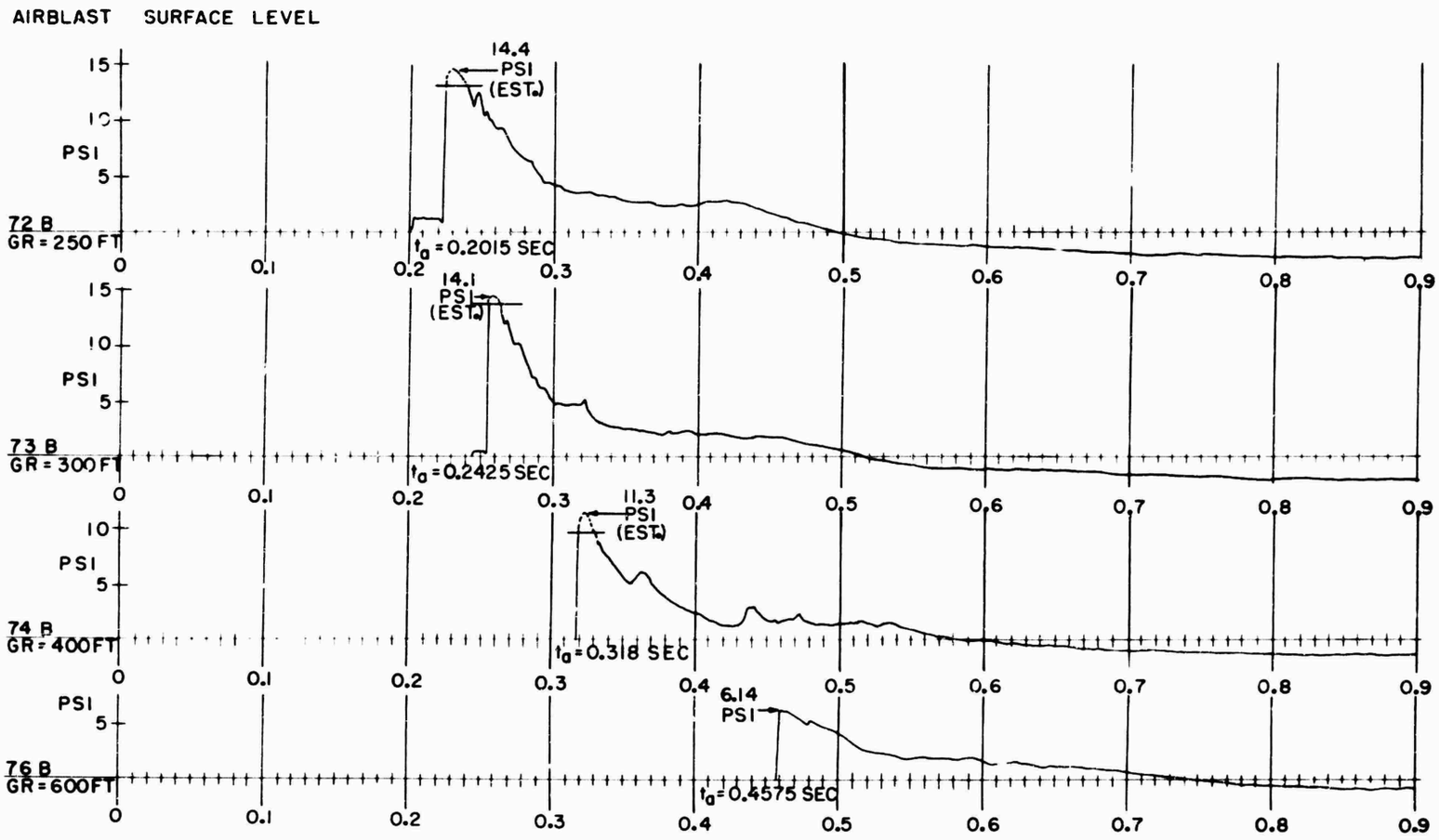

4.6 Gage record tracings, surface level air pressure.

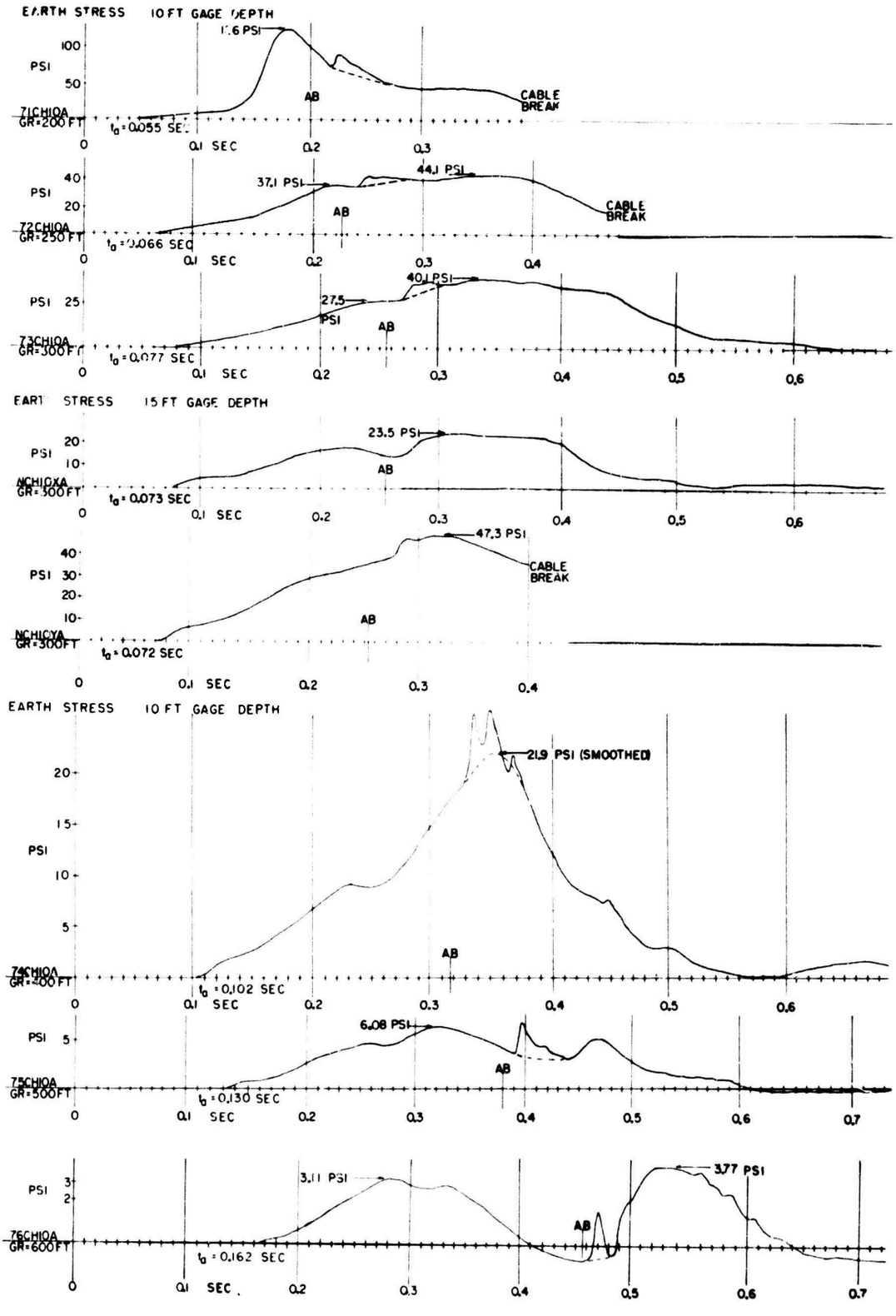

4.7 Gage record tracings, horizontal earth stress 10 feet deep.

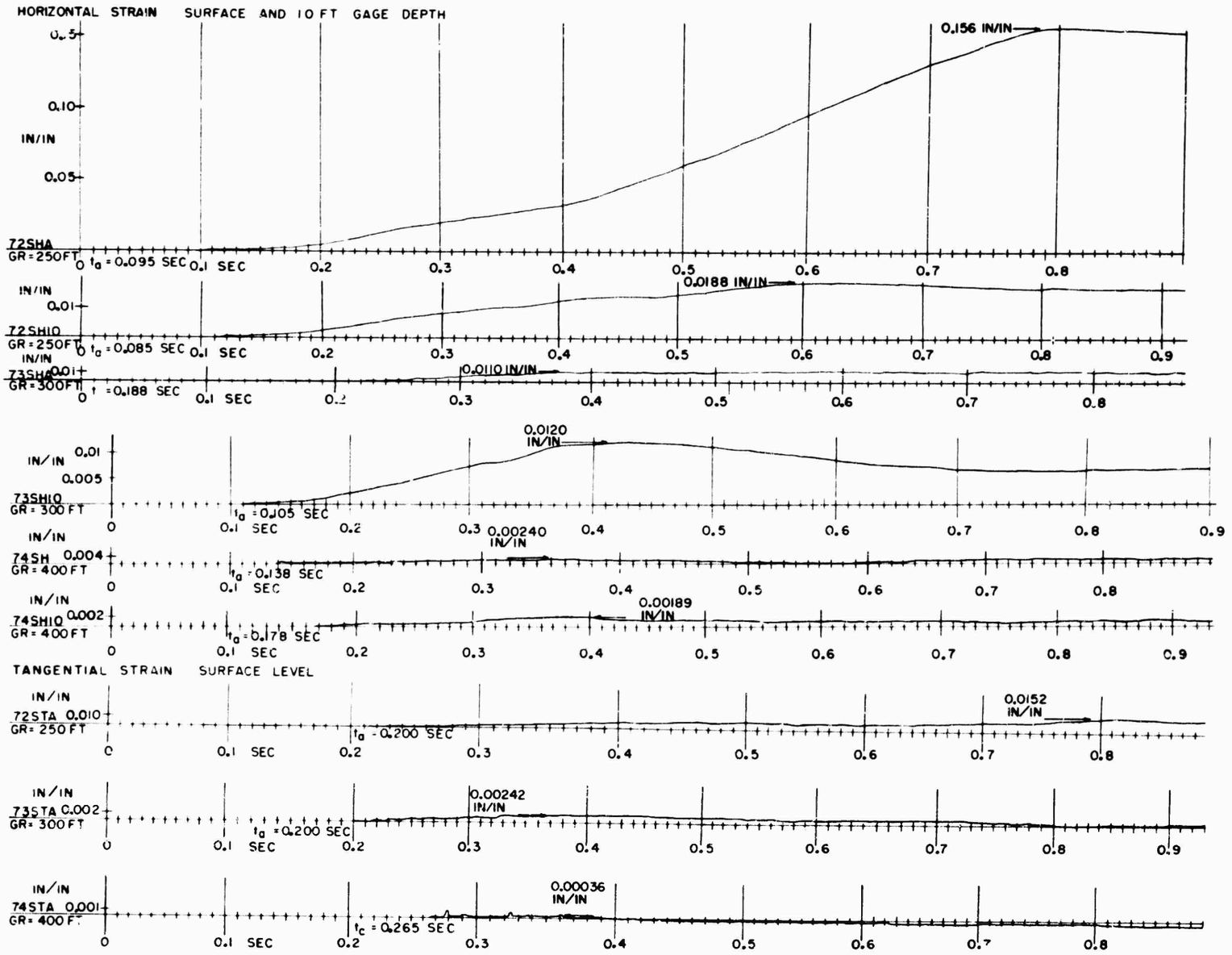

4.8 Gage record tracings, earth strain; surface level (long-span gages) and 10 feet deep (short-span gages).

Chapter 5
DISCUSSION

In this chapter the TEAPOT Shot 7 free-field results are discussed in the following order: (1) earth acceleration and particle velocity, (2) earth stress and strain, (3) earth dynamic and permanent displacement, and (4) airblast. In each case, the TEAPOT data are compared with pretest predictions and the prediction method based upon crater radius is evaluated. Also, where data are available, comparisons are made with results from the JANGLE U and S Shots. Some aspects of seismology and soil mechanics as applied to underground explosion phenomena are presented, and, finally the most significant HE explosion results are summarized.

5.1 EARTH ACCELERATION AND PARTICLE VELOCITY

5.1.1 Earth Acceleration. The TEAPOT Shot 7 peak horizontal acceleration data, excluding the effect of air-blast slap, are summarized in Figure 5.1. The solid curve corresponds to the first positive peak and the dashed curve shows the variation of the first negative peak with ground range. Referring to Table 4.1, it is clear that, at the farthest three stations (400-, 500-, and 600-foot ground ranges), a second positive peak, higher than the first peak, is recorded. The curves of Figure 5.1 indicate that, although at close-in stations the positive horizontal peaks exceed the negative values, the relative magnitudes are reversed beyond 300-foot ground range. The few measurements at 1-foot depth show no consistent behavior; that is, at 250-foot range the shallow-buried gage indicated slightly lower response, whereas at 400 feet the 10-foot depth record shows lower-amplitude accelerations. A possible explanation for this behavior is that the Rayleigh surface waves gain more relative prominence at the larger ground ranges. The single vertical acceleration measurement at 300-foot range yielded peaks which are significantly less than indicated on the horizontal gage at the same ground range.

Also shown on Figure 5.1 (dotted curve) is the prediction curve for acceleration versus ground range based upon the measured 146-foot crater radius (Reference 23). The conclusion is that the early decay (slope) of peak horizontal acceleration follows predictions very well; however, the measured magnitudes are significantly greater than the prediction would indicate. In addition, at the greater ground ranges the measured values fall slightly below predictions.

Reference to the accelerometer record tracings (Figures 4.4 and 4.5) shows that the acceleration wave form is constant as recorded at the various Shot 7 stations. The horizontal acceleration shows a slow rise (100-150 msec) to a positive peak, followed by a negative peak of comparable magnitude. The arrival time of the air-blast pressure (surface gage) at the respective stations is indicated by a symbol "AP" on each record

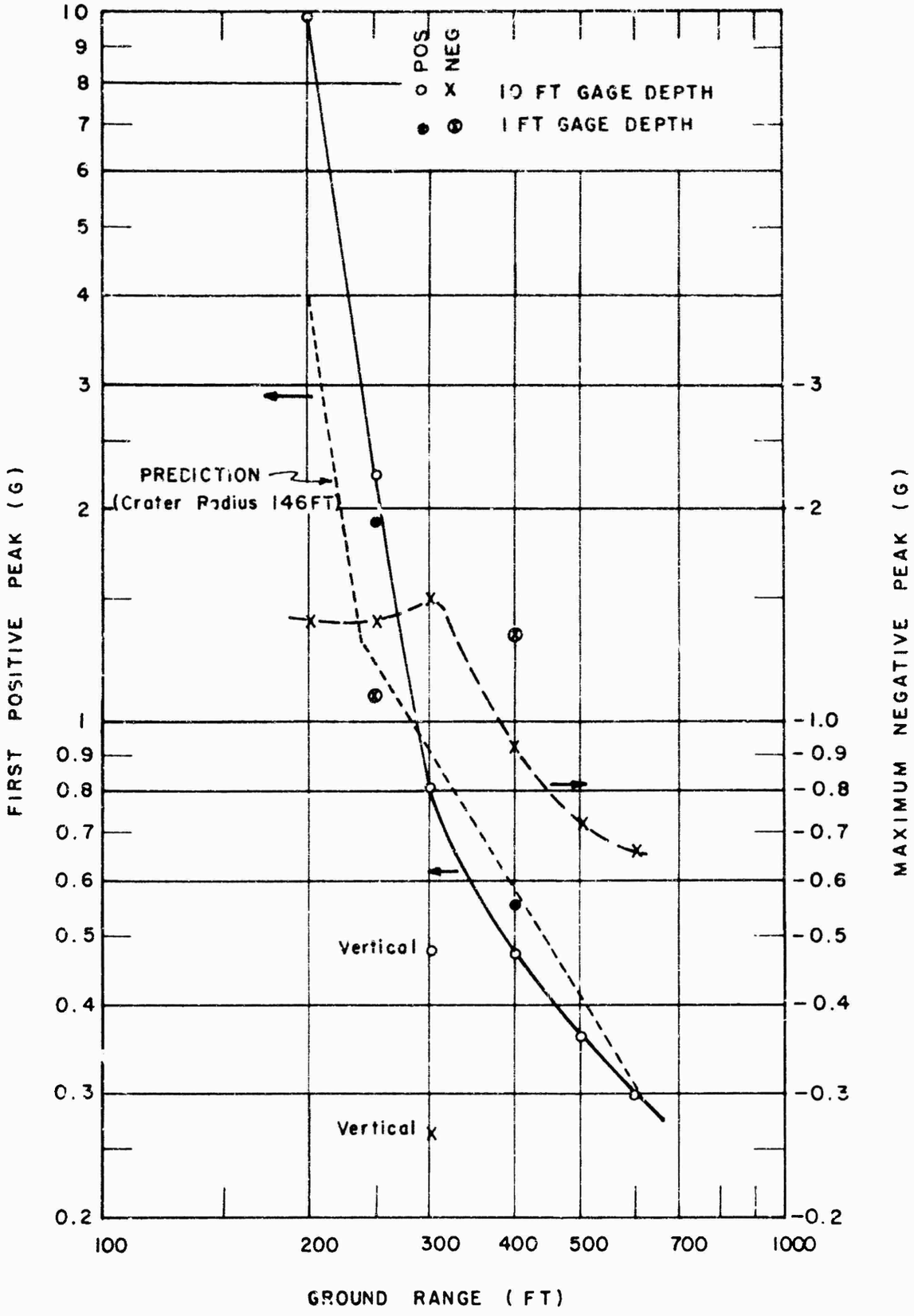

5.1 Maximum earth acceleration, excluding airblast slap, TEAPOT Shot 7, JANGLE U and S.

tracing. It appears that although the characteristic air-blast slap acceleration is in evidence, the record is not seriously disturbed and "recovers" soon after the slap, making it a simple process to separate the air-blast effect.

Figure 5.2 shows some comparisons of horizontal acceleration wave forms from the three pertinent nuclear detonations: TEAPOT Shot 7, JANGLE U, and JANGLE S. The comparisons are made at similar, but not exactly the same, ground ranges. In general, it is obvious that the two JANGLE shots produced results which are characterized by an initial high-frequency disturbance, followed by relatively low-amplitude response. The basic difference between these JANGLE results and TEAPOT Shot 7 is apparently caused by the airblast-induced slap. Specifically, for the JANGLE shots, the air-blast arrival was almost simultaneous with the arrival of the earth disturbance, thereby introducing the high-frequency slap accelerations during the most significant portions of the record. Also, the air-blast pressures were higher (i.e., more energy transferred) at the same ranges for the JANGLE shots. This factor also partly accounts for the close-in acceleration predictions being too low (Figure 5.1); in using JANGLE data for prediction purposes it was necessary to estimate what the peaks would be excluding air-blast effects, because it was thought that airblast effects would be greatly reduced on TEAPOT. However, the effort to edit out the airblast slap acceleration probably contributed greatly to the fact that the predicted values (at close-in ranges) were low. From the comparisons of Figure 5.2, it is apparent that for the surface (JANGLE S) and near-surface (JANGLE U) shots the airblast slap accelerations mask the direct earth-transmitted effects, whereas the deep shot (TEAPOT Shot 7) results are much less disturbed by the slap effect.

The peak horizontal acceleration data (excluding air-blast slap) from the three pertinent Nevada Test Site nuclear shots are presented in Figures 5.3 and 5.4. If the effect of charge depth was manifest in the horizontal acceleration parameter, the peaks would be largest for the deepest shot (TEAPOT Shot 7). Although there is some indication that this is true beyond a ground range of about 500 feet, there appears to be no similar consistency at the closer ranges. Of course, here again, efforts to eliminate the effect of the airblast slap may have introduced some error into the determination of peak values.

Figure 5.5 presents a summary of the peak vertical acceleration data (including air-blast slap) from the JANGLE U and S shots; for comparison, the two data points from TEAPOT Shot 7 are also included. Since the vertical component of acceleration should be more sensitive to airblast-induced effects than is the horizontal component, it would be expected that the peak acceleration would decrease with increased depth of charge. This general behavior is illustrated in Figure 5.5, particularly at close-in ground ranges, where the JANGLE S measured peaks are notably highest. In addition, there is evidence that the negative-going peaks are larger than the positive maxima at the same gage station. This result is consistent with the assumption that the slap acceleration is due to energy transfer from the airblast wave to the ground and that the positive vertical acceleration may be identified with the recovery of the earth from the shock-like compressive forces.

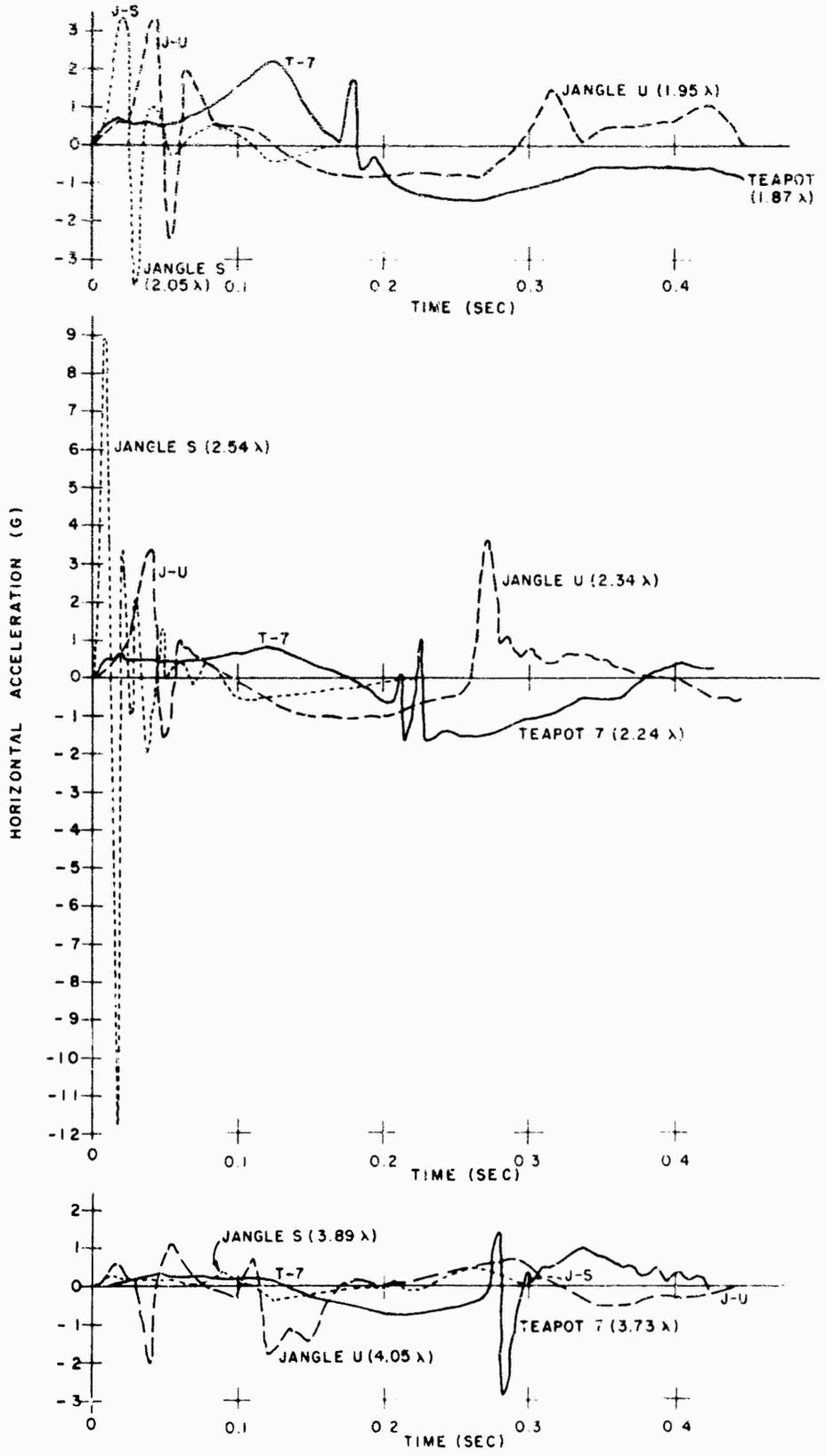

5.2 Wave form comparison, horizontal earth acceleration, excluding airblast slap, TEAPOT Shot 7, JANGLE U and S.

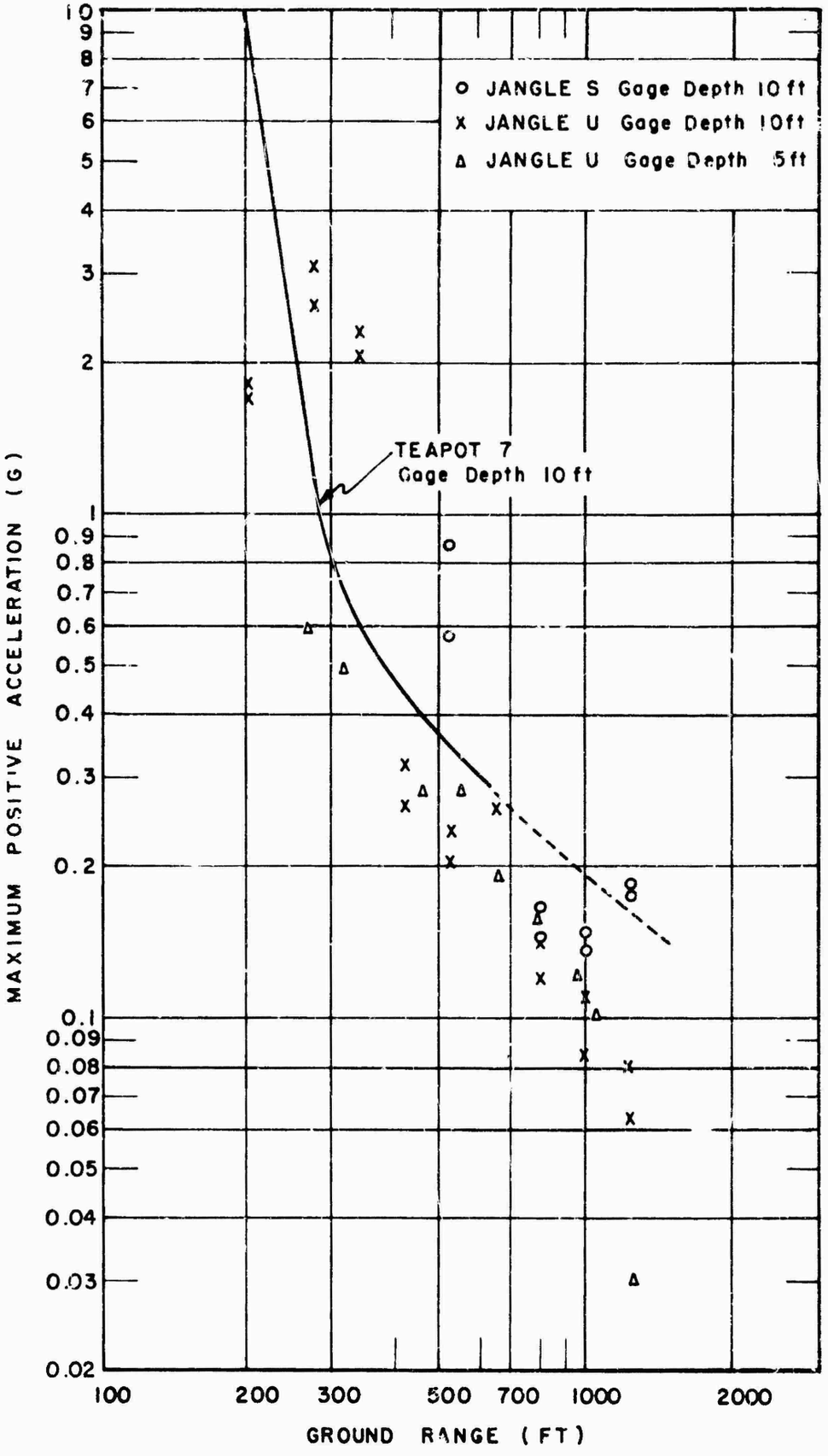

5.3 Maximum outward horizontal earth acceleration, excluding airblast slap, TEAPOT Shot 7, JANGLE U and S.

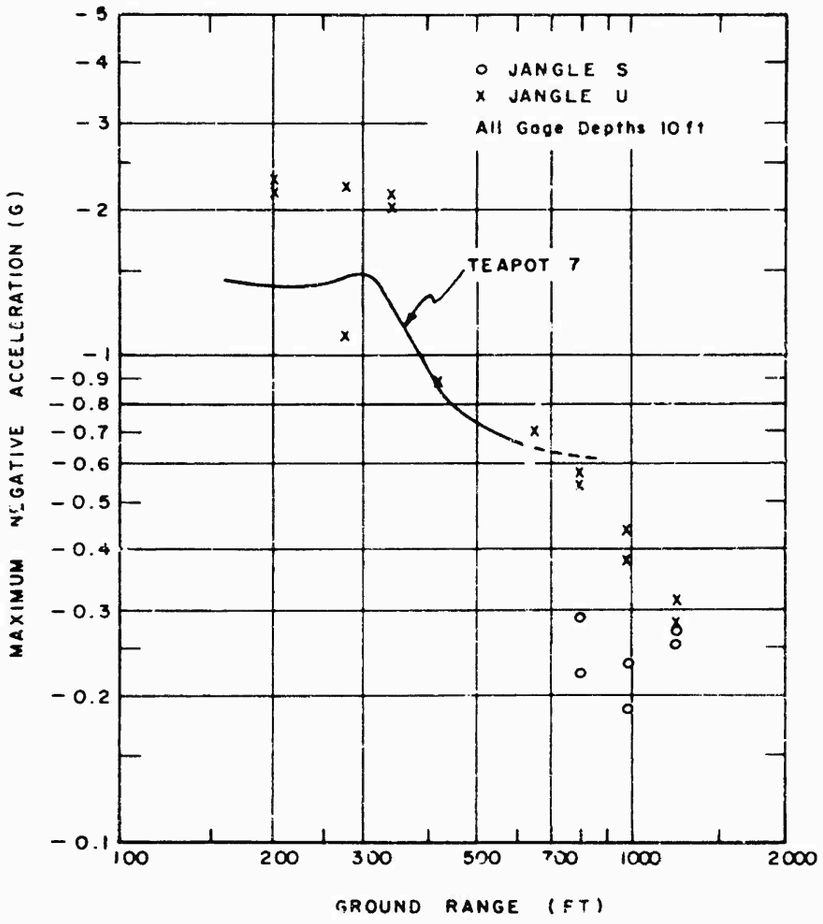

5.4 Maximum inward horizontal earth acceleration, excluding airblast slap, TEAPOT Shot 7, JANGLE U and S.

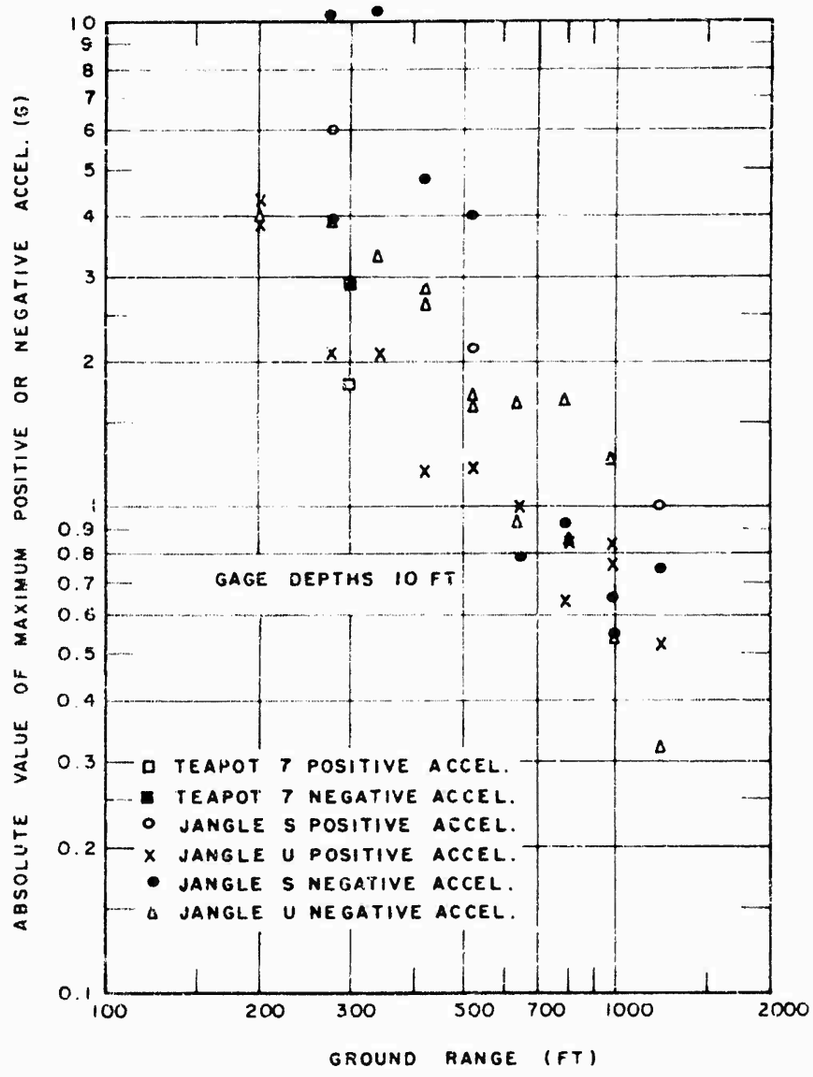

5.5 Maximum vertical earth acceleration, including airblast slap, TEAPOT Shot 7, JANGLE U and S.

A word of caution should be interjected here concerning the use of maximum acceleration data without regard to wave form, i.e., the frequency content. Small charge HE underground work (Reference 9) indicated that peak acceleration is not a reliable parameter and not a good parameter for effects comparisons. This conclusion is based partly upon the wave form comparisons and partly upon the fact that it is not possible to ascertain the effect of high-amplitude, short-duration acceleration peaks upon damage to underground structures. For this reason, the usefulness of the earth acceleration as a damage parameter is limited and more emphasis should be placed upon the earth velocity and displacement data, which are derived from the acceleration by numerical integrations. Nevertheless, it must be noted that, although the acceleration-time data may not lead to good structural damage predictions, this parameter could become important in the problem of damage to components stored inside an underground structure.

5.1.2 Earth Particle Velocity. The TEAPOT Shot 7 peak-to-peak horizontal particle velocity data are presented in Figure 5.6. Because of a cable break, the data obtained at the 200-foot ground range are somewhat uncertain; as shown in Table 4.2, it was possible to determine the maximum positive velocity only, which established a lower limit for the peak-to-peak value. The two 1-foot deep measurements indicate that at the close-in radius (250 feet) the velocity was somewhat less at 1 foot than at 10 feet, i.e., a small velocity gradient between these depths, while at the 400-foot ground range the shallower gage recorded a higher peak-to-peak velocity, which substantiates the previous conclusion that the surface waves assume greater relative importance at the larger ranges. The single peak-to-peak vertical velocity determination at 300 feet is about a third of the corresponding horizontal component.

Also shown on Figure 5.6 (dashed curve) is the curve for peak-to-peak velocity versus ground range based upon the measured 146-foot crater radius. It is concluded that the measured values agree very well with the predicted curve; it is only at the 600-foot range that the divergence is significant. The improved agreement with predictions observed when proceeding from the peak acceleration to the peak velocity parameter may be partly explained by the fact that, upon integration, the high-frequency slap acceleration contributes relatively little to the peak velocity.

Figure 5.7 shows some comparisons of horizontal velocity versus time wave forms from the TEAPOT Shot 7, and JANGLE U and S detonations. There is evidently considerable variation between shots in the duration of the velocity pulse, the deepest shot yielding the longest durations. At the larger range (near 4.0 λ), the wave forms are similar for the three shots.

The maximum peak-to-peak velocity data from the three nuclear shots considered are presented in Figure 5.8, where the curve for TEAPOT Shot 7 is taken from Figure 5.6. Unlike the acceleration case (Figures 5.3 and 5.4), the peak-to-peak velocity parameter exhibits a consistent charge depth effect; in fact, the JANGLE U data, like the TEAPOT data, appear

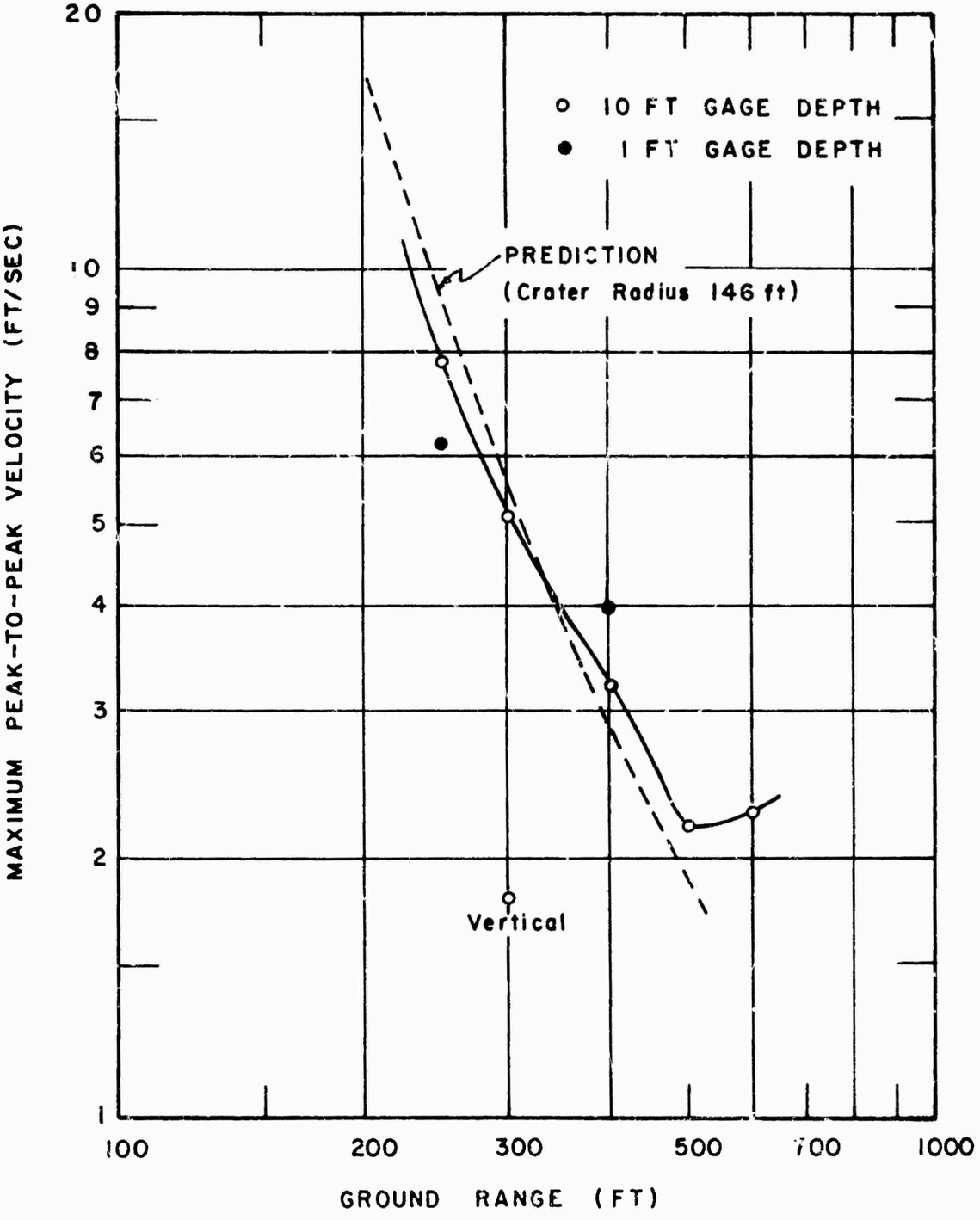

5.6 Maximum horizontal peak-to-peak earth particle velocity, TEAPOT Shot 7.

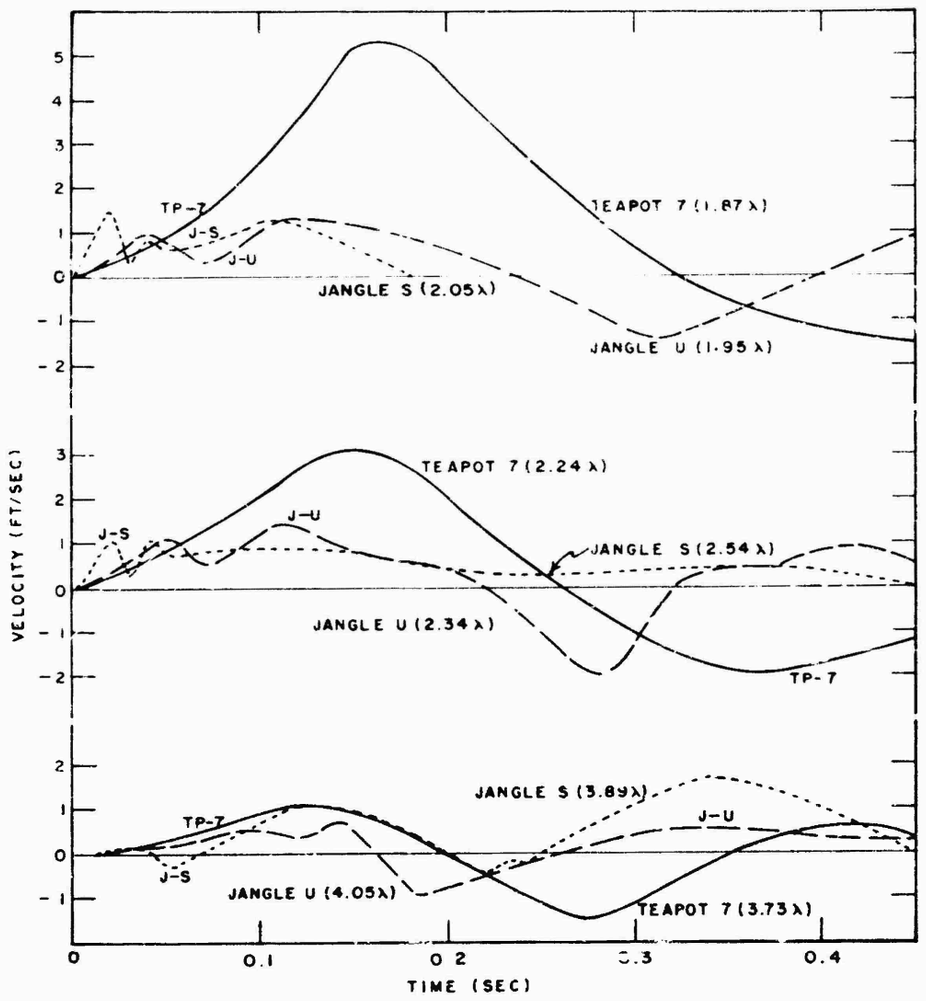

5.7 Wave form comparison, horizontal earth particle velocity, TEAPOT Shot 7, JANGLE U and S.

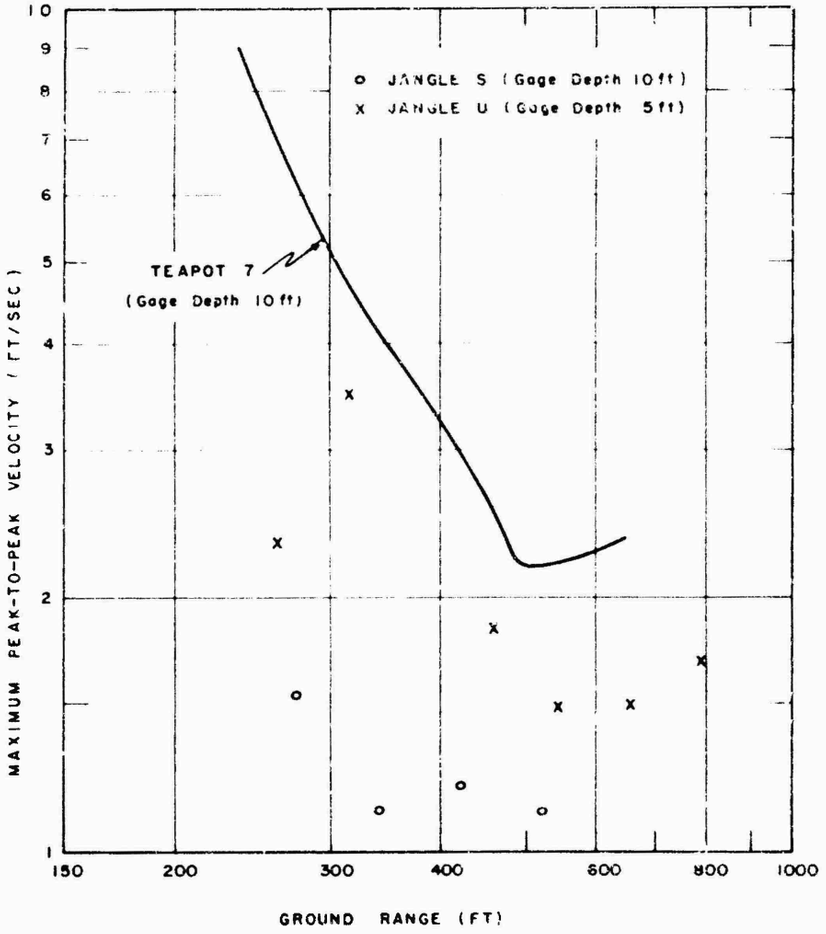

5.8 Maximum horizontal peak-to-peak earth particle velocity, TEAPOT Shot 7, JANGLE U and S.

to level off near 500-foot ground range. At the close-in ranges, the deep shot velocities are about four times larger than those measured on the surface shot.

5.2 EARTH STRESS AND STRAIN

5.2.1 Earth Stress. The results of the TEAPOT Shot 7 horizontal earth stress (Carlson gage) measurements are listed in Table 4.3. Reference to the record tracings in Figure 4.7 shows that the recorded earth stress was little disturbed by airblast-induced effects. The wave forms are similar to the various ground ranges; the only exception being the record at the last gage station (600-foot ground range), which exhibits two separate positive stress peaks at widely different times. This sort of wave form change at large ranges is common on underground measurements from HE explosions (Reference 9). The rise time to peak stress varies from 0.125 to 0.260 second, increasing with ground range.

The maximum values of horizontal earth stress are plotted against ground range in Figure 5.9. The data obtained at 300- and 400-foot stations tend to give the curve a pronounced hump in this region. A similar hump in the stress-distance curve is not uncommon in underground HE work, (Reference 9) and is usually ascribed to variations in subsurface soil characteristics. Also included on Figure 5.9 is the preshot prediction curve based upon a crater radius of 146 feet. It is evident that the results agree with prediction only at ground ranges of 500 and 600 feet; however, at close-in ranges the measured values are much larger than would be predicted. The preshot prediction of peak horizontal earth stress was made rather tenuous by the fact that no data were available on this parameter from the other nuclear detonations in Nevada (U and S). Therefore, it was necessary to base the predictions upon small-charge HE data. It becomes obvious that, considering earth stress from underground nuclear detonations, this procedure yields values which are too low.

Whitman (Reference 15), in his discussion of the reliability of the Carlson-Wiancko gage as a true stress detector, uses an interesting example. He first computes the static overburden pressure of the soil above the gage. Second, from the data on permanent horizontal and vertical displacement, he finds the radius at which these displacements are zero or very small. Third, from the stress records, he finds the radius at which peak recorded stress corresponds approximately to the calculated static overburden pressure. Then, if the two radii (that where peak stress corresponds to static pressure and that where displacement is small) agree, the stress gage is probably measuring true earth stress. For small-charge HE underground explosions in Nevada the agreement is good at 2.0 to 2.5 crater radii. For TEAPOT Shot 7, a similar analysis is possible: In Section 5.5 it is shown that the permanent horizontal and vertical displacements approach zero at ground ranges of 300 to 350 feet, that is, at approximately 2.0 to 2.3 crater radii. Reference to Figure 5.9 shows that at these ranges the peak horizontal earth stress is 33 to 40 psi, whereas the static overburden pressure for a 10-foot deep gage in Nevada soil is about 42 psi. This good agreement

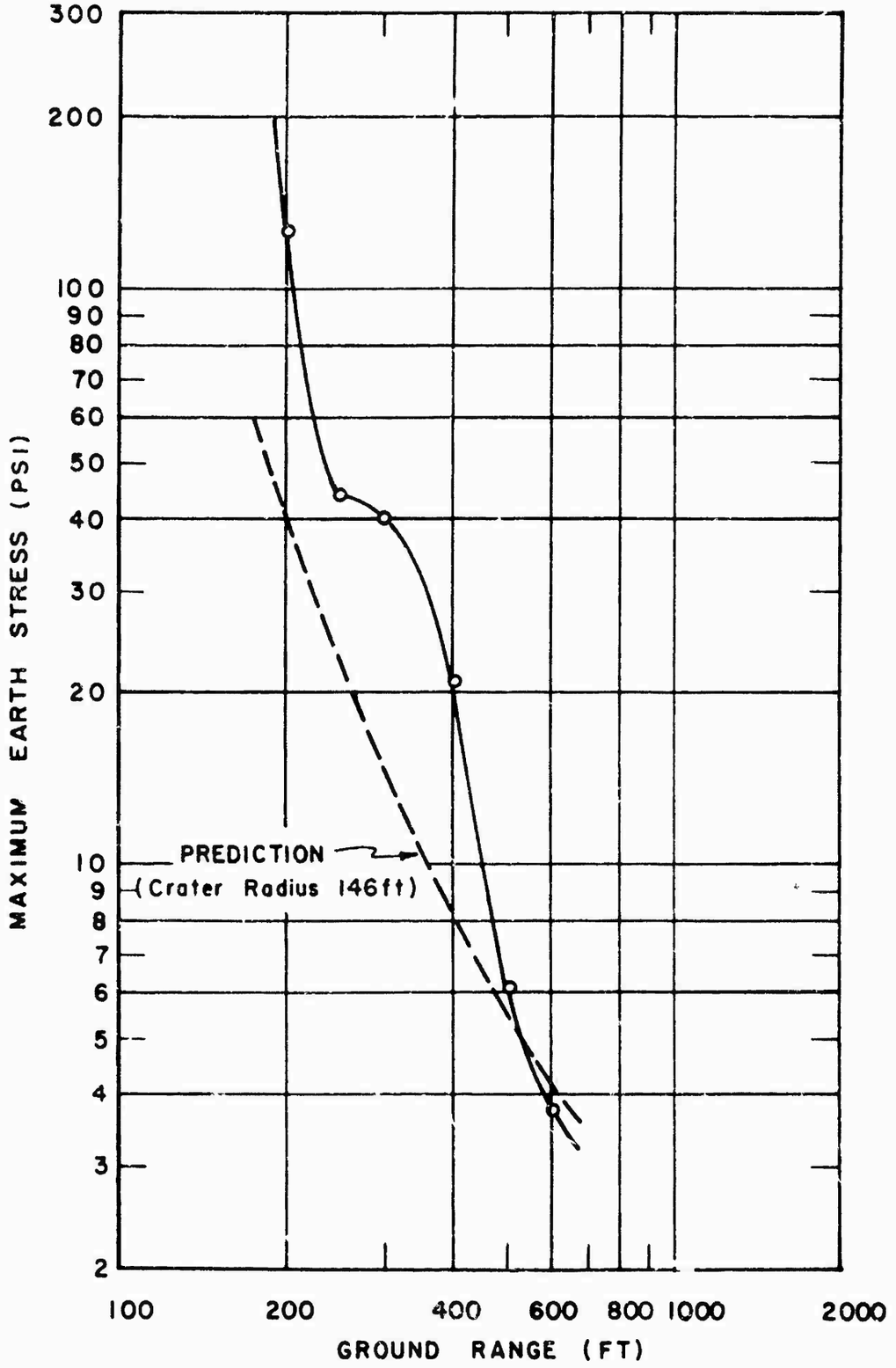

5.9 Maximum horizontal earth stress, TEAPOT Shot 7.

lends some confidence to the method of measuring earth stress using Carlson-Wiancko gages.

5.2.2 Earth Strain. The results of the Shot 7 horizontal radial earth strain measurements are listed in Table 4.4 and illustrated in Figure 5.10. The strain is presented in units of parts per thousand (ppk). In the figure, two curves are shown; one for surface measurements using long-span strain gages and the other corresponding to the 10-foot depth data obtained with the short-span gages. At ground ranges of 300 and 400 feet, the two measurements are practically identical, but at a range of 250 feet the strain recorded at the surface is markedly larger than the underground strain. Although little previous data were available, it had been expected that the subsurface strains would be consistently less than those at the surface, i.e., negative strain gradient with depth. Nevertheless, the data indicate that this behavior is confined to relatively close-in ground ranges for TEAPOT Shot 7.

The values of postshot residual strain are also listed in Table 4.4. It is evident from these data that the surface strains are more permanent than those at 10-foot depths; that is, the residual horizontal strain at the surface is approximately equal to the maximum value. Therefore, although the measured maximum strains are very similar for the two depths at 300 and 400 feet, the 10-foot deep strains appear to recover better following the passage of the disturbance.

Table 4.4 also lists the maximum values of the observed surface level tangential strain. From these data, assuming a uniform symmetrically expanding medium, it is possible to compute, at the surface, peak horizontal displacement values. In fact, displacement is the product of the tangential strain and the radius. Figure 5.11 shows these values plotted against ground range, indicating severe attenuation with increased range. Also shown on the figure is the peak displacement curve from 10-foot deep accelerometers (Table 4.2). As was the case for horizontal strain, it is evident that the vertical gradient is appreciable near the crater, but practically disappears at two or more crater radii.

5.3 DYNAMIC AND PERMANENT EARTH DISPLACEMENT

5.3.1 Dynamic Earth Displacement. Dynamic earth displacement may be obtained by double integration of acceleration-time records. This method is admittedly subject to some unavoidable errors, the magnitude of which can only be estimated.

Some wave forms for horizontal displacement versus time obtained from the TEAPOT Shot 7 and JANGLE U measurements are presented in Figure 5.12. In each case the records rise slowly to a broad maximum, followed by a long decay; it appears that the TEAPOT records achieve maximum value later in time. The displacement-time wave form comparisons indicate that the first maximum is probably the only meaningful comparison parameter.

The peak horizontal displacement data from the three nuclear detonations of interest are summarized in Figure 5.13. From the figure, it can

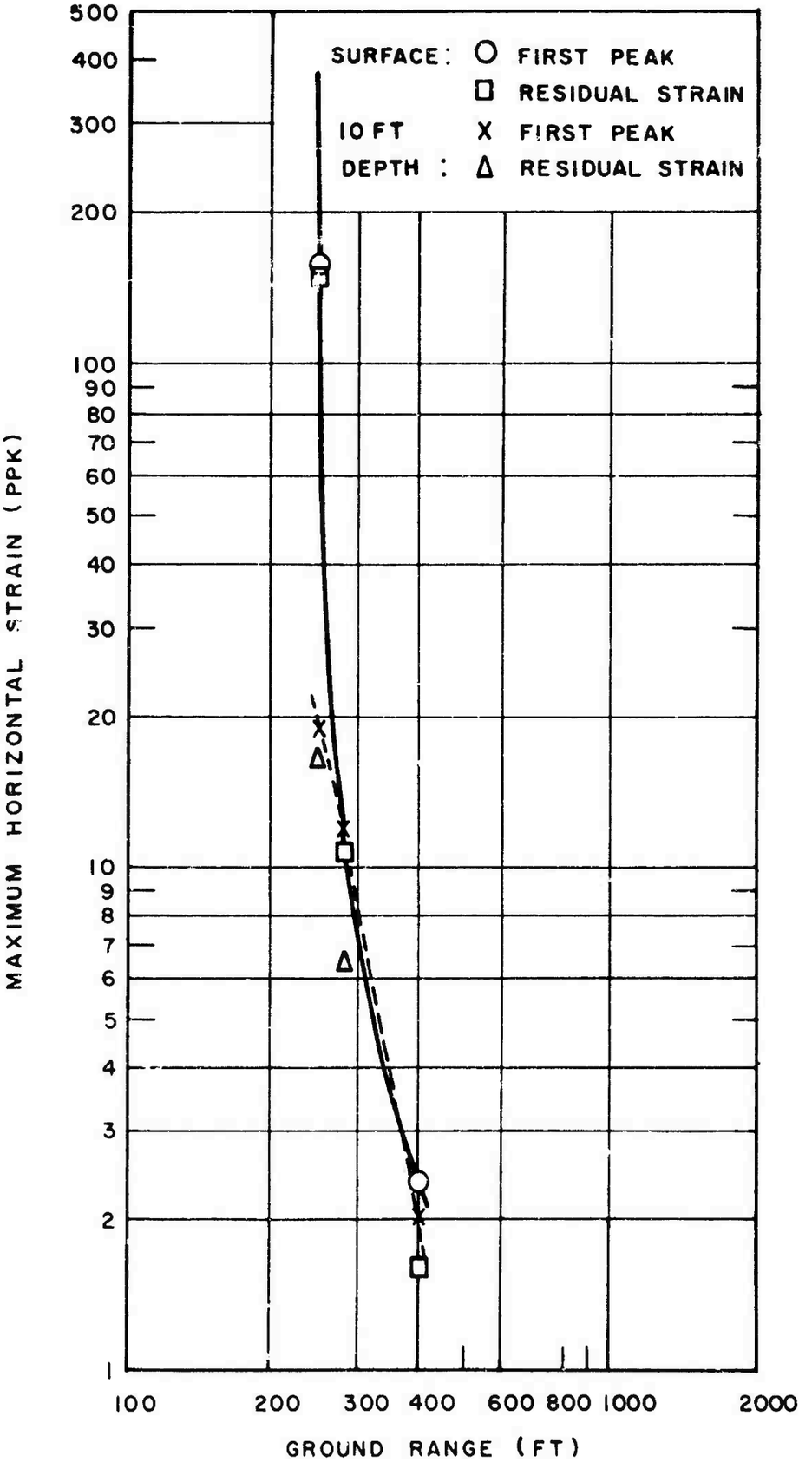

5.10 Maximum horizontal earth strain, TEAPOT Shot 7.

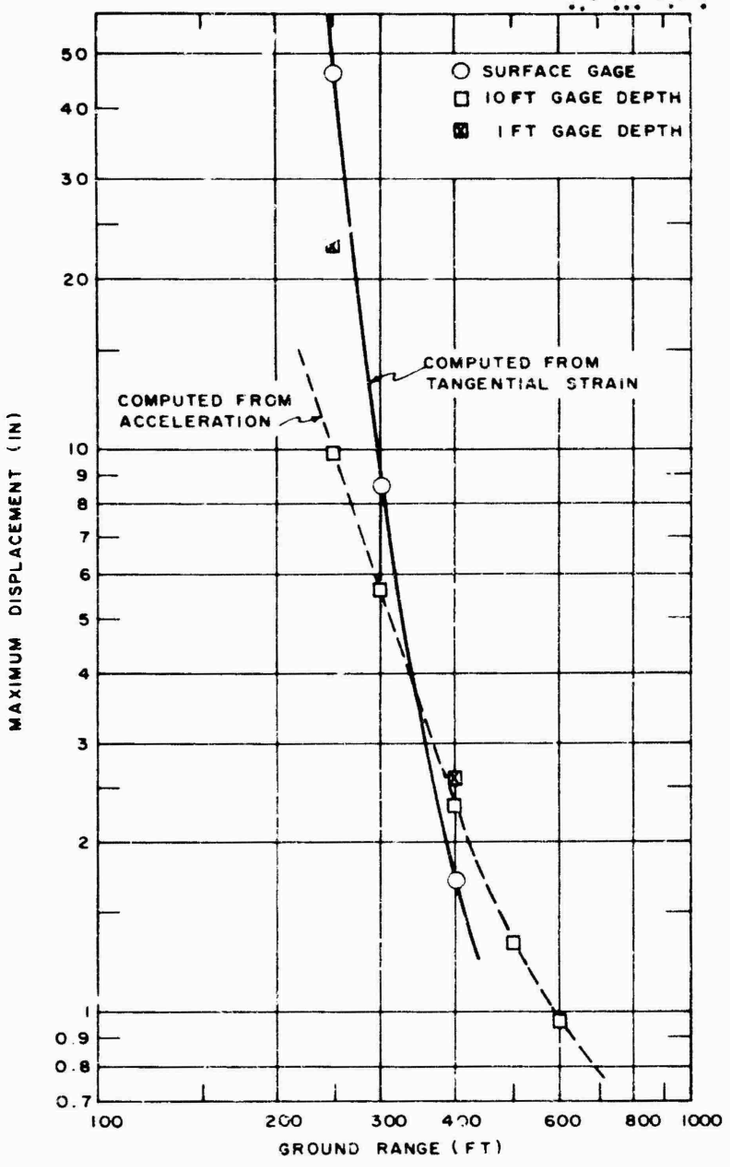

5.11 Maximum horizontal earth particle displacement, computed from tangential strain and from double integration of acceleration, TEAPOT Shot 7.

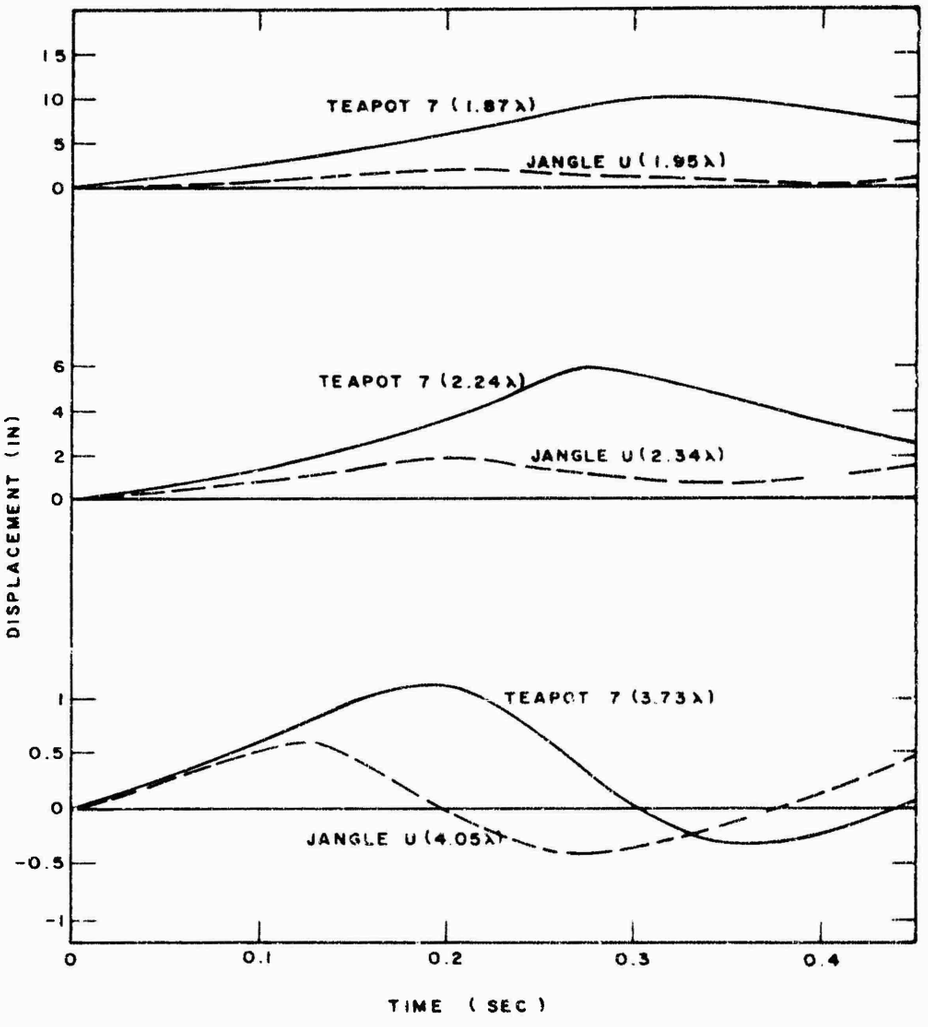

5.12 Wave form comparison, horizontal earth particle displacement, TEAPOT Shot 7 and JANGLE U.

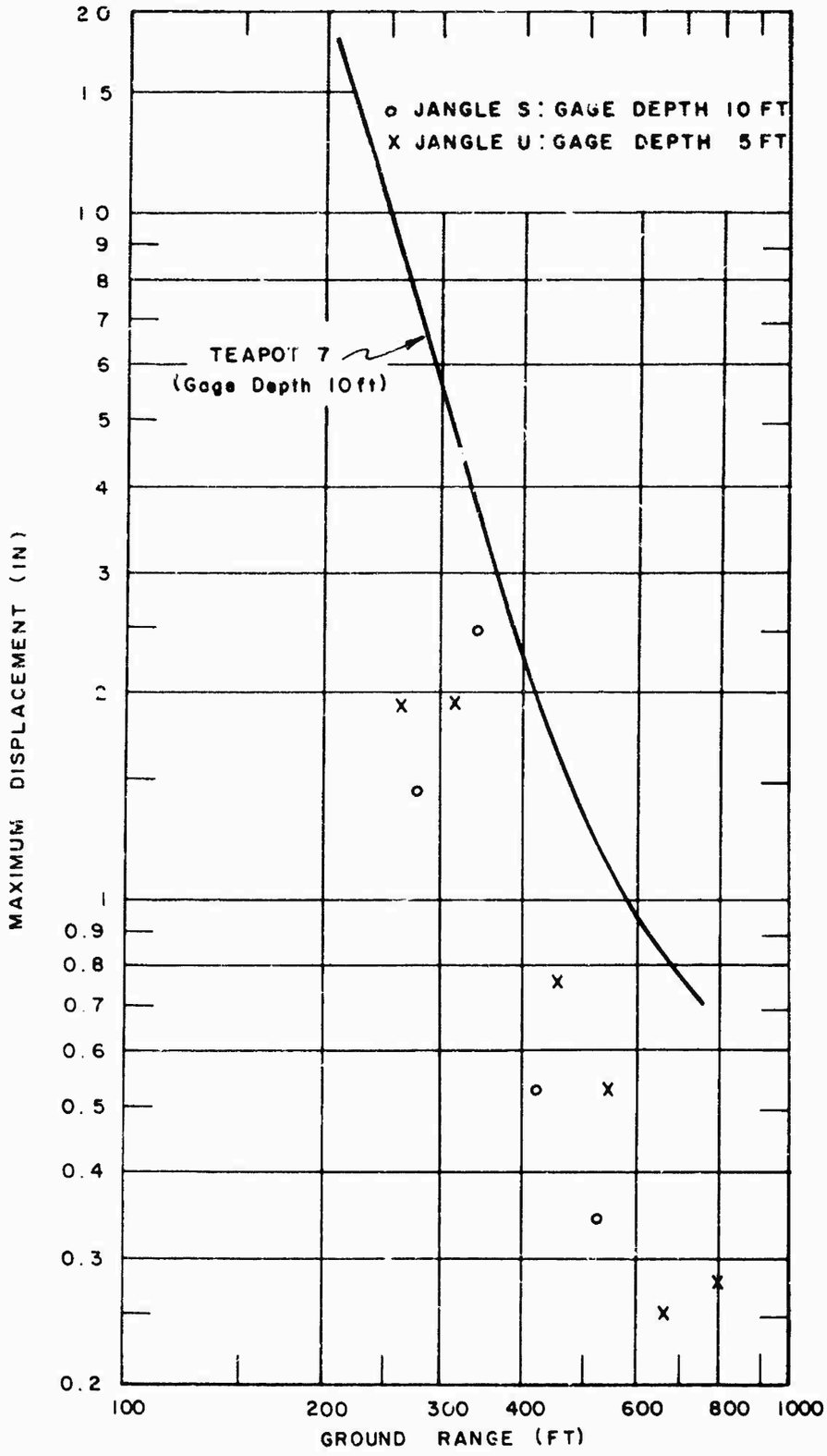

5.13 Maximum horizontal earth particle displacement, TEAPOT Shot 7, JANGLE U and S.

be said that the TEAPOT shot yielded significantly higher displacements than did the JANGLE shots; however, there appears to be no real difference between the available U and S data, which is inconsistent with a charge depth effect. It should be noted that the U and S gages were at different depths; nevertheless, the shallower gage burial on the U shot would tend to favor higher displacements, which were not observed.

In an effort to check the internal consistency of this strain measurement plan, the slope of the surface displacement-vs-ground range was calculated for a number of ranges using the tangential strain data, which produced the horizontal strain-distance curve of Figure 5.14. When this curve is compared with the observed values of horizontal strain (Figure 5.10), the closeness of the comparison is striking, which results in some degree of confidence in the observations. It is recognized that the above procedure is approximate to the extent that displacement peaks do not occur simultaneously, but the broad peaks encountered make this correction negligible.

Using the data available from Shot 7, it is possible to make one additional interesting comparison. In Figure 5.15 a comparison is made between the surface horizontal displacement versus time (computed from the tangential strain data) and the 1-foot depth displacement obtained from the results of integrated acceleration-vs-time. It is probably not wise to generalize extensively from such meager data; however, Figure 5.15 indicates that, within the reliability of the measurements, the horizontal displacement of the surface at 250-foot ground range on Shot 7 is significantly higher than that at 1-foot depth. Also, at the 400-foot range, the behavior appears to be reversed, which is consistent with the comparisons between the surface and 10-foot deep displacements.

5.3.2 Permanent Earth Displacements. The vertical and horizontal components of permanent displacement for TEAPOT Shot 7 were determined from pre- and post-shot survey data on the location of concrete monuments set in the ground. Since these monuments are only 3 feet long, the measured displacements are characteristic of the motion of a near-surface earth layer.

The permanent earth displacement data from Shot 7 are summarized in Table 4.5. The horizontal displacements as measured along the four radial lines are shown in Figure 5.16. It is obvious that the displacements along the S52°W line are significantly larger than indicated on the other lines. Figure 5.17 shows a similar plot for the vertical displacements; in this case, there appears to be an anomaly in the data at 250-foot ground range.

A more graphic presentation of the permanent displacement data is included in Figures 5.18 and 5.19. These figures show the contours of equal displacement surrounding the Shot 7 ground zero point. Referring to the horizontal displacement contours (Figure 5.18), it is obvious that the pattern is asymmetrical, indicating a bulge in the southwest direction. Since the JANGLE U shot crater is northeast of the Shot 7 ground zero, its proximity cannot be the explanation for the aforesaid asymmetry. The

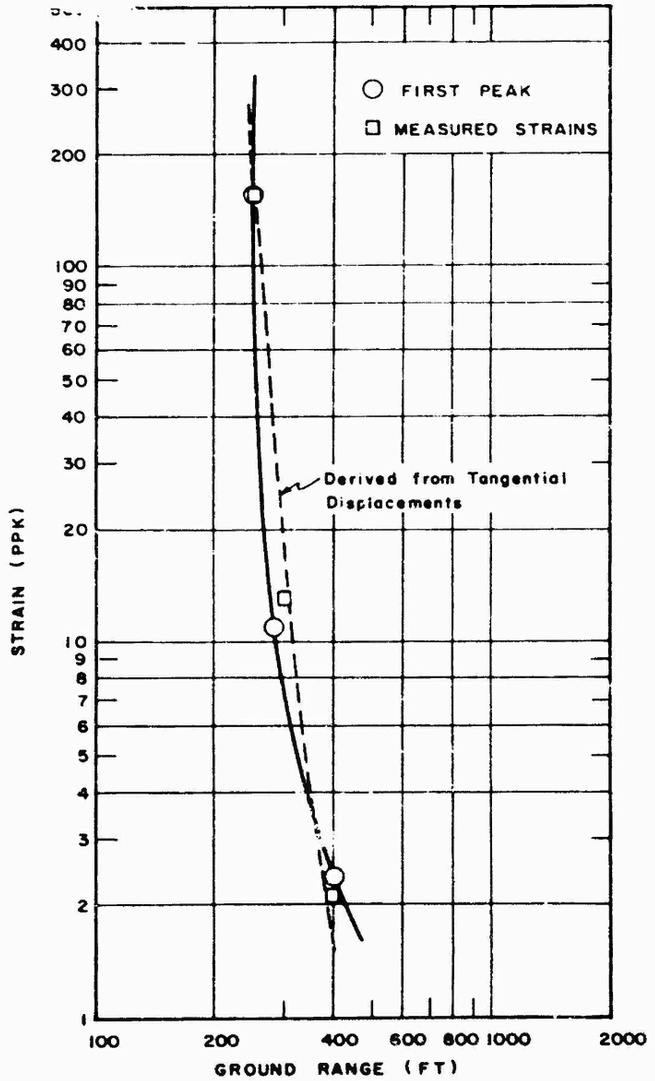

5.14 Maximum horisontal earth strain, compared to strain computed from tangential strain.

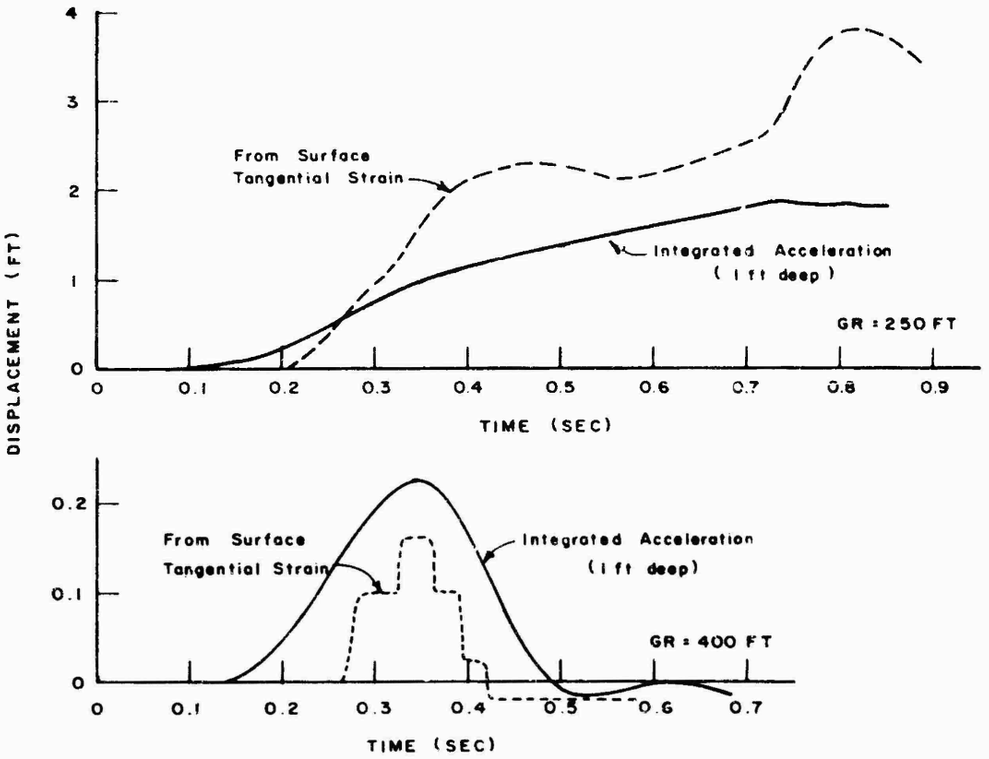

5.15 Horisontal earth displacement vs time, computed from tangential strain and from double integration of acceleration.

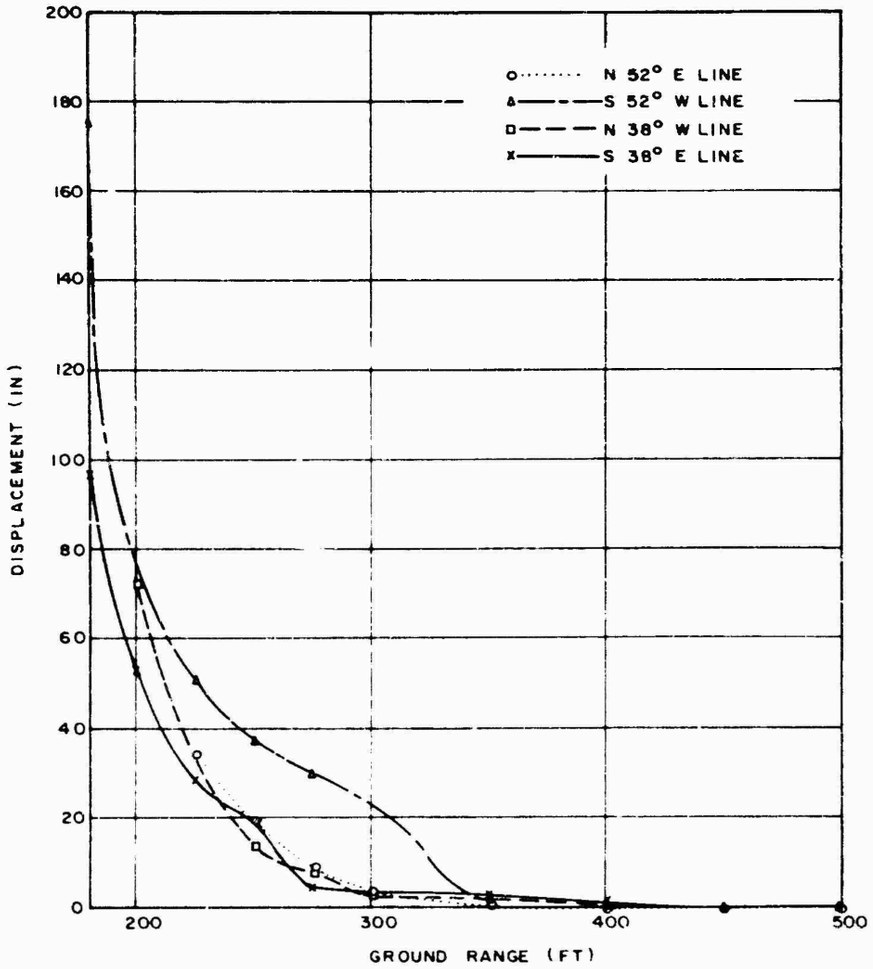

5.16 Permanent horizontal earth displacement, TEAPOT Shot 7.

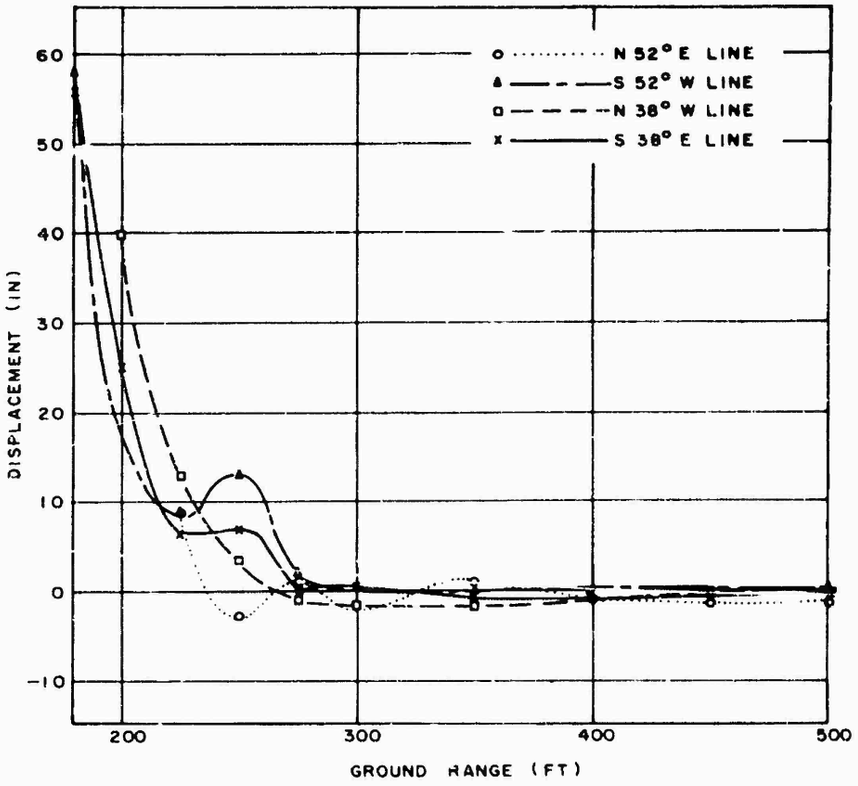

5.17 Permanent vertical earth displacement, TEAPOT Shot 7.

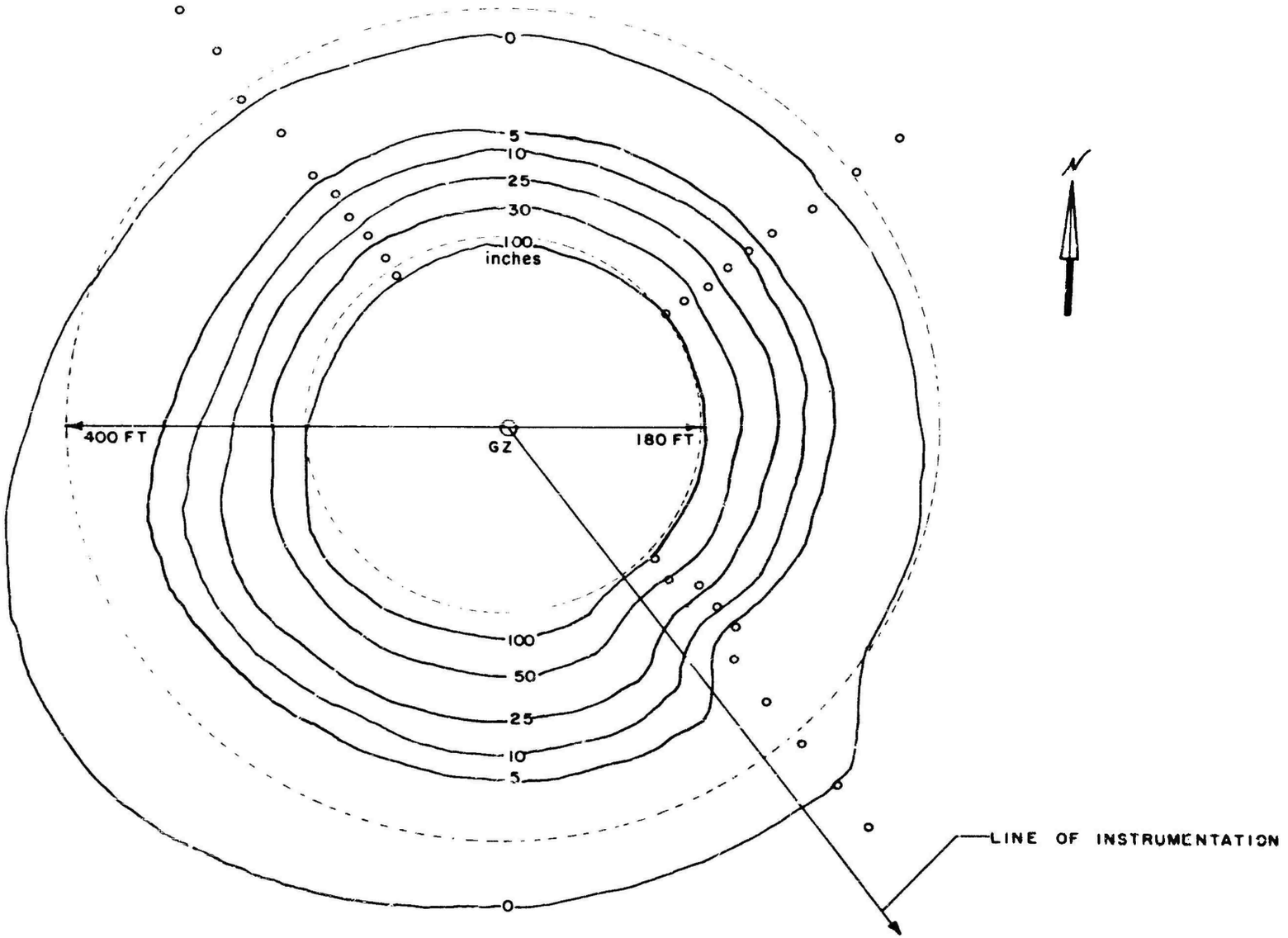

5.18 Contour map of permanent horizontal earth displacement, TEAPOT Shot 7.

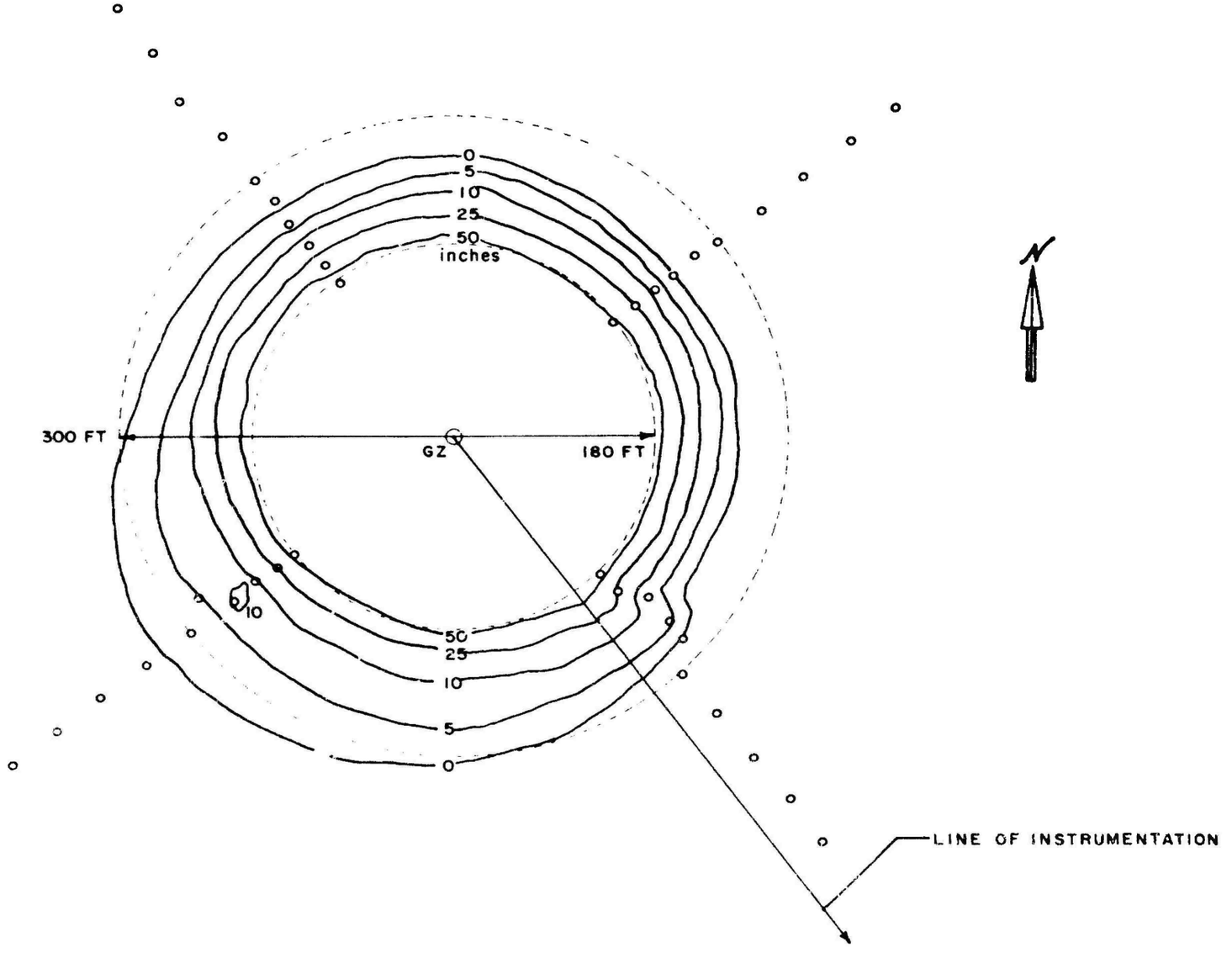

5.19 Contour map of permanent vertical earth displacement, TEAPOT Shot 7.

instrumentation line is indicated on the figure. Figure 5.19, showing the Shot 7 vertical displacement contours, illustrates the fact that the vertical component of displacement was much smaller than the horizontal. Also, the same general type of asymmetry appears to be characteristic of both components. Finally, it should be mentioned that many of the monuments beyond 300-foot ground range indicated negative (away from the ground surface) vertical displacements; this seems to indicate that, beyond a certain range, the airblast slap has more influence on near surface vertical displacements than do the directly transmitted earth waves.

5.4 AIR-BLAST PHENOMENA

The record tracings in Figure 4.6 show the wave form of the air-blast pressure versus time measurements obtained on Shot 7. In addition to the classical airblast wave form, which is characterized by a sharp increase in pressure to a peak value followed by a logarithmic decay, there was observed on the 250-foot and 300-foot records a preshock disturbance commonly referred to as the "front porch." An explanation can be advanced to identify the possible mechanisms leading to this shock wave shape.

Briefly, it is assumed that immediately following an underground detonation, the earth first rises relatively slowly but steadily. This fact is supported by measurements taken from high-speed motion pictures. The resultant air shock from this "earth piston" should thus be of small but relatively constant amplitude. However, the explosion gases soon pierce the curtain of rising earth. Since the velocity of the gas jet is considerably greater than that of the rising earth, the air shock resulting from this "gas jet piston" is stronger than that from the earth rise. Moreover, the jet decelerates much faster than the earth, so the air-blast pressure decays from the peak much more rapidly than does the pressure from the earth rise alone. Also, the jet shock, by virtue of its higher pressure level, travels faster than the relatively low-pressure earth rise (front porch) disturbance. Hence, the jet shock starts late, but eventually overtakes the earth piston shock and merges to produce a single shock.

This explanation also accounts for the absence of a front porch pressure on air pressure records from shallow buried charges; that is, for shallow burial, the time interval between earth rise and jet break-through is so short that the jet shock overtakes the earth rise effect before the wave reaches the closest air-blast pressure gage.

Brode (Reference 24) in his theoretical paper on strong-shock spherical blast waves, derives some relations for the pressure decay behind a spherical shock moving through an ideal gas medium. He finds that the decay is, in general, not a simple exponential, since the early portion of the pressure-time function decays more rapidly than do the later parts. It should be noted that this method of computation is strictly limited to the case of free-air wave propagation. Thus, any application to shock phenomena which are influenced by energy transfer from one medium into

another (underground detonations) necessarily involves approximations of unknown magnitude. Nevertheless, it seems worthwhile to make some comparisons between free-air theory and experimental underground-explosion airblast data.

Figure 5.20 presents the comparisons between the Shot 7 measured and theoretical air-blast pressure-time wave forms. It is obvious from this figure that the recorded pressure consistently decays more abruptly than would be predicted on the basis of free-air point source theory. Also, the general form is nonclassical in appearance; specifically, the records exhibit, after the abrupt decay, a long-duration pressure plateau before the negative phase develops. In fact, if the initial decay were extrapolated to zero pressure, the indicated positive-phase duration would be about one-half the duration actually observed. This nonclassic characteristic is possible due to the effect of the "extended" source (i.e., jet of expanding gases) identified with underground detonations.

Similar wave-form comparisons are made in Figure 5.21, using data from the JANGLE U (shallow) underground shot. In this case, the agreement between point source theory and experimental data is quite good, although the close-in pressure record (300-foot ground range) shows a tendency toward the pressure plateau which is characteristic of the TEAPOT results (Figure 5.20). The foregoing discussion indicates that the deviations of airblast pressure wave forms from classical form are more pronounced the deeper the charge is buried.

The airblast maximum pressures observed during Shot 7 were greater than expected, as is shown in Figure 5.22, where the peak observed airblast pressures are compared with the predictions based on small-charge HE data (Reference 9) and with the results from JANGLE U. It is obvious that the peak pressures are higher than were predicted, about one-half those of JANGLE U (also included on Figure 5.22). The rapid change in slope of the pressure-distance curve near 300 feet is not unexpected; similar results have been observed on HE shots, in that pressures close to the crater lip on deep shots are sometimes less than or no greater than the pressures at larger distances. However, it should be noted that the predominant decay of peak pressure versus distance is similar for the three nuclear shots and unlike the HE data behavior. It is also evident that the peak pressure exhibits a definite charge depth effect. Although data from the two JANGLE shots are comparable, the TEAPOT values are significantly lower. In addition, if S data were available at close-in ranges, they would probably deviate markedly from the U pressures.

Air-blast gage records at 250- and 300-foot ground range showed the predicted small front porch with a magnitude of about 5 percent of the maximum. Naturally, this was soon overtaken by the main shock wave, and the more remote gages (400 and 600 feet) show only a single shock (see Figure 4.6). Consideration of the arrival time data reveals that the front porch travels at approximately 1,160 ft/sec and is overtaken at about 350 feet by the main shock, which at that range has a velocity of approximately 1,550 ft/sec, later decreasing to 1,320 ft/sec at 600-foot ground range.

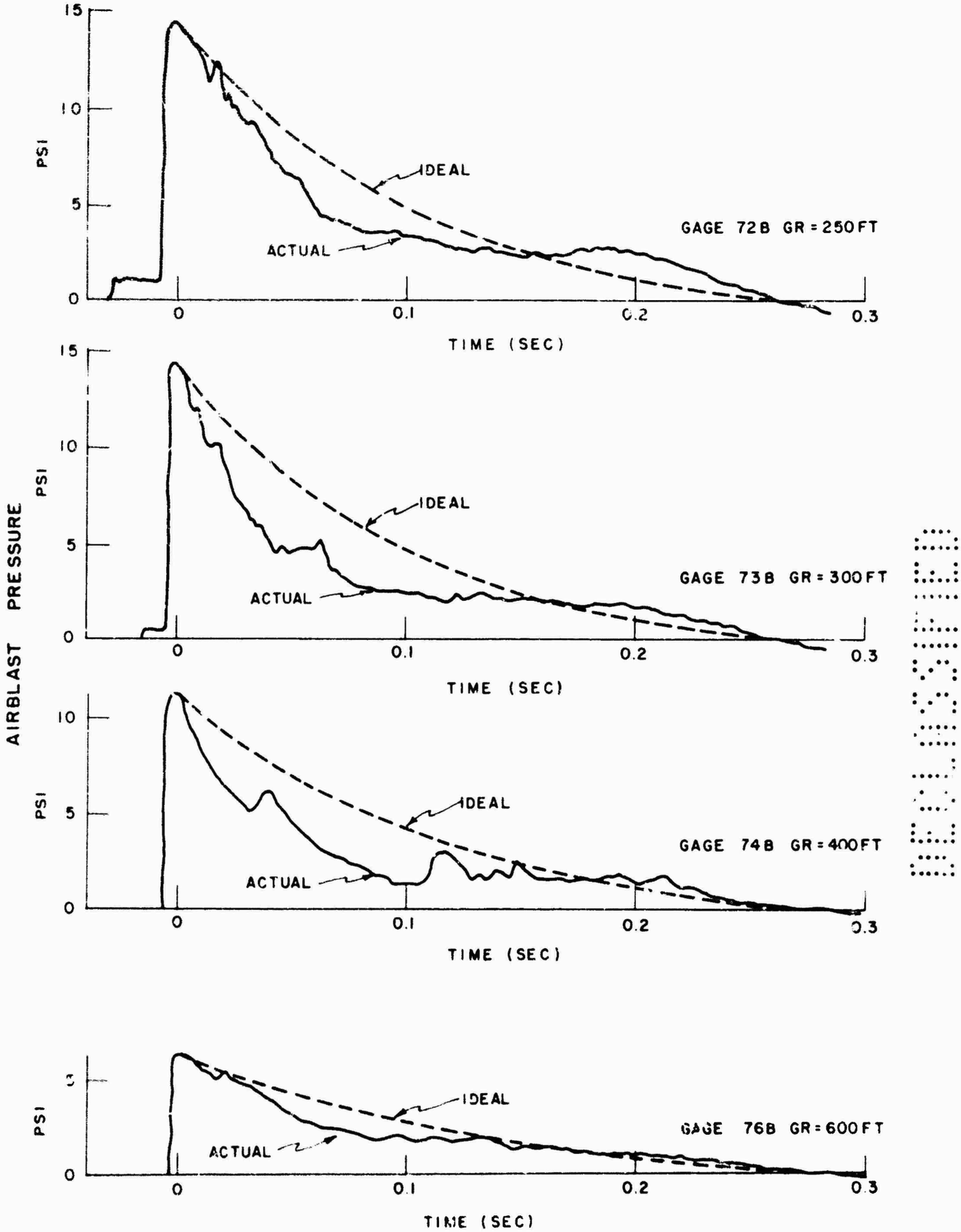

5.20 Comparison of measured airblast pressure with Brode's calculated wave form for free air pressure, TEAPOT Shot 7.

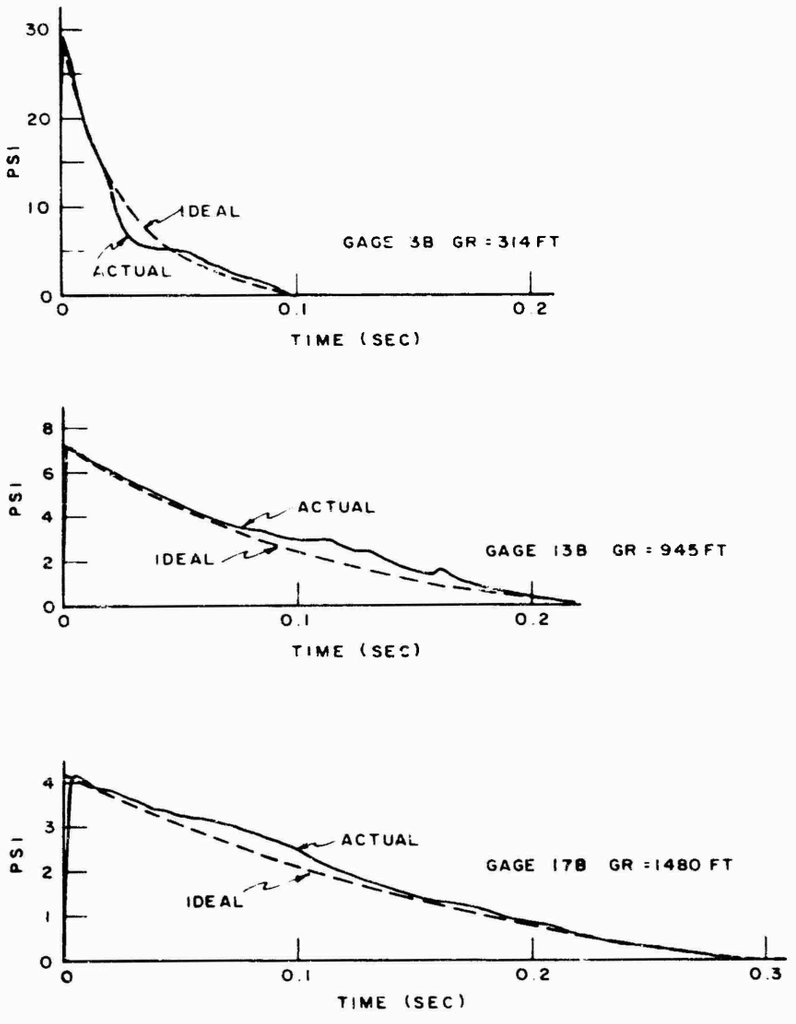

5.21 Comperison of measured airblast pressure with Brode's calculated wave form for free air pressure, JANGLE U.

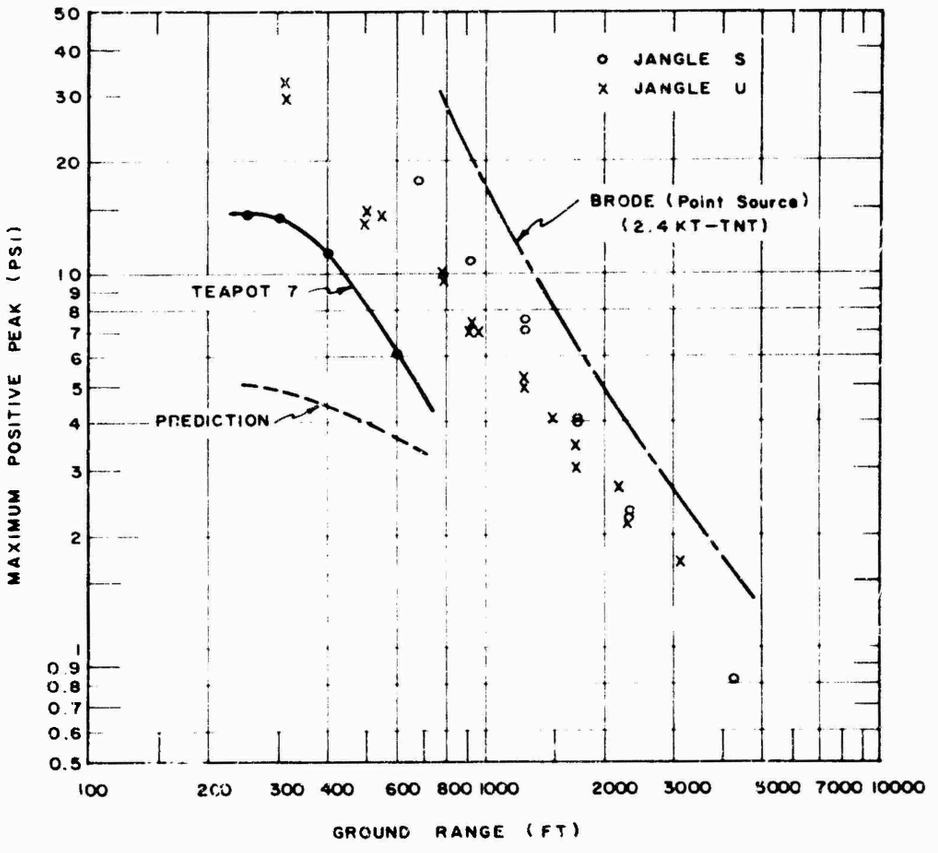

5.22 Maximum airblast pressure, TEAPOT Shot 7, JANGLE U and S.

Included on Figure 5.22 is the Brode point source pressure-distance curve (Reference 24). To explain: if the surface of the earth were an ideal reflector for shock waves, then image theory should apply for low burst heights, and the pressure produced near the surface at any distance from a charge fired above the surface should be equivalent to the pressure in free air (with no surface) that would be produced by the original charge plus an equal image charge at the image distance below the now imaginary surface. As the point of measurement is removed to greater and greater radii, the pressure produced by the charge and its image becomes more and more closely equivalent to the pressure produced by a single charge of twice the weight, located at the surface.

On this basis, the Brode curve in Figure 5.22 has been drawn to describe the pressure to be expected from a 2.4-kt TNT charge. Consideration of the JANGLE S data on this figure yields the result that this surface nuclear detonation was about 35 to 40 percent efficient (when compared with TNT) in producing peak airblast pressure. A considerable mass of data obtained from nuclear air bursts indicate about a 45 percent efficiency, which indicates that the JANGLE S peak air-blast pressure data are reasonable.

Figures 5.23 and 5.24 present the positive duration and positive impulse data obtained from the three pertinent nuclear shots. Although the duration data from the two JANGLE shots agree well, the TEAPOT airblast positive durations are much higher. This result is traceable to the deviation from the classic wave form observed on the TEAPOT records (Figure 5.20); the long pressure plateau contributes significantly to an increased positive duration. Similarly, it appears that the lengthening of the positive pressure pulse leads to large impulse values, which are summarized in Figure 5.24. Here, the data from the JANGLE shots are consistent with an assumption of a charge depth effect; however, at close-in ranges the TEAPOT Shot 7 impulses exceed the JANGLE U data. In this connection it is worthwhile to point out that the pressure plateau portion of the TEAPOT records makes a substantial contribution to the total positive impulse.

5.5 EVALUATION OF PREDICTION METHOD

It appears desirable to devote a part of this report to an over-all evaluation of the prediction method which is based upon measured crater radius. As stated previously, this method results in predicted values lower than would be obtained from direct $W^{1/3}$ scaling of HE results. However, except for airblast, measured nuclear results are also lower than direct $W^{1/3}$ scaling of HE results would obtain. It is considered that using free-field effects data from HE charges in terms of crater radius to predict nuclear effects in a given soil partially compensates for the TNT efficiency of the nuclear charge.

The fact that the predictions and measured results do not agree precisely indicates that the TNT efficiency for cratering is not exactly the same as for other free-field phenomena or that possibly there may be

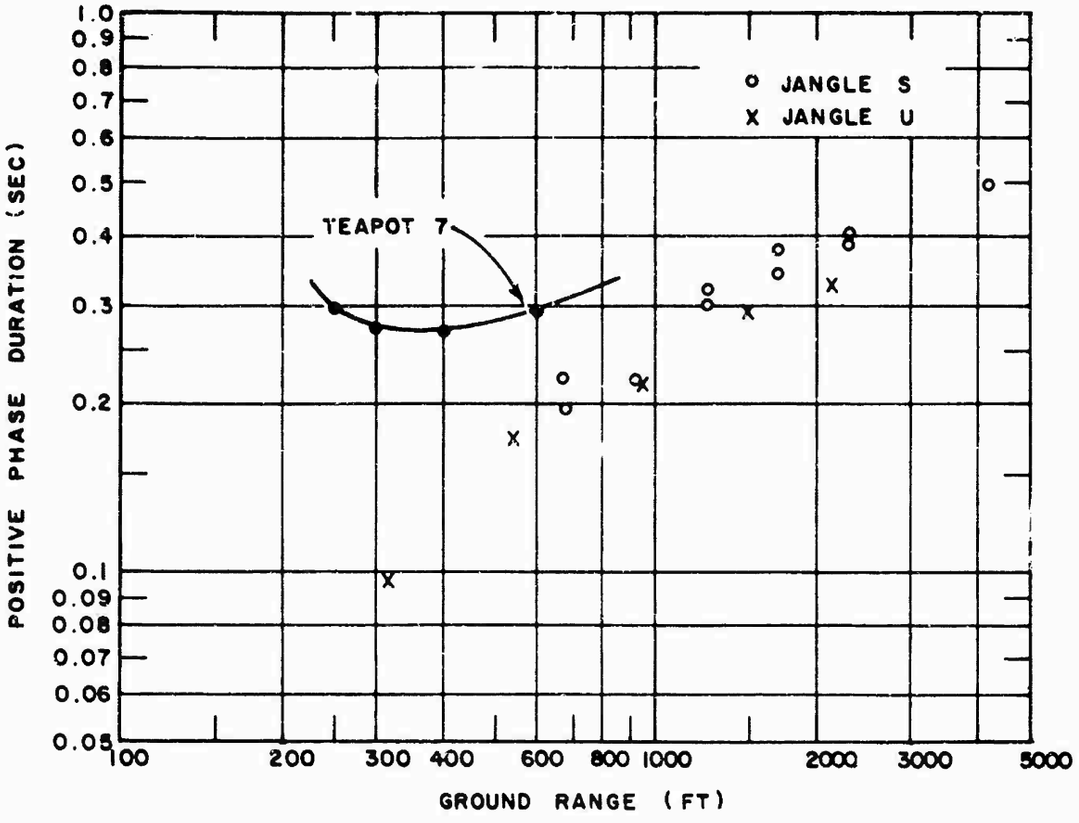

5.23 Airblast positive phase duration, TEAPOT Shot 7, JANGLE U and S.

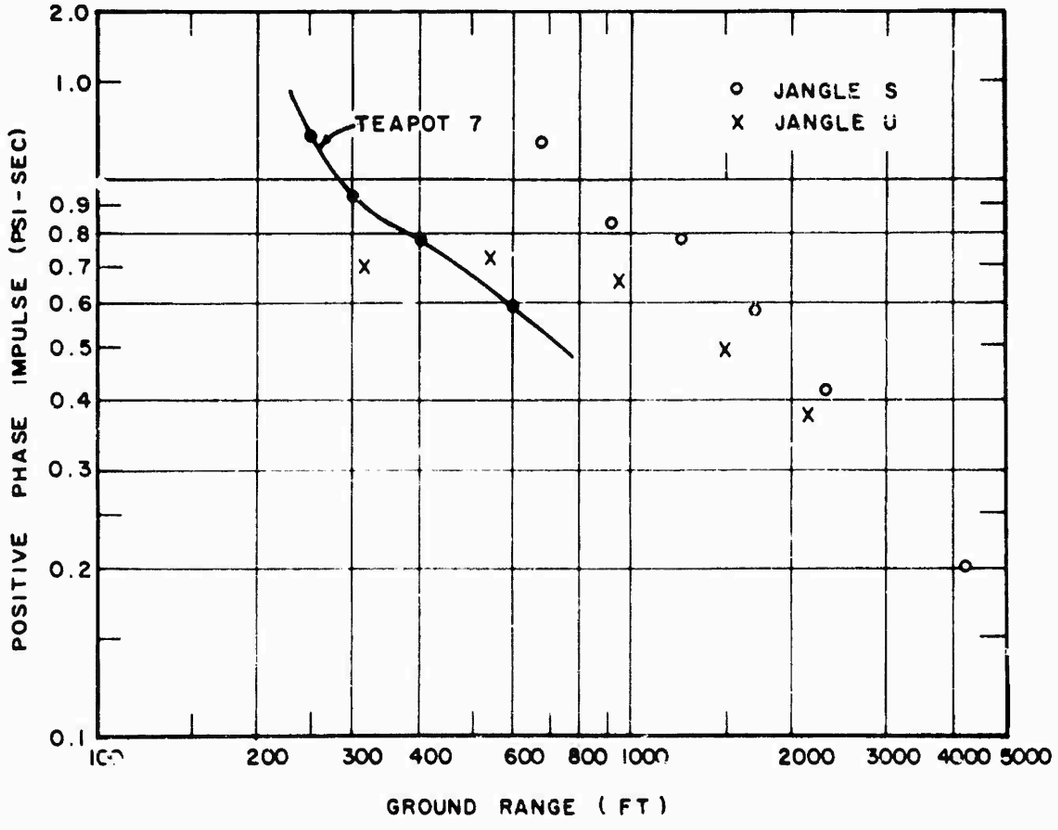

5.24 Airblast positive phase impulse, TEAPOT Shot 7, JANGLE U and S.

some variation due to the change in energy density. However, it would appear that this method is more realistic that direct $W^{1/3}$ scaling with 100 percent mechanical efficiency assumed. It is noteworthy that, for the crater radius prediction method, it was necessary to use apparent crater radius data. This procedure was dictated by the fact that reliable "true" crater data are not available for most detonations.

Some measurements of true craters (or, more exactly, the spatial extent of the disassociation zone) were made on the pre-TEAPOT Mole operation in Nevada (Reference 23), using the technique of colored-sand columns. These measurements indicate that the deviation of the true crater from the apparent becomes most serious as the charge depth is increased. The foregoing result suggests that if the true crater radius had been used for the TEAPOT Shot 7 predictions the agreement between prediction and measurement would have been improved. A detailed procedure for "correcting" apparent crater radius data and an extension of the prediction method is described in Reference 9, the final report of Project Mole.

5.6 SEISMOLOGY AND SOIL MECHANICS

The acceleration-time and earth stress-time records from the three nuclear shots and some pertinent HE tests were used to plot travel-time curves familiar to seismologists. In addition, it is possible, using the TEAPOT Shot 7 data, to obtain an approximate stress-strain relation for the soil found at the Nevada Test Site.

5.6.1 Seismic Considerations. The travel-time plots corresponding to the pertinent larger-charge shots conducted at the Nevada Test Site (Yucca Flat) are shown in Figures 5.25 through 5.31. It should be noted that arrivals of earth acceleration, and, where appropriate, stress and airblast are plotted; velocity is computed. The data from these plots are summarized in Table 5.1.

Reference to the travel-time plots of the JANGLE HE series (Figures 5.25 through 5.28) makes it clear that the curves of first arrivals detected by the close gages are linear within experimental error, indicating that the velocity of the first arrivals is constant and that propagation is not affected by the magnitude of the signal beyond the smallest gage distance, 72 feet (2.1 λ) for the large charge (HE-2) and 28 feet (2.05 λ) for the smaller charges. It would be desirable to have data closer to the explosive to study the transition zone between magnitude-dependent and magnitude-independent propagation.

The seismic survey carried out by the United Geophysical Company (Reference 25) sheds considerable light on the Nevada Test Site's geologic structure, although the closest profile and drill hole are over 7,000 feet away from the site of the JANGLE HE test series. In the light of these seismic results, the travel-time curves obtained on the form profiles of Figures 5.25 through 5.28 become more understandable. On HE-3 (Figure 5.25), a 3,937 ft/sec line is observed out to 1,340 feet, with a 4,651 ft/sec line breaking out at 100 feet. For HE-1 (Figure 5.26),

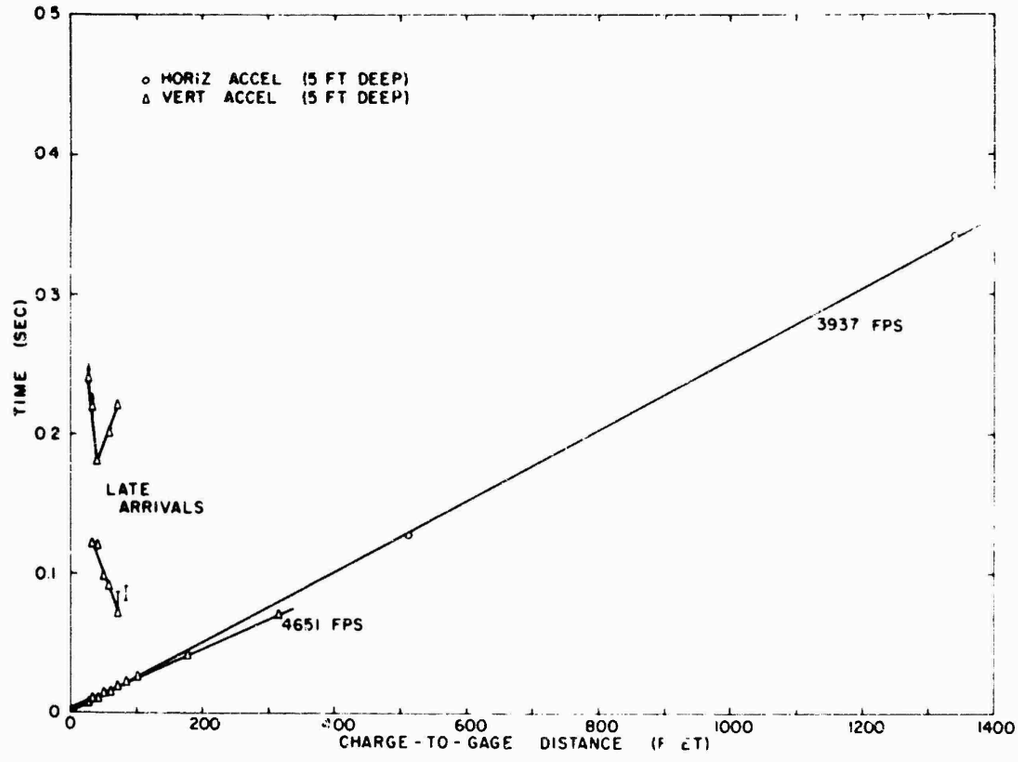

5.25 Travel-time plot, JANGLE HE-3, λ_c=0.5

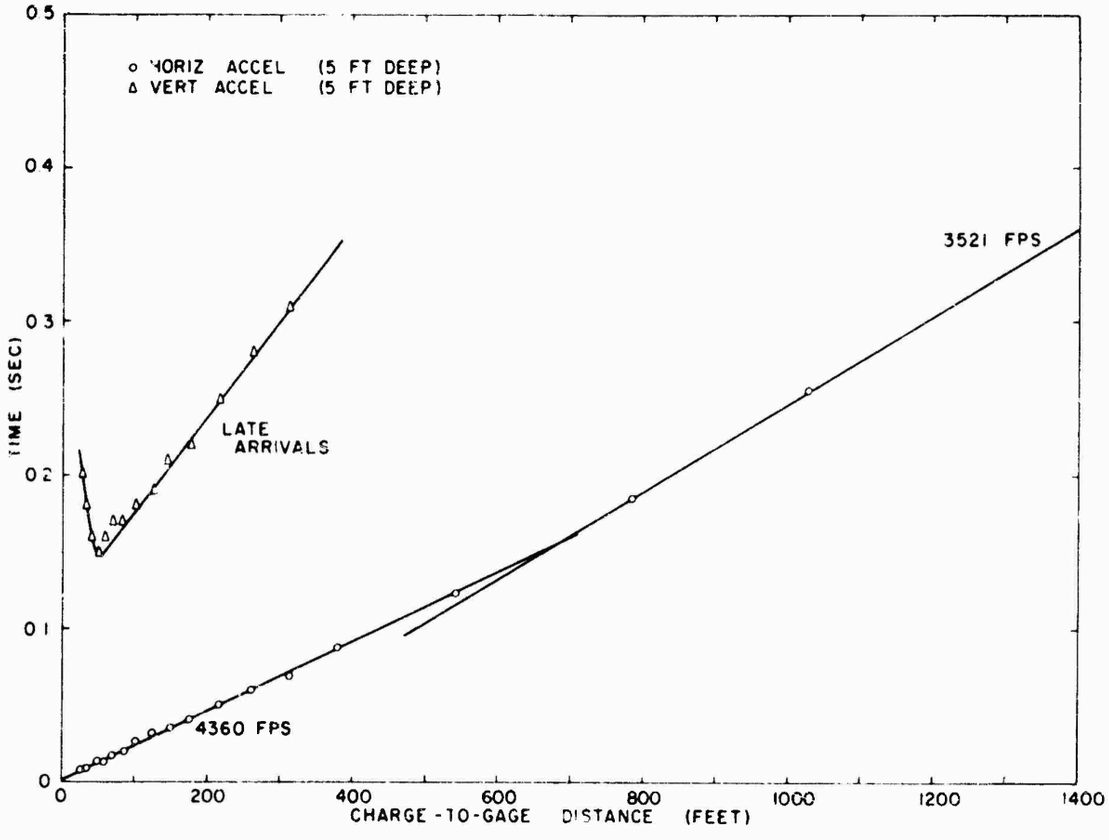

5.26 Travel-time plot, JANGLE HE-1, λ_c=0.15

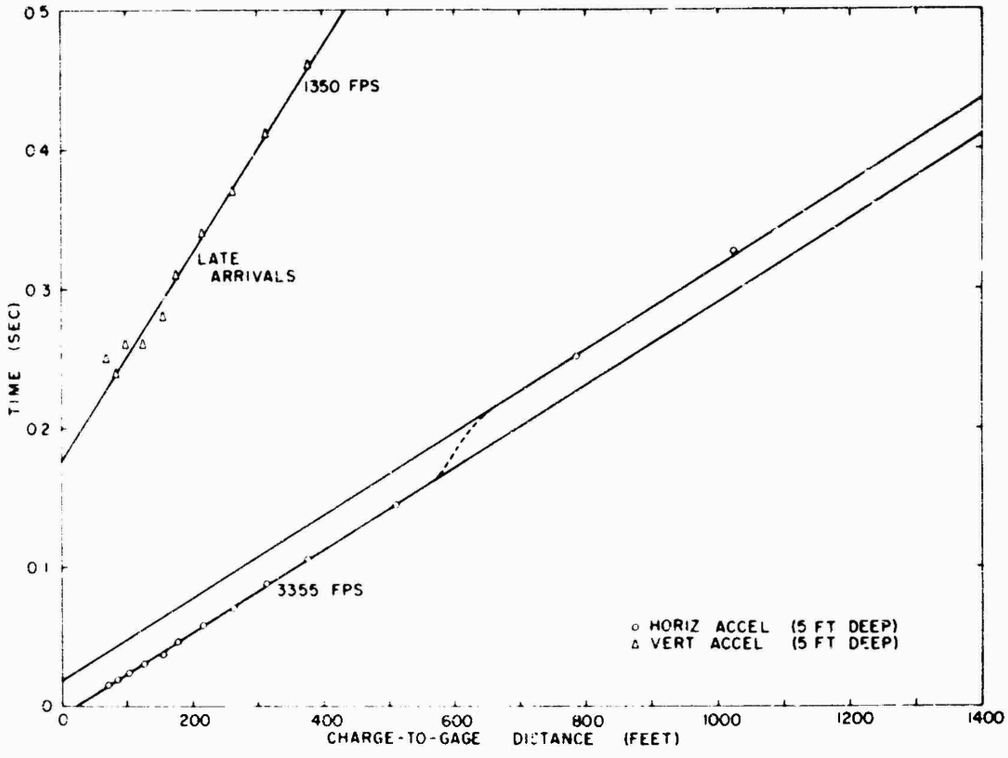

5.27 Travel-time plot, JANGLE HE-2, λ_c=0.15

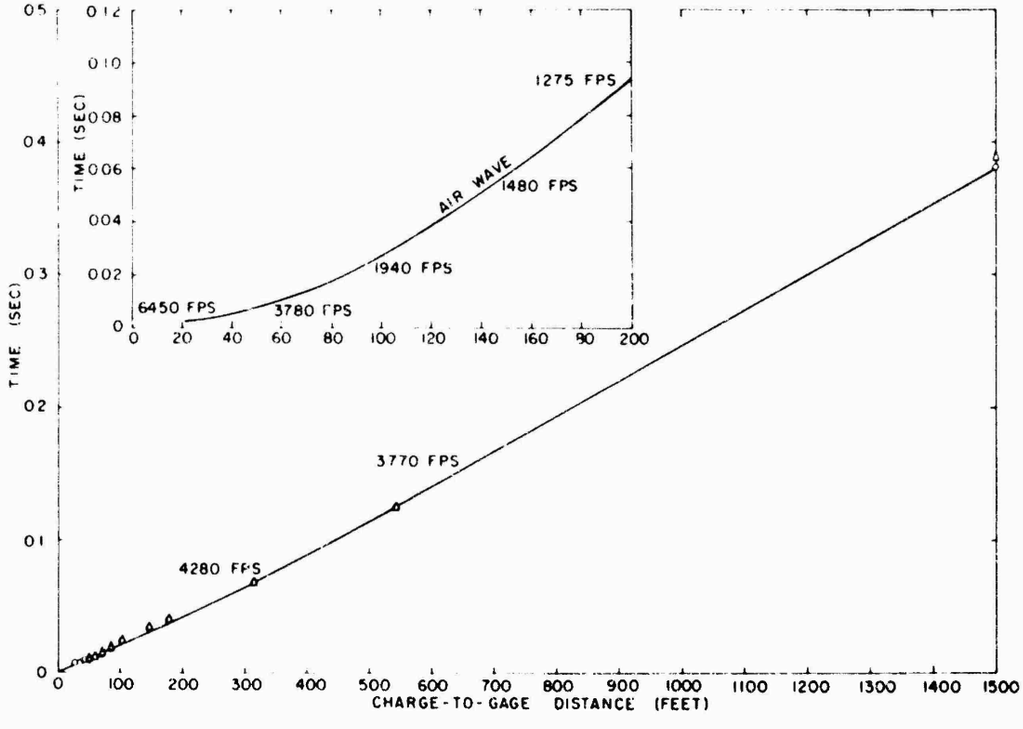

5.28 Travel-time plot, JANGLE HE-4, λ_c=-0.15

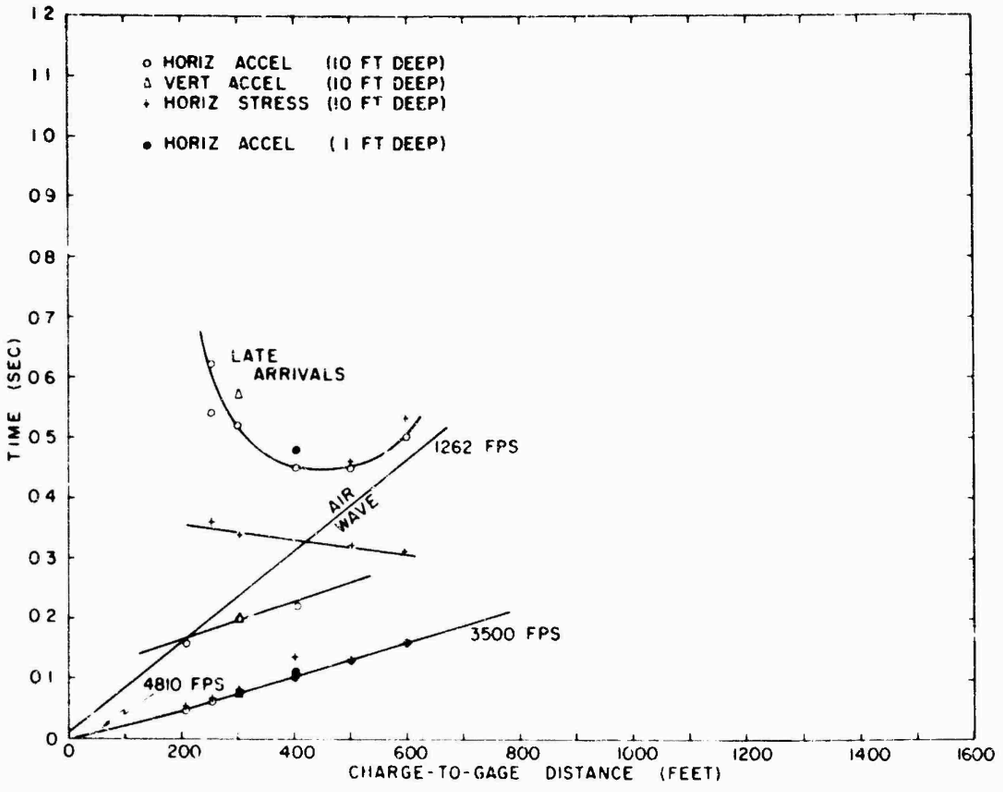

5.29 Travel-time plot, TEAPOT Shot 7

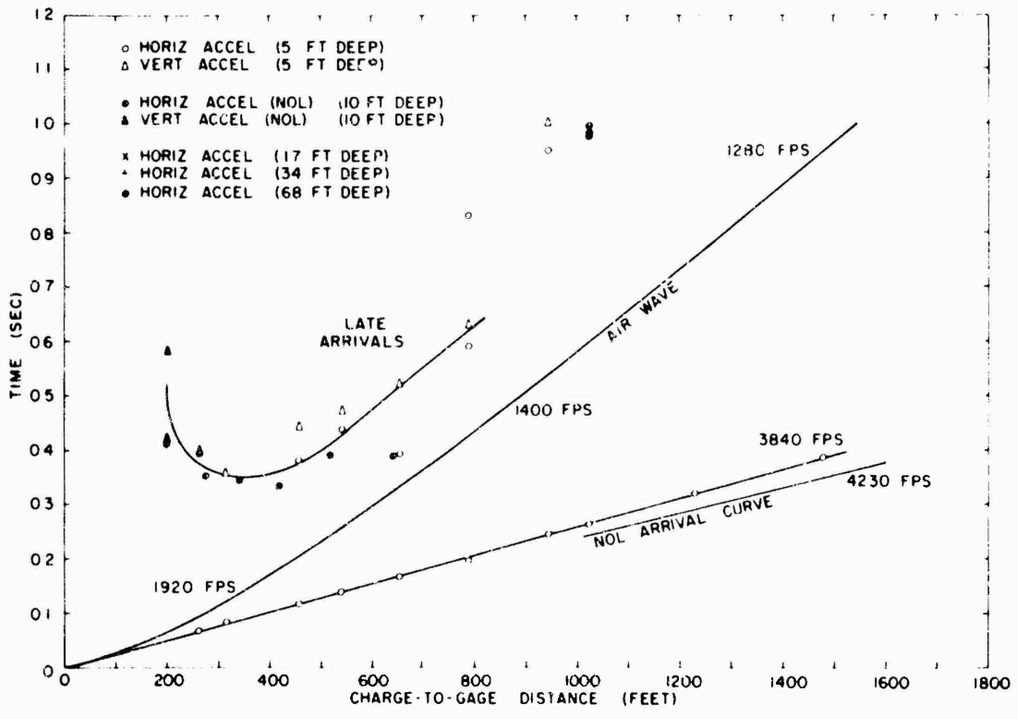

5.30 Travel-time plot, JANGLE Underground Shot

TABLE 5.1 - WAVE VELOCITIES FROM TRAVEL-TIME PLOTS
(NEVADA SAND-GRAVEL MIX)

Shot	λ_c	Observed Velocities			Air Wave (ft/sec)
		First Arrivals (ft/sec)	Later Arrivals[1] Normal (ft/sec)	Later Arrivals[1] Reverse (ft/sec)	
HE-3	0.5	3940	---[3]	100-360	---
HE-1	0.15	4360-3521[2]	---	120-1600	---
HE-2	0.15	3355	1350	---	---
HE-4	-0.15	4280-3770[2]	---	---	6450-3780-1275[2]
TEAPOT Underground		4810-3500[2]	3100	400-1200	1262
JANGLE Underground		3840	---[3]	340-1270	1920-1400-1280[2]
JANGLE Surface		3780	Data unavailable		2270-1620-1186[2]

1. Velocity of later arrivals = shot-gage distance/travel-time.
2. Higher velocity nearest ground zero.
3. Some additional late arrivals noted which do not fit standard pattern.

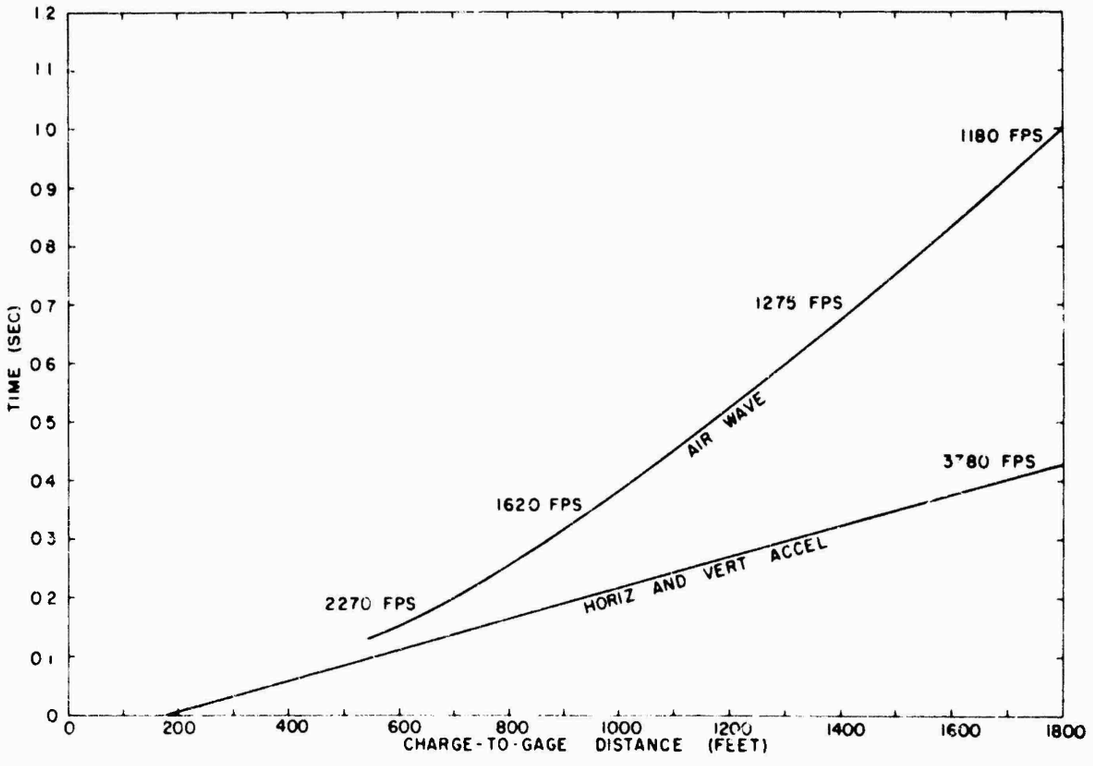

5.31 Travel-time plot, JANGLE Surface Shot

the 4,360 ft/sec line with an intercept of less than 0.001 second breaks into a lower velocity (3,521 ft/sec) line near 700 feet. A 3,355 ft/sec line on HE-2 (Figure 5.27) is offset about 0.024 second at about 600 feet, with the same velocity on each side of the offset. These data indicate higher velocity (4,100 ft/sec) material in the area within 700 feet southwest of HE-B, shown on the geologic map of Figure 5.32, and lower velocity material (3,500 ft/sec) south of HE-A. In addition, a low velocity (2,100 ft/sec) material overlies the 3,355 ft/sec materials beyond about 600 feet south of HE-A.

The results of HE-4 (Figure 5.28) require special attention. After plotting the travel-times of the air pressure arrivals as a function of distance, it is evident that the air wave velocity diminishes from 6,450 ft/sec at 28.4 feet (2.08λ) to about 1,275 ft/sec at 200 feet. The air wave is the first arrival out to about 70 feet, where the ground arrival overtakes it. Actually, for some distance beyond this, ground motion data and resulting velocity determinations are governed by air-ground coupling, which should be especially strong where the velocities are comparable (in the neighborhood of 40 feet).

Later arrivals are observed on all these shots, except HE-4. These arrivals possess characteristics similar to those observed for the Project Mole rounds; that is, at closest gage stations the late arrival amplitudes are smaller than that associated with the first pulse, but by the 6λ range they are comparable to or even larger than the first arrival amplitudes. In addition, characteristic reverse velocity of later arrivals is observed on these shots, with the "turn-around" point usually near 6λ.

The travel time for the later arrivals is of the order of 0.10 second. If these arrivals were reflections from a subsurface reflector, this reflector would be at a depth of about 150 feet. No such reflector was observed on the seismic surveys and none can be expected from reference to the geologic sketch map of Figure 5.32. Furthermore, late arrivals which fall into the same pattern are observed in different soils and in different areas. They cannot be identified either as shear or Rayleigh surface waves, since their velocity is too low and their travel-time curves do not pass through the origin. Therefore, it is desirable to look to the mechanics of wave propagation in soils for an explanation of these late arrivals.

For the JANGLE HE series, later arrivals are observed on all gage records down to gage depths of 68 feet, appearing later the deeper the gage. The amplitude of these waves changes slowly with depth. The only gages set at various depths were at ground ranges beyond 6λ. For these data, the velocity of the later wave is normal (not reversed) at about 600 ft/sec. The later waves appear most prominently on the vertical acceleration records and to a lesser extent on the horizontal acceleration and earth pressure gage records; also, these later arrivals bear no evident relationship to the arrival of the air-blast pressure at the gage station.

The travel-time plots from the three pertinent nuclear detonations are shown in Figures 5.29, 5.30, and 5.31. These results show first

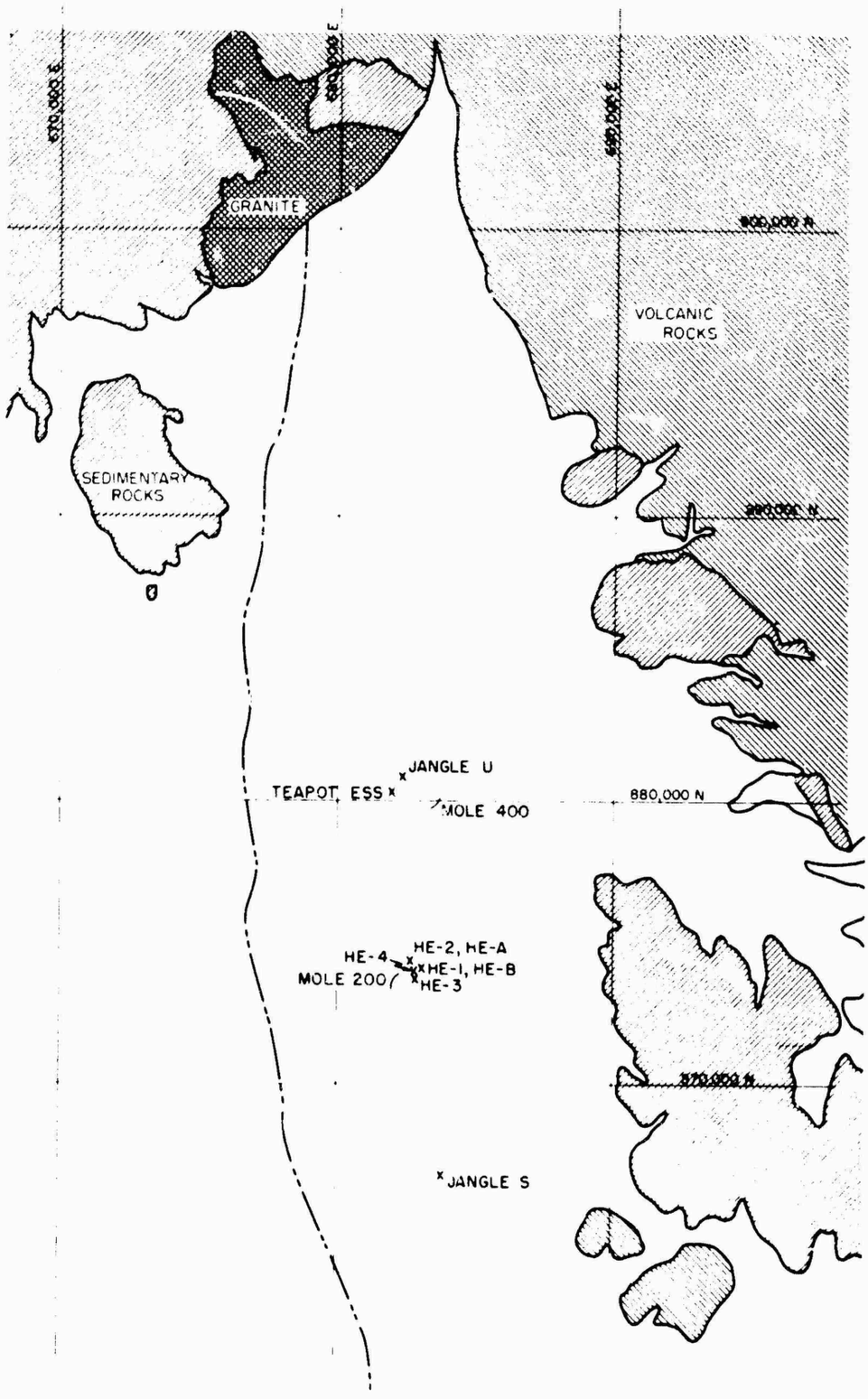

5.32 Geologic sketch map, Yucca Flat, showing location of all Nevada Test Site detonations.

arrival velocities for the three shots in the range 3,500 to 4,200 ft/sec, which compares well with the JANGLE HE results. Late arrivals are observed on the two underground nuclear detonations; the absence of late arrival data for the surface shot (Figure 5.31) could be misinterpreted. Actually, complete gage records from this shot are not available in the published literature; therefore, only tabulations of acceleration and airblast first arrivals could be included on the figure. Hence, the JANGLE surface shot must be eliminated from any discussion of late arrivals. Concerning the underground shots, both exhibit reverse velocity for the later arrivals; the turn-around radius for the shallower detonation (JANGLE U shot) occurs at about 300 feet, whereas the same effect is apparent at about 400 feet for the TEAPOT Shot 7 data, which may be evidence that the turn-around point is a function of charge depth. For both these nuclear shots, the velocities corresponding to the late arrivals are in the range 400-1,200 ft/sec (see Table 5.1). This velocity range is significantly higher than the 50 to 700 ft/sec range often observed for the Mole grounds, which suggests that these velocities are not independent of charge weight or magnitude of disturbance.

Finally, it can be said, even from this brief look at the seismic picture, that a real contribution to the problem of understanding underground explosions could be made by applying the principles of seismology. It is hoped that this avenue of investigation will eventually lead to better explanations for the propagation of waves through elastoplastic media.

5.6.2 Soil Stress-Strain Comparisons. Reference to the gage layout for the TEAPOT underground shot (Figure 3.1) shows that at three gage stations (Stations 72, 73, and 74) a short-span strain gage was installed in close proximity with an earth stress gage, both buried 10 feet deep. Using these data, it is possible to construct "free-field stress-strain diagrams" for the soil. When this is done, using the available data, the curves shown in Figure 5.33 result. Several significant conclusions can be stated on the basis of these results:

1. Assuming, as is the case in conventional materials testing procedure, that the area enclosed by the stress-strain diagram is a measure of the energy absorbed by the soil as the disturbance passes through it, Figure 5.33 indicates that the most energy is absorbed at the closest gage station to the charge and the least absorption occurs at the most remote gage station.

2. The stress-strain diagram corresponding to Station 74 (400-foot ground range) is the sort of result expected in the elastic regime where the soil is not stressed beyond its yield point.

3. However, the diagrams for the other two stations indicate that the soil was stressed beyond yield and, therefore, the deformation was plastic.

4. For the strain-rates encountered on the TEAPOT Shot 7 test, it appears that the yield stress for the Nevada sand-gravel soil is in the

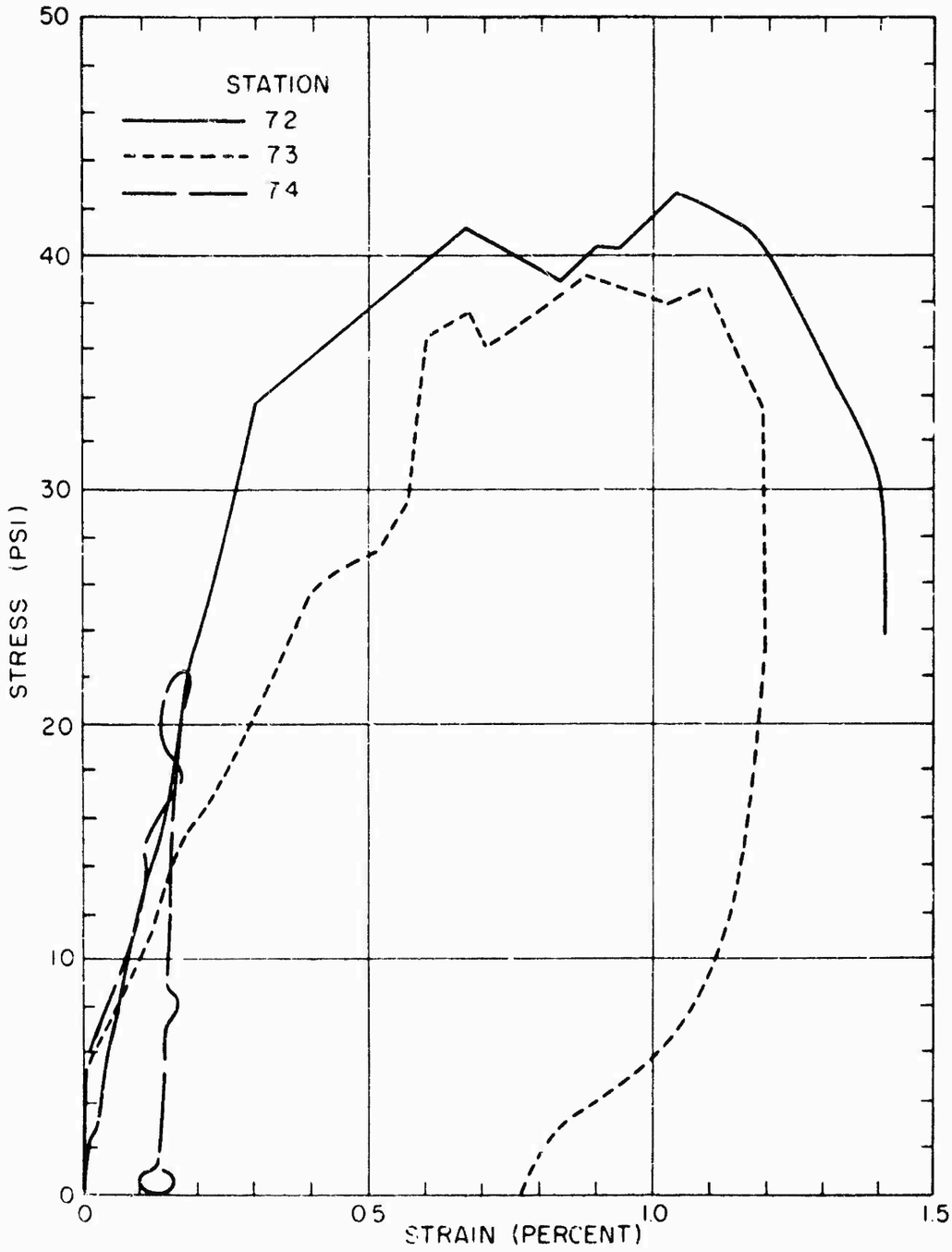

5.33 Horizontal earth stress vs horizontal earth strain, short-span gages, 10 feet deep, TEAPOT Shot 7.

25-40 psi range. No laboratory transient test data on this soil are available for comparison purposes.

The evident change between 300 and 400 feet in the mode of propagation of energy through the soil (Figure 5.33) might be related in some way to the radius of the turn-around point of the late arrival travel-time curve discussed in Section 5.6.1. However, the fact that the same two effects occur at approximately the same ground range may be fortui-

tous. In any case, it would be unwise to base an analysis on such meager stress-strain data. The suggestion of possible correlation here points up the need for more complete data of this type, so that a clearer picture of wave propagation in earth can be formed.

5.7 SIGNIFICANT HE RESULTS

To conclude the discussion of the TEAPOT Shot 7 free-field underground measurements, it seems profitable to review briefly the significant conclusions which have resulted from analyses of HE test data obtained at various soil sites and using various charge sizes.

Referring to the Project Mole data (Reference 9) it is possible to make some general statements:

1. The response in wet and damp soils was greater than in dry soils for all measured parameters, except airblast phenomena.

2. For dry soils, the more cohesive (dry clay) produced larger response than did the moderately cohesive soil (sand-gravel mix).

3. Only airblast and postshot static measurements (craters and permanent displacement) show consistent charge depth effects in all soils tested.

4. The only dynamic earth parameter which indicates a charge depth effect in all soils tested is the maximum horizontal velocity.

The consideration of the possible application of the $W^{1/3}$ modeling procedures to underground explosion phenomena may logically be divided into two main sections, the first dealing with the effects of increasing the TNT charge weight and the second with the effects of larger nuclear detonations where both charge type and weight must be considered. In the Project Mole final report (Reference 9), the value of strict $W^{1/3}$ modeling was tested using data (see Tables 3.1 and 3.2) obtained at the Utah dry clay site (Dugway Proving Grounds) and the Nevada sand-gravel site (Nevada Test Site). The modeling technique, when applied to TNT detonations only, has been found wanting in several respects. However, it should be clearly understood that the model laws are not questioned, but rather the ability to conduct idealized model experiments is subject to doubt.

Some progress has been made, in terms of cratering, by applying $W^{1/3}$ modeling to the results of surface and underground nuclear detonations when the charge weight is taken as some lesser fraction than 100 percent of the total radiochemical yield. For example, the TNT efficiency for cratering for TEAPOT Shot 7 is approximately 30 percent in terms of the Project Mole data at Nevada (Reference 23). This efficiency leads to a scaled charge depth of $\lambda_{TNT} = 0.75$, whereas the radiochemical data gives $\lambda_{RC} = 0.50$. If it is assumed that the TNT efficiencies of other free-field phenomena are essentially the same as that for cratering, the earth

parameters could be scaled for comparison with nuclear data using this factor and $W^{1/3}$ modeling. This idea is the basis for the crater radius prediction method referred to previously.

Because it is not within the scope of this project, little has been said in this report about damage to actual underground and surface structures due to an underground detonation. However, it seems obvious that any future efforts in the underground effects field should include a detailed consideration of the physical quantities which are most pertinent to structural response and damage. The basic question must be raised as to whether the most useful quantities are being measured and compared; this question should be answered by those dealing with the effects of underground explosions upon underground and surface structures.

Chapter 6
CONCLUSIONS and RECOMMENDATIONS

6.1 CONCLUSIONS

The instrumentation performance on Operation TEAPOT Project 1.7 (Shot 7) was excellent; records were obtained from 75 of the 76 connected channels of information. The results of the structural measurements for Projects 3.2.1 and 3.2.2 have been transmitted to the proper agencies for analysis; the conclusions in this chapter are restricted to analysis of the free-field data obtained on Project 1.7.

In general, the wave forms of the various gage records of free-field earth measurements obtained on TEAPOT Shot 7 are quite uniform with respect to ground range and gage burial depth. In addition, the induced effects which may be identified with airblast appear to be small and of short duration. For this reason, unlike results from previous underground detonations, separation of airblast effects from direct earth-transmitted effects seems straightforward.

6.1.1 Earth Acceleration and Particle Velocity. The influence of airblast-induced effects appear to be most pronounced upon the earth acceleration parameter, particularly upon the vertical component of acceleration. For the Shot 7 detonation, the surface (Rayleigh) waves exhibit an overriding influence at the larger ground ranges. Evidence points to the fact that the frequency content of the acceleration-time disturbance is a pertinent consideration in attempts to correlate with structure damage. It is considered that earth particle velocity (and displacement) are probably better damage parameters than acceleration. However, it must be emphasized that when considering damage to the contents of an underground structure, earth acceleration may be the most important parameter.

Results regarding horizontal radial earth velocity from three nuclear detonations at the Nevada Test Site indicate a consistent charge depth effect for this variable; that is, the deeper the charge burial, the greater the peak-to-peak earth velocity at comparable ground ranges. The predictions based upon previous data and the measured crater radius agree well with the velocity data obtained on Shot 7.

6.1.2 Earth Displacement. Although the deep underground shot (Shot 7) yielded large underground dynamic earth displacements, a consistent effect of charge depth was not evidenced in the data from the shallower (JANGLE U) and surface (JANGLE S) shots. The surface dynamic displacement, as computed from the tangential strain observations on Shot 7, indicates that, at close-in ranges, the displacements decrease markedly from the

ground surface to 10-foot depth; however, at larger ground ranges, the surface and underground displacements are comparable.

For permanent displacement, the Shot 7 vertical component is significantly smaller than the horizontal component. The permanent displacement contours indicate an asymmetry which cannot be ascribed to the proximity of the JANGLE U shot crater. However, the main asymmetry appears to occur in the general area where excavation (and backfills) were made for underground test structures.

6.1.3 Earth Stress and Strain. The horizontal earth stress measurements were little affected by airblast-induced effects. Preshot predictions of peak earth stress, based upon the small-charge HE data only, yielded values which were too low, particularly at close-in ground ranges.

From horizontal earth strain measurements, it is concluded that only at close-in ranges (250 feet on Shot 7) is there a significant positive strain gradient with decreased depth of measurement. At two crater radii and beyond, the strain gradient with depth is practically zero. Tangential strain measurements appear to be consistent with the concept of a uniformly expanding soil medium.

6.1.4 Airblast. Maximum airblast pressures observed on Shot 7 were two or three times greater than would be predicted using pertinent data from previous nuclear tests and underground HE experiments. Some significant deviations from the classical airblast wave form were observed on the Shot 7 records. Generally there is a pronounced tendency toward an abnormally long positive phase; consequently, the airblast positive impulse from Shot 7 is larger than would be expected.

Maximum blast pressure exhibits a charge depth effect, in that the JANGLE U and S data are significantly higher than those from TEAPOT Shot 7.

6.1.5 Seismology and Soil Mechanics. The analysis of the seismic travel-time data from the three pertinent nuclear tests, as well as some selected HE tests, shows first-disturbance velocities which approximate the measured seismic (elastic wave) velocities. Also, for the nuclear shots late arrivals are observed which exhibit a reverse velocity behavior characteristic of small-charge HE results.

Use of Shot 7 data to construct some free-field stress-strain diagrams leads to the conclusion that at the 400-foot ground range the soil disturbance remained in the elastic regime, whereas, closer to ground zero, the deformation was plastic. It is possible to identify tentatively the turn-around point of the curve of late-arrival travel time with this transition between plastic and elastic deformation.

From a brief analysis of the seismic and soil mechanics picture, it can be concluded that further consideration is merited; it is hoped that the work would lead to a better understanding of wave propagation through elastoplastic media.

6.1.6 HE Results. A review of the underground HE results yields some useful conclusions, the most significant of which is the fact that all attempts to conduct scaled experiments have met with little success. That is, the data obtained from HE tests employing various charge weights are not consistent with model laws, and when the nuclear charge weight is assumed to be the radiochemical equivalent, the $W^{1/3}$ modeling cannot be applied to nuclear test observations. Thus, at present, the only hope lies in the determination of TNT efficiences to be assigned to the nuclear charge for the various phenomena arising out of underground nuclear detonations. It is possible that, for military purposes, this approach will provide adequately accurate predictions of the significant parameters.

6.2 RECOMMENDATIONS

The following are recommendations to guide future work in the field of underground explosion phenomena;

1. The need is apparent for a more complete determination of the influence of airblast-induced effects upon such parameters as earth acceleration and earth stress. For this purpose, it would be desirable to concentrate on the measurement of the vertical component of acceleration and stress.

2. More information, both theoretical and experimental, is required concerning the attenuation of free-field earth response with increasing depth below the ground surface, response due to both airblast-induced and earth-transmitted effects.

3. There is a serious lack of definitive free-field underground measurements from a surface nuclear detonation; it is recommended that this deficiency be considered in future test plans.

4. In addition to the more conventional underground instrumentation, it is desirable that, for any future tests, the measurement of surface and subsurface strain be included.

5. Work should be continued in an attempt to place the laboratory and field determination of soil stress-strain relationships on a common basis so that current and future data will be more understandable. Also, it would be desirable on future tests to obtain complete travel-time and seismic survey data.

6. It would be advisable to initiate a thorough survey and subsequent laboratory testing program of underground effects instrumentation.

7. It is recommended that a detailed review of the available free-field earth response and structural damage data be undertaken to determine which free-field parameters are most pertinent to damage.

8. For any future underground effects tests, it would be desirable to include free-field earth response measurements as well as structural response and damage data.

Appendix

UNDERGROUND EXPLOSION EFFECTS FROM HIGH-EXPLOSIVE TESTS AT SHOT 7 SITE

Preliminary data reduction of the measurements taken on the underground structures of Project 3.3.2 from TEAPOT Shot 7 showed that the forces, accelerations, and relative displacements on these structures deviated markedly from the predictions based on HE data. In general, these functions were lower than were expected, and the pressures measured on the faces of the structures, particularly, were even lower than those measured in the free field.

There were, naturally, questions as to whether these results were typical of structures of these types under these conditions or whether they were due to a peculiarity of this individual experiment, such as improper backfilling of the structures, improper placement of the gages, or gross failure of the gages themselves to respond properly. It was decided at that time to conduct a series of tests on these structures using HE charges when the radiation level in the area permitted. It was hoped that these tests would provide definitive data as to the cause of the deviations noted and would also provide more general information as to the loading of structures from underground explosions.

These tests were conducted in October of 1955 in conjunction with operations in the area of Project 1.6 for the determination of crater characteristics and with the final measurements on permanent displacement monuments, a part of Project 1.7.

A.1 SHOT LAYOUT

A total of three rounds were fired; the explosive in each case consisting of a 256-pound spherical TNT charge detonated at the center, buried at a depth corresponding to the center of the structure involved (8 feet 2 inches from the nominal ground surface). The location of the charges and the gage layouts are shown in Figures A.1 and A.2. Prior to the tests the throwout from TEAPOT Shot 7 was cut away and the surface leveled in the vicinity of the structures, so that the height of the surface above the structures was approximately the same as in the original experiment design, and the interior of the structures was excavated to the original level.

A.2 GAGE LAYOUT

Gages were located on the structures at the same points as on Shot 7. The earth pressure gages on the surfaces of the structures were the identical gages used on Shot 7; they had not been excavated, so no question was

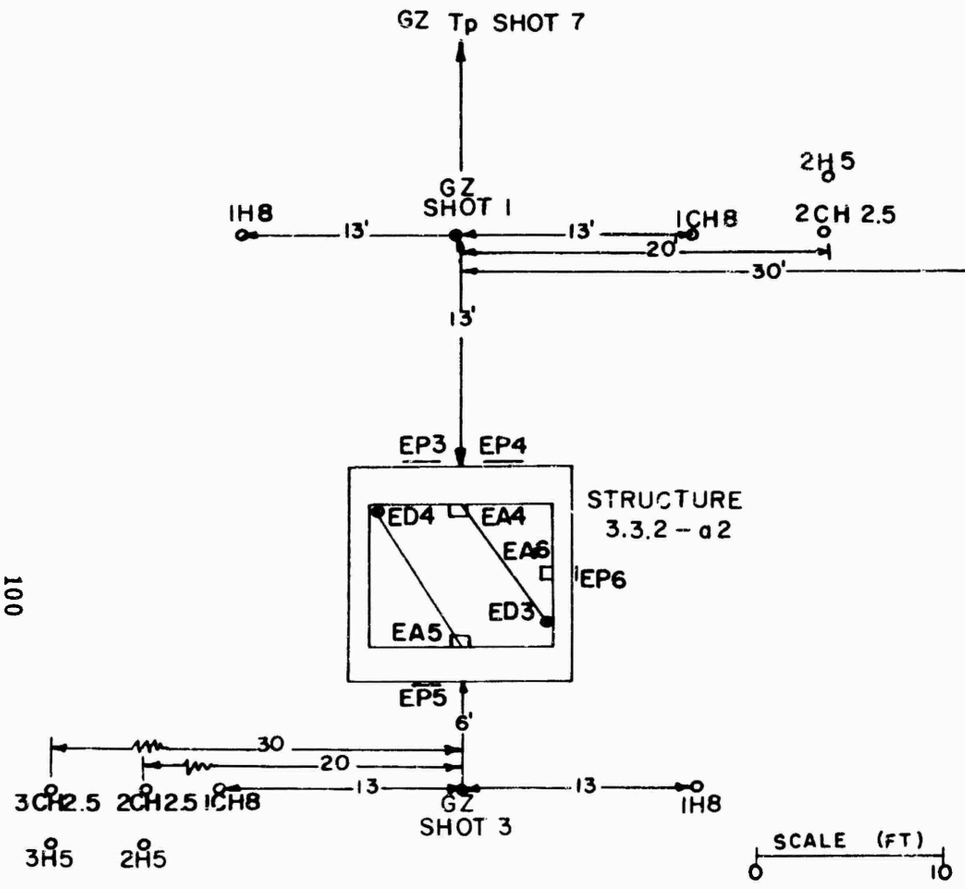

A.1 Gage layout, Shots 1 and 3.

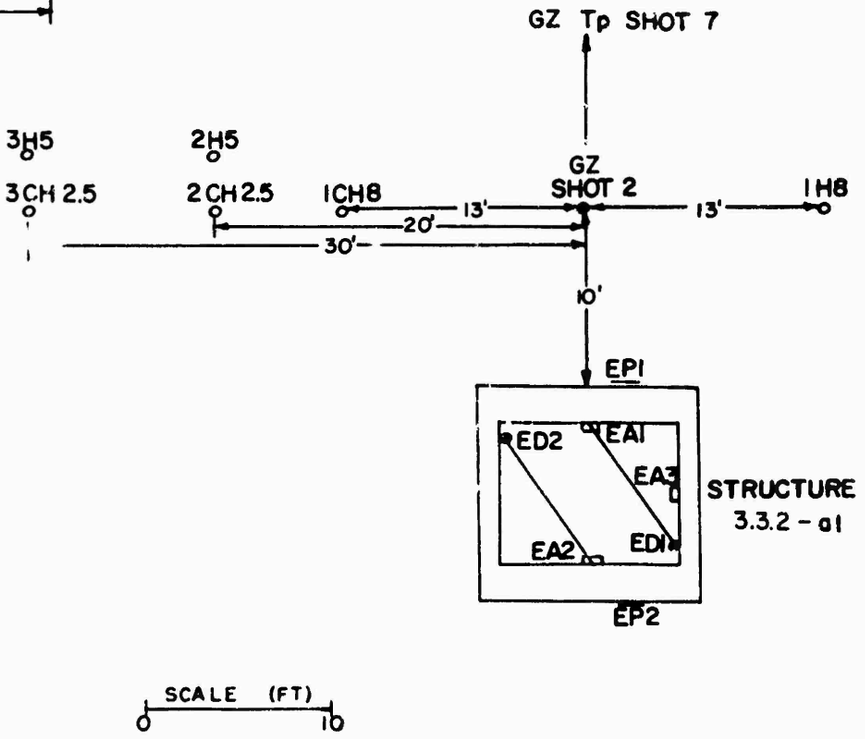

A.2 Gage layout, Shot 2.

1CH8	Horizontal stress at 8-foot depth at 13-foot radius (depth of center of structure).
2CH2.5	Horizontal stress at 2.5-foot depth at 20-foot radius.
3CH2.5	Horizontal stress at 2.5-foot depth at 30-foot radius.
1H8	Horizontal acceleration at 8-foot depth at 13-foot radius.
2H5	Horizontal acceleration at 5-foot depth at 20-foot radius.
3H5	Horizontal acceleration at 5-foot depth at 30-foot radius.

Structural gages same locations as on Shot 7.

introduced as to the similarity of the planting of these gages between Shot 7 and these HE tests. Accelerometers and displacement gages originally mounted inside the structures had been damaged by the throwout from Shot 7, so it was necessary to remount and recalibrate them, but they were remounted under conditions identical to the original. On each shot an array of free-field earth stress gages and accelerometers was included for purposes of correlation between shots with other tests. Free-field gages were located at radii of 13, 20, and 30 feet on each shot. At the 13-foot radius, both the accelerometer and the stress gage were buried to a depth of 8 feet 2 inches (the depth of the center of the structure and the depth of the center of the explosive). At the other radii the stress gages were buried at a depth of 2-1/2 feet, corresponding to the depth used on the majority of the Project Mole shots; the accelerometers were buried at 5 feet for similar reasons. It was originally desired to place the nearest stress gage and accelerometer at the same radius as the front wall of the structure involved, but this was found to be impossible on the later shots since such placement would put these gages within the crater and records would not have been obtained. In all cases, the free-field layouts were along radii at right angles to the line between the charge and the structure, as is shown in Figures A.1 and A.2.

A.3 PERMANENT DISPLACEMENTS AND CRATERS

On all shots an array of two radial lines of permanent displacement monuments was established prior to the shot, using the same techniques as were used on Project Mole. These monuments were located at a number of radii between 13 and 50 feet. Their vertical and horizontal location with respect to fixed monuments were determined prior to the shot and after the shot, thus giving data as to the variation of permanent displacement with ground range. After each shot the crater was surveyed along two diameters to determine its shape and size. All measurements were made on the apparent crater only and have been referred as accurately as possible to the original ground level.

A.4 PREPARATIONS

The Stanford Research Institute Field Party began operations on these tests on October 12, 1955. Prior to this time, contractors' personnel under the direction of John E. Lewis, Project 1.6, had commenced clearing the area and removing surface soil for decontamination, as well as recovering and resurveying the Project 1.7 permanent displacement monuments. This work continued until October 18. In the meantime the instruments remaining in the recording shelter from Shot 7 were rechecked and reconnected to the recording oscillographs which had been removed subsequent to Shot 7.

It was found that all gage cables had been broken at ranges up to 700 feet from ground zero by throwout and earth strain, so it was necessary to replace portions of all cables. Fortunately, it was found possible to identify the cables leading to the external earth pressure gages at points some 50 feet from the structures, so it was unnecessary to excavate these

gages. These particular gages were connected to the same channels as were used on Shot 7, so that a minimum of question would exist as to the similarity of their performance. All other gages on each test, including those used in the free-field measurements, were connected to their respective channels and calibrated prior to each test.

A.5 SHOT SCHEDULE

Shot 1 was fired on October 20, 1955. All channels gave usable results, and the preliminary data obtained therefrom permitted the decision to be made as to the location of Shot 2, which was fired on October 22, 1955, and Shot 3, which was fired on October 25. After the completion of the test series all gages were excavated, including these earth pressure gages associated with the structures. The latter were then reconnected to their respective channels and recalibrated, with the exception of Gage EP5, which was damaged beyond repair by Shot 3.

A.6 RECOVERY

Opportunity was taken at this time to recover the gages used in free-field measurements on Shot 7 with the exception of those at Stations 71 and 72 (excavation of which would have interfered with the operations of Project 1.6). Operations were completed on October 27, and the field party left the Nevada Test Site at that time.

A.7 RESULTS

Of the total of 42 gage channels installed on the three shots, 39 usable records were obtained, although several of these were of rather short duration, due to early cable breaks. The channels which failed to produce useful data were the two displacement gages, ED3, and ED4, and the front face accelerometer EA5, on Shot 3. The latter was seriously overranged and failed to return to zero, indicating that the instrument had been damaged. One of the displacement gages suffered an early cable break, and the other produced a record which was apparently meaningless because of displacement of the gage itself rather than the point of attachment. The peak data obtained from the records that were considered usable are presented in Tables A.1 and A.2, and tracings of the records themselves are presented in Figures A.3 through A.8.

A.7.1 Free-Field Data. The free-field gages were used on these shots to form a basis of comparison among shots and with other tests made under similar conditions. Several perturbations were introduced into these experiments: The tests were located in an area where considerable excavation had taken place prior to TEAPOT Shot 7, including Operation Jangle, and after Shot 7, in removing the added overburden. In excavations and drilling before and after these tests, old cable trenches, structure foundations, and miscellaneous junk were found. These conditions represented marked departures from a homogeneous free field. In addition, the

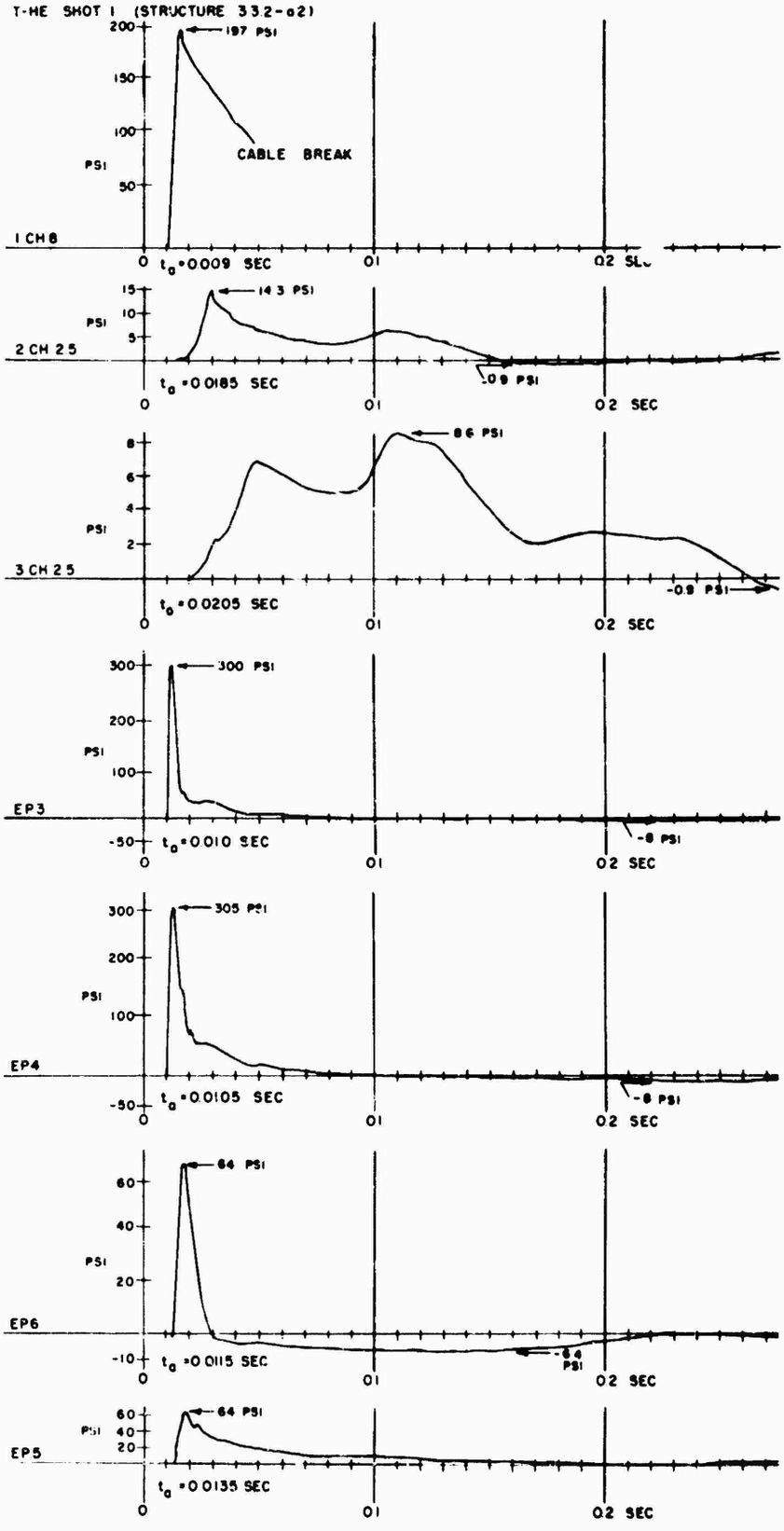

A.3 Record tracings, stresses and pressures, Shot 1.

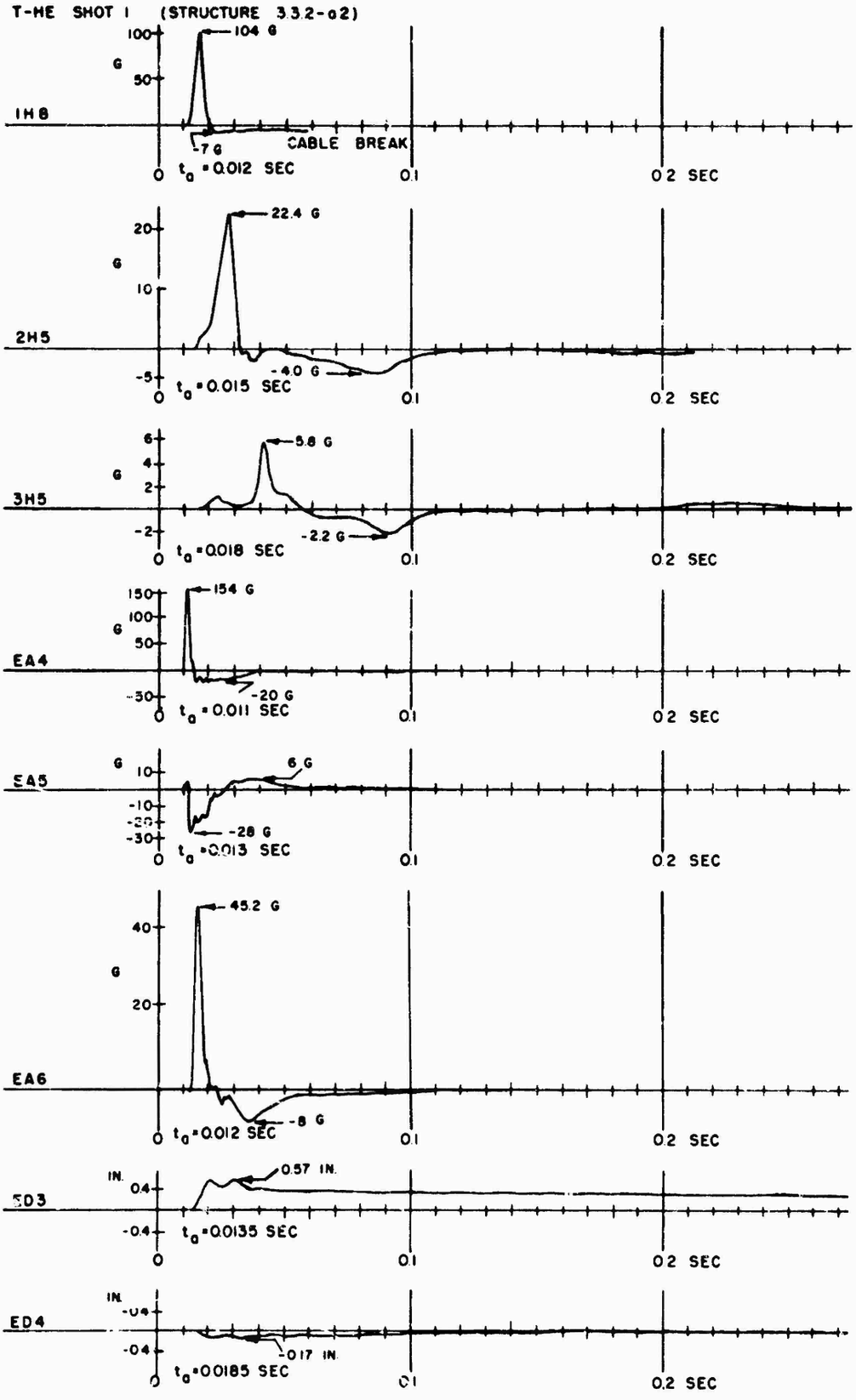

A.4 Record tracings, accelerations and displacements, Shot 1.

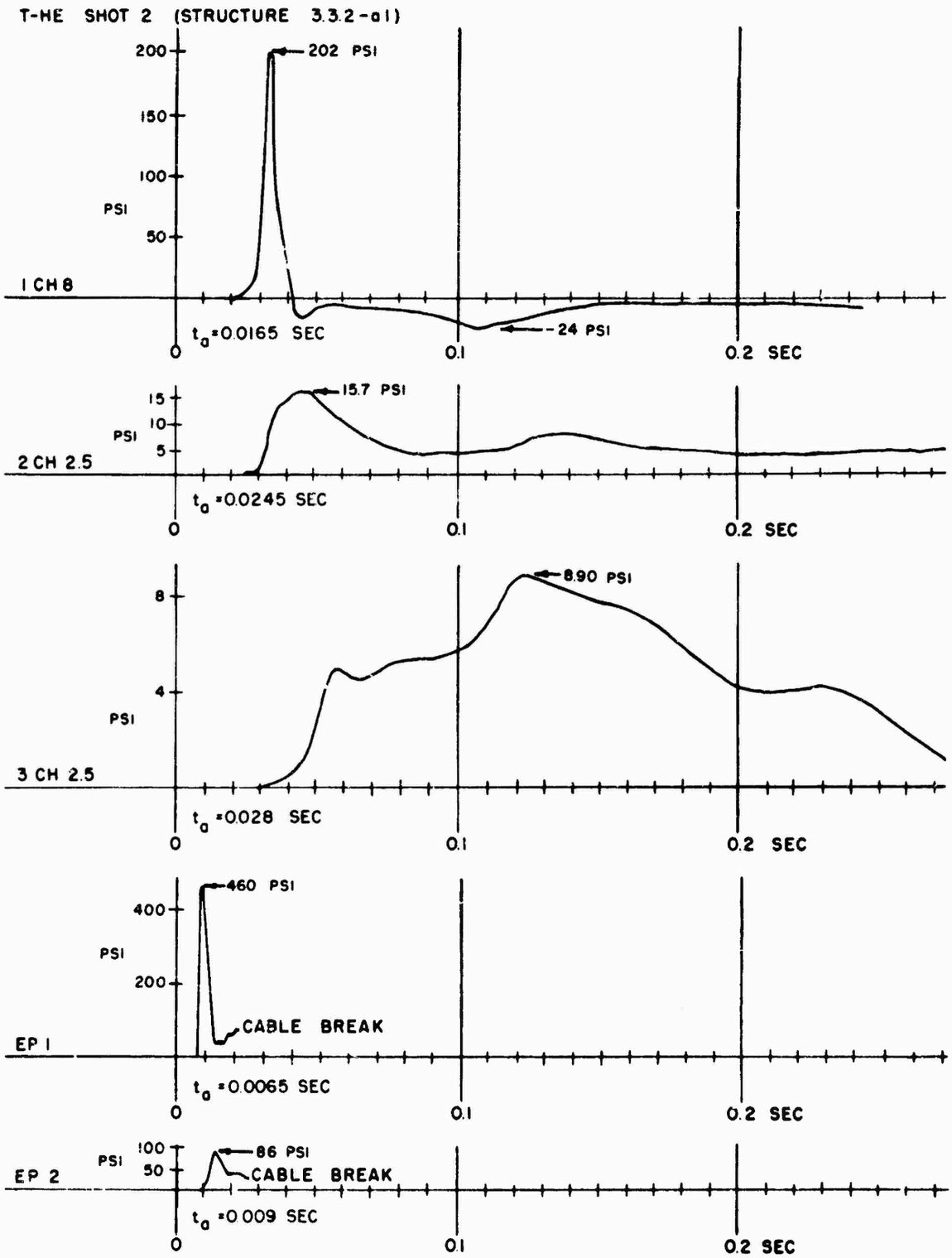

A.5 Record tracings, stresses and pressures, Shot 2.

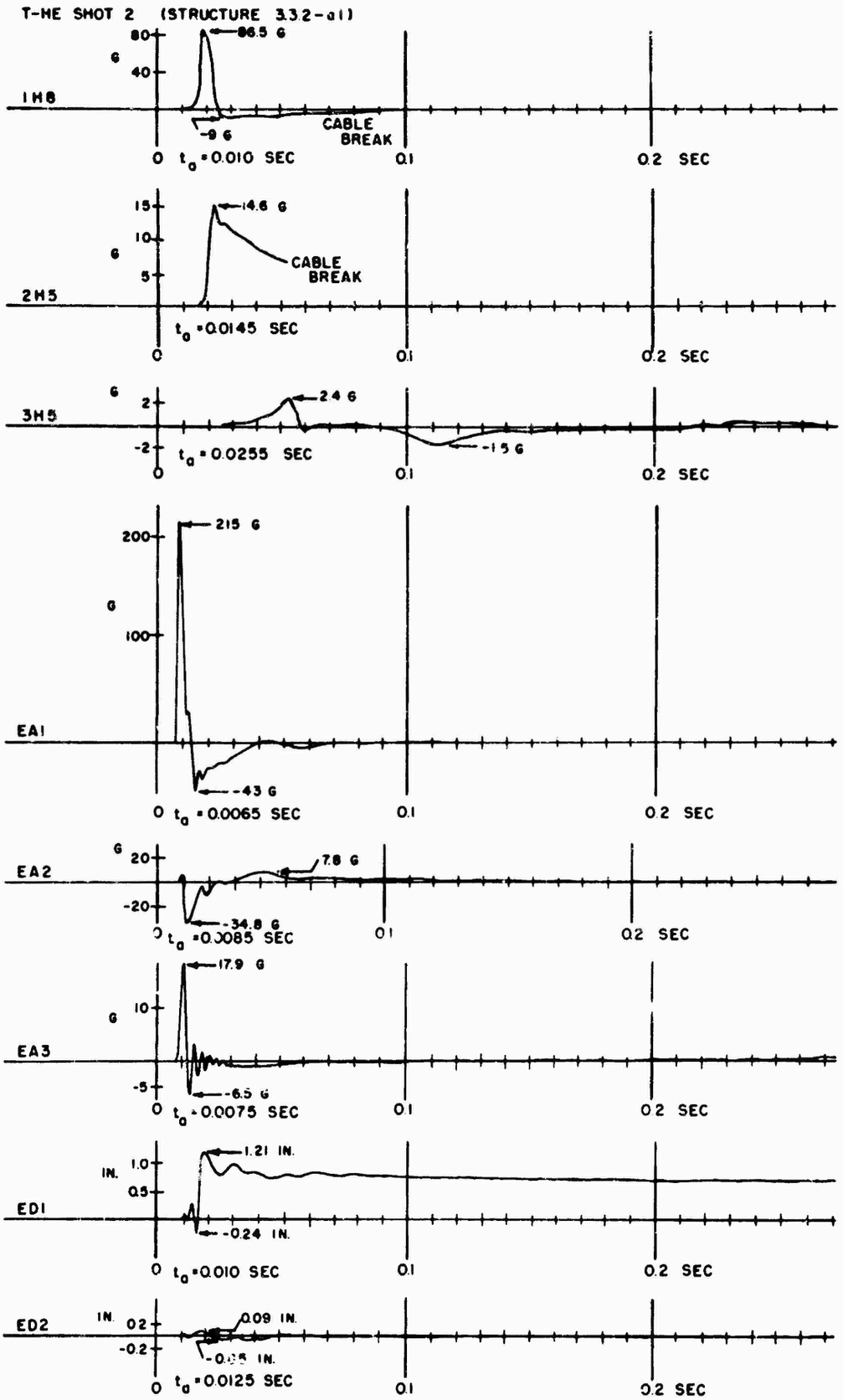

A.6 Record tracings, accelerations and displacements, Shot 2.

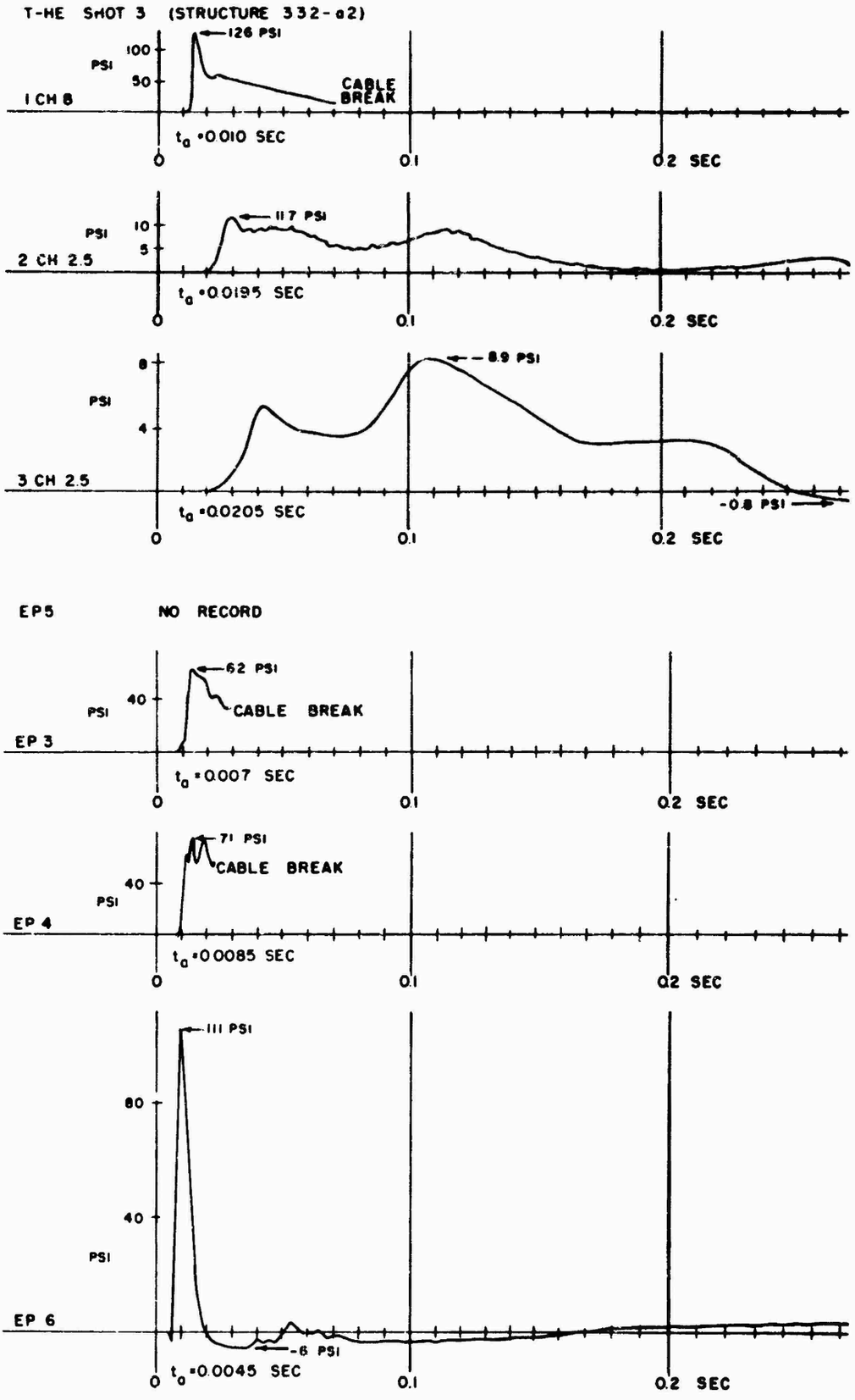

A.7 Record tracings, stresses and pressures, Shot 3.

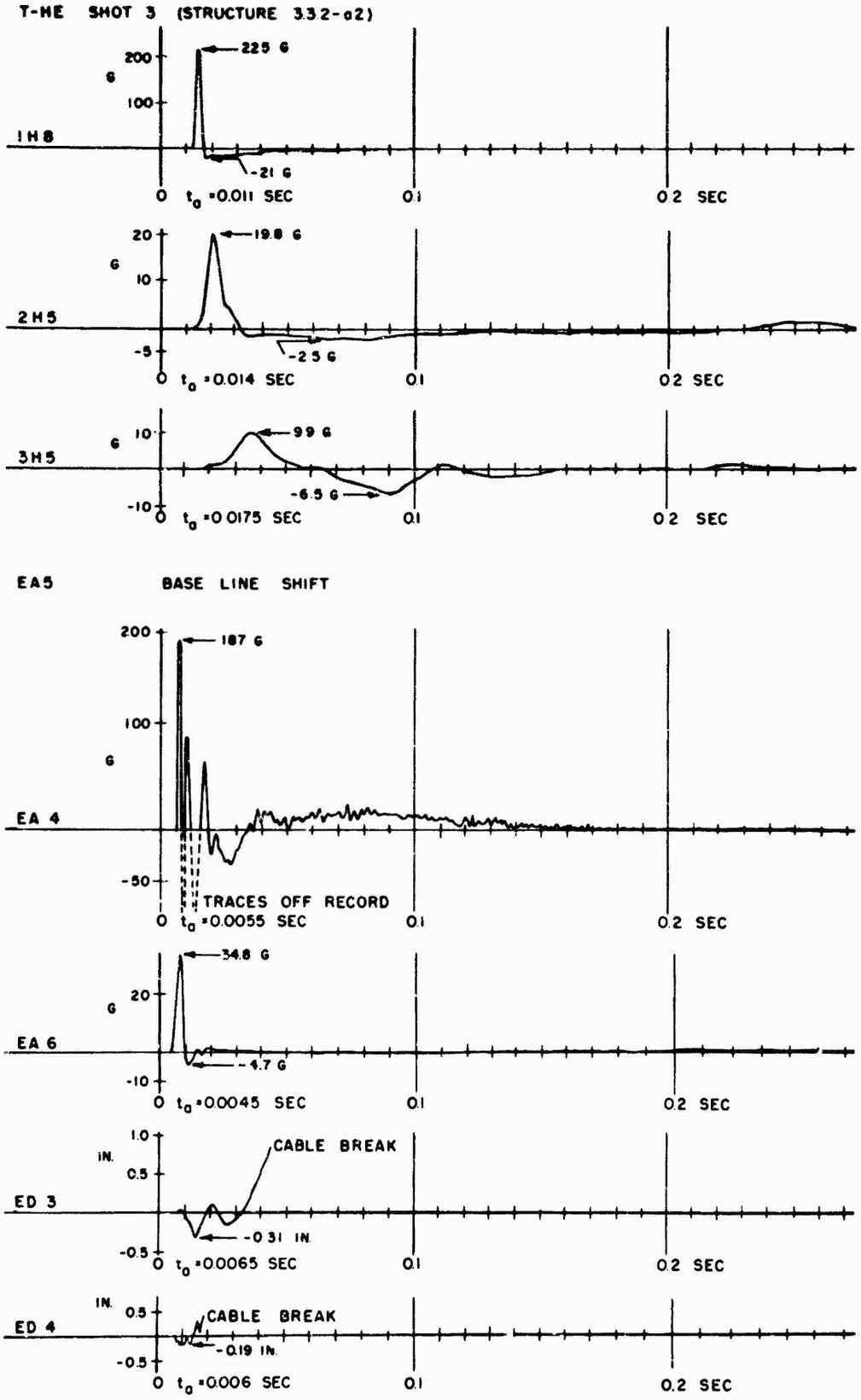

A.8 Record tracings, accelerations and displacements, Shot 3.

presence of the structures being tested undoubtedly caused perturbations of the free-field conditions, particularly on Shot 3, where the shot was very close to the structure and the structure failed, causing a severe assymetry of effects.

The wave forms of free-field earth stress shown in Figure A.3, A.5, and A.7 are similar for the three shots. There is a noticeable tendency toward development of a second peak with increased ground range, causing a marked increase in positive-phase duration, associated with a similar increase in rise time. These effects are consistent with those observed on the 400 series of Project Mole (Reference 1), although the time scales are increased (probably due to the greater depths of burial). In the case of 1CH8, Shot 1, there is some question as to the validity of the record between 0.020 and 0.050 second, immediately prior to the cable break. This wave form appears unnatural and is similar to those observed on 1CH8, Shot 3; 2H5, Shot 2; and EP3 and EP4, Shot 3. The same warning applies to the latter parts of these records. There appears to be no reason to question the validity of the peak values observed on these records. It is possible, though doubtful, that the peculiar wave forms are the cause, rather than a result of the cable break.

The peak values of earth stress are compared among shots and Mole Rounds 404 (charge depth 6 feet 4 inches) and 402 (charge depth 4 feet 9 inches) in Figure A.9. It will be seen here that the scatter among Shots 1, 2, and 3 is considerably less than that between the two Mole shots. It should be noted that the measurements at 13 feet ground range were at a depth of 5 feet, whereas all other measurements shown were at 2.5 feet.

It may be concluded that the measured free-field stresses were well within the range to be expected and that the wave forms were not abnormal.

The wave forms of the observed free-field horizontal acceleration shown in Figures A.4, A.6, A.8 are similar for the three shots (with the exception of 2H5, Shot 2). The variations with ground range are similar to those of earth stress and are consistent with those of the Mole 400 series (Reference 20).

The peak values of horizontal earth acceleration are compared with similar Mole data in Figure A.10. Here the scatter between Shots 1, 2, and 3 is approximately the same as that between Mole 404 and 402. In spite of the differences in depth of burial, the similarity of peak values versus ground range is pronounced. There is a marked tendency for the Shot 2 values to drop below those for the other shots, presumably due to variations in soil conditions.

A.7.2 Structural Data. No effort will be made in this report to analyze the structural data in detail. A few comments on the records presented may be useful, however.

The similarity between gage records EP3 and EP4, nominally in symmetrical positions, is excellent on Shot 1 and fair on Shot 3. This correspondence increases the confidence in the remainder of the data.

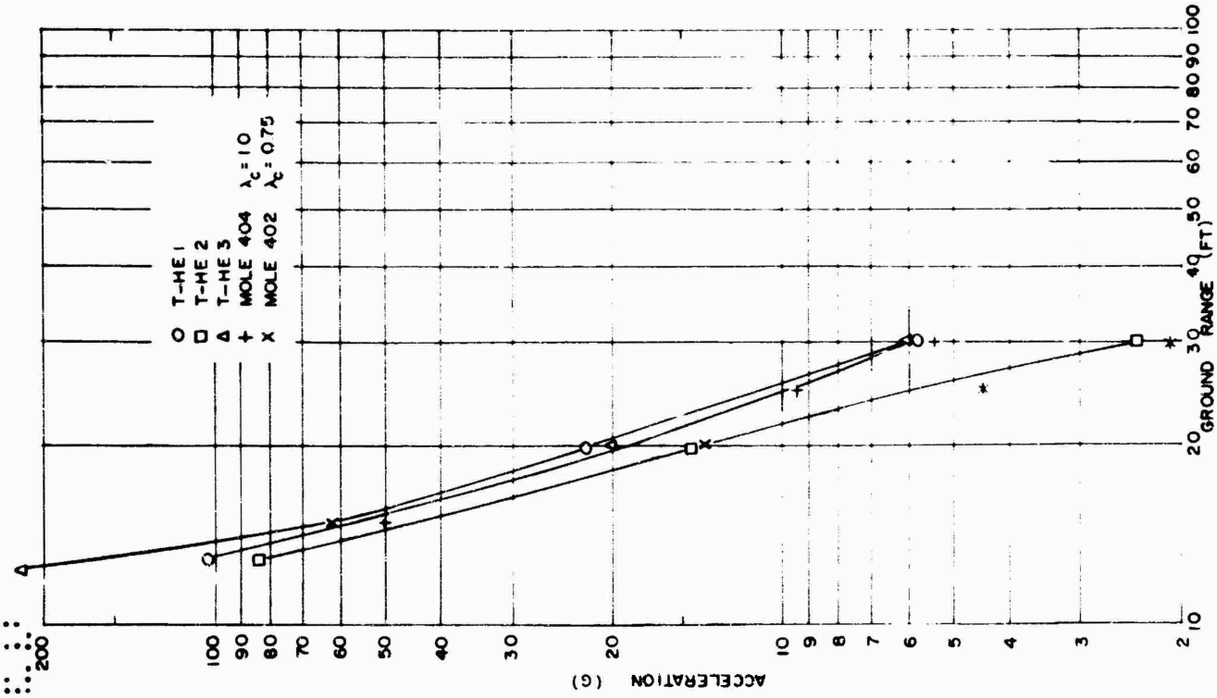

A.10 Peak acceleration versus ground range.

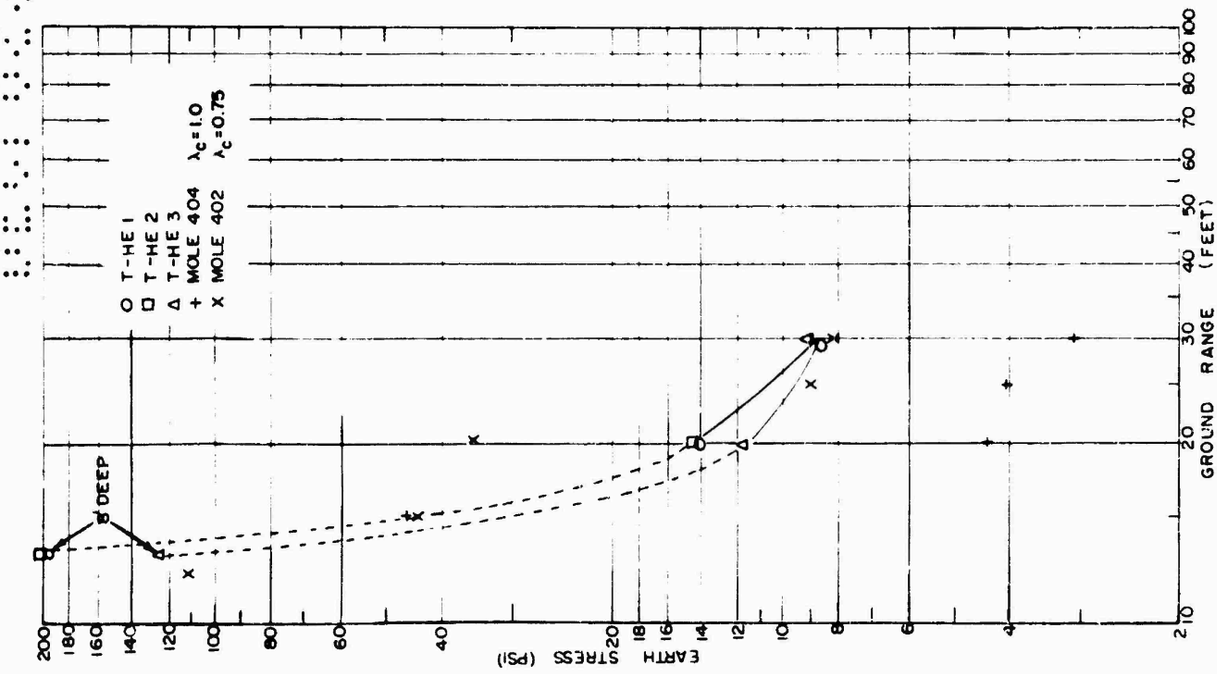

A.9 Peak Earth Stress versus Ground Range.

An examination of the peak values of Table A.1 shows that, where comparison with corresponding peaks in the free-field is possible, the measured pressure on the structure faces is higher than in the free field. Although no data are available, extrapolation of the curves of Figure A.9 would indicate that EP1, Shot 2, was lower than the free-field pressure at 10 feet ground range. This reading represents an overrange of the gage used, however, and the reading may be low.

It should be observed that the arrival times of the pressures on the side and back faces of the structures (Table A.2) are earlier than those at similar ranges in the free field. This indicates different modes of propagation, probably through the structure.

The fact that the peak pressure on the back face on Shot 3 was lower than on the other shots may be taken as an indication that the failure of the front wall relieved the forces transmitted through the side walls. Any slight asymmetry in this failure would explain the 15 percent difference between the two readings of back wall pressure.

Many of these measurements must be used with some reservations. On Shot 1, EA4 shows a very short duration. It is possible that the frequency range of the gage (425 cps undamped natural frequency) was exceeded, and that the reading was lower than the true peak. This also applies to EA1, Shot 2, and possibly to a lesser degree to other acceleration records.

EA3, Shot 2, and EA4, Shot 3, show severe ringing. The nature of this ringing implies overshoot, and a consequent high observed peak, but this cannot be considered to follow implicitly, since the source of the ringing cannot be determined. The same gages, on other shots, did not ring. Comparison of acceleration peaks with those at similar ranges in the free field are probably meaningless, since the mechanism of propagation is quite complex. The times of arrival and peak will be seen in Table A.2 to be earlier than the free-field arrivals, at comparable ranges, which indicates significant propagation through the structure.

The values quoted for deflection (gages ED1, -2, -3, -4) in this report are not corrected for the geometry of the gage system. This geometry is shown in Figures A.1 and A.2 and the correction to be applied is such as to make the true deflections some 1.22 times those reported. No results are given for deflection measurements on Shot 3, since cable breaks occurred before any peaks had been reached (see Figure A.8).

A.7.3 Permanent Displacements. Location of wooden stakes at a number of ground ranges were measured before and after the shot. Because of interference from the structures being studied and other topographic features, it was not found possible to measure permanent displacements on more than two radial lines. These lines formed a diameter that was parallel to the free-field gage line on Shots 1 and 3, and was displaced 15° from the gage line on Shot 2.

Figures A.11 and A.12 show the observed permanent displacements as a function of ground range. It will be seen that no displacements of

TABLE A.1 MEASURED PEAK VALUES

Function Measured	Gage Location	Shot 1 Gage Code	Shot 1 Peak	Shot 2 Gage Code	Shot 2 Peak	Shot 3 Gage Code	Shot 3 Peak
Structure[1]							
Unit Pressure	Front Wall	EP3	300	EP1	460 OR		
	Front Wall	EP4	305				
	Side Wall	EP6	64			EP6	111
	Back Wall	EP5	64	EP2	86	EP3	62
	Back Wall					EP4	71
Acceleration	Front Wall	EA4	154 S	EA1	215 S	EA5	NR
	Side Wall	EA6	45.2	EA3	17.9 R	EA6	34.8
	Back Wall	EA5	-28	EA2	-34.8	EA4	187 R
Displacement[3]	Front Wall	ED3	0.57	ED1	1.21	ED4	CB
	Back Wall	ED4	- 0.17	ED2	0.09	ED3	CB
Free-Field[2]							
Earth Stress	13 ft GR, 8 ft deep	1CH8	197	1CH8	202	1CH8	126
	20 ft GR, 2.5 ft deep	2CH2.5	14.3	2CH2.5	15.7	2CH2.5	11.7
	30 ft GR, 2.5 ft deep	3CH2.5	8.6	3CH2.5	8.9	3CH2.5	8.9
Earth Accel.	13 ft GR, 8 ft deep	1H8	104	1H8	86.5	1H8	225
	20 ft GR, 5 ft deep	2H5	22.4	2H5	14.6	2H5	19.8
	30 ft GR, 5 ft deep	3H5	5.8	3H5	2.4	3H5	9.9

1. Structure faces designated with reference to these shots. For pressure, displacement, and front and back face acceleration, positive direction is inward towards center of structure. For side wall acceleration, positive direction is away from shot.

2. Positive direction away from shot.

3. Displacement values quoted as read, without correction for gage geometry.

NR No record; gage damaged
CB Cable break before peak
R Severe ringing; values questionable
OR Over-ranged gage; reading may be low
S Very short duration; probably exceeds frequency response of gage and readings may be low

TABLE A.2 ARRIVAL AND PEAK TIMES

Shot 1 Gage	Shot 1 Arrival Time (sec)	Shot 1 Peak Time (sec)	Shot 2 Gage	Shot 2 Arrival Time (sec)	Shot 2 Peak Time (sec)	Shot 3 Gage	Shot 3 Arrival Time (sec)	Shot 3 Peak Time (sec)
EP3	0.010	0.0125	EP1	0.0065	0.0085			
EP4	0.0105	0.0135						
EP6	0.0115	0.0175				EP6	0.0045	0.0085
EP5	0.0135	0.019	EP2	0.009	0.0145	EP3	0.007	0.014
						EP4	0.0085	0.014
EA4	0.011	0.013	EA1	0.0065	0.009	EA5	0.0035	0.007
EA6	0.012	0.0165	EA3	0.0075	0.0105	EA6	0.0045	0.0085
EA5	0.013	0.016	EA2	0.0085	0.012	EA4	0.0055	0.007
ED3	0.0135	0.021	ED1	0.010	0.018	ED4	0.006	CB
ED4	0.0185	0.024	ED2	0.0125	0.0175	ED3	0.0065	CB
1CH8	0.009	0.020		0.0165	0.034		0.010[1]	0.0145
2CH2.5	0.0185	0.0305		0.0245	0.0445		0.0195[1]	0.0285
3CH2.5	0.0205	0.1105		0.028	0.124		0.0205	0.108
1H8	0.012	0.018		0.010	0.019		0.011	0.015
2H5	0.015	0.0285		0.0145	0.0225		0.014	0.024
3H5	0.018	0.043		0.0255	0.0535		0.0175	0.0355

1. Rough trace -- could be 0.0155 sec

CB Cable break before peak

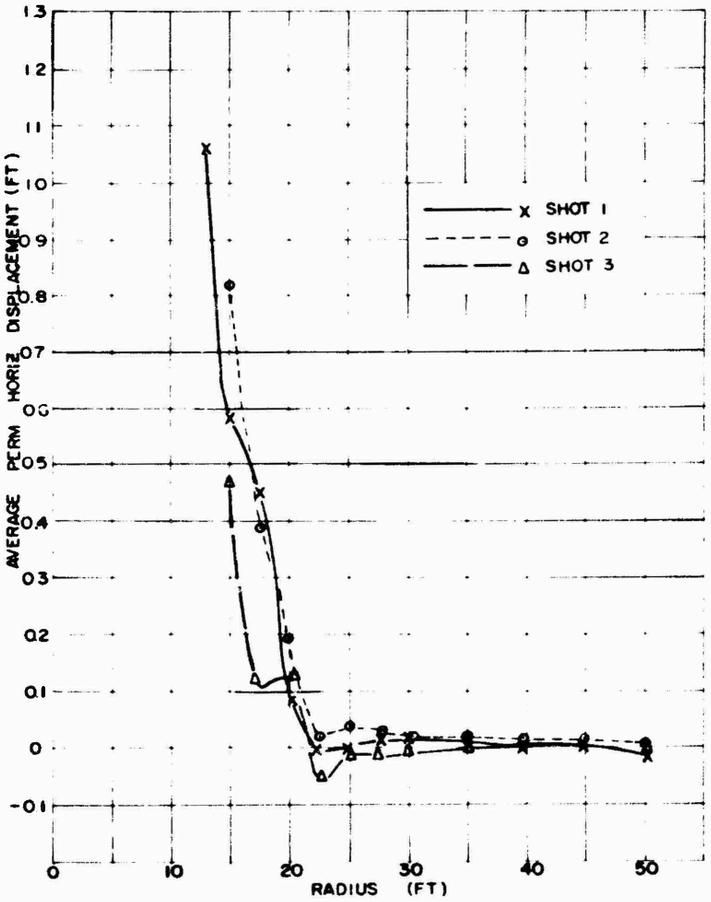

A.11 Permanent horizontal displacements.

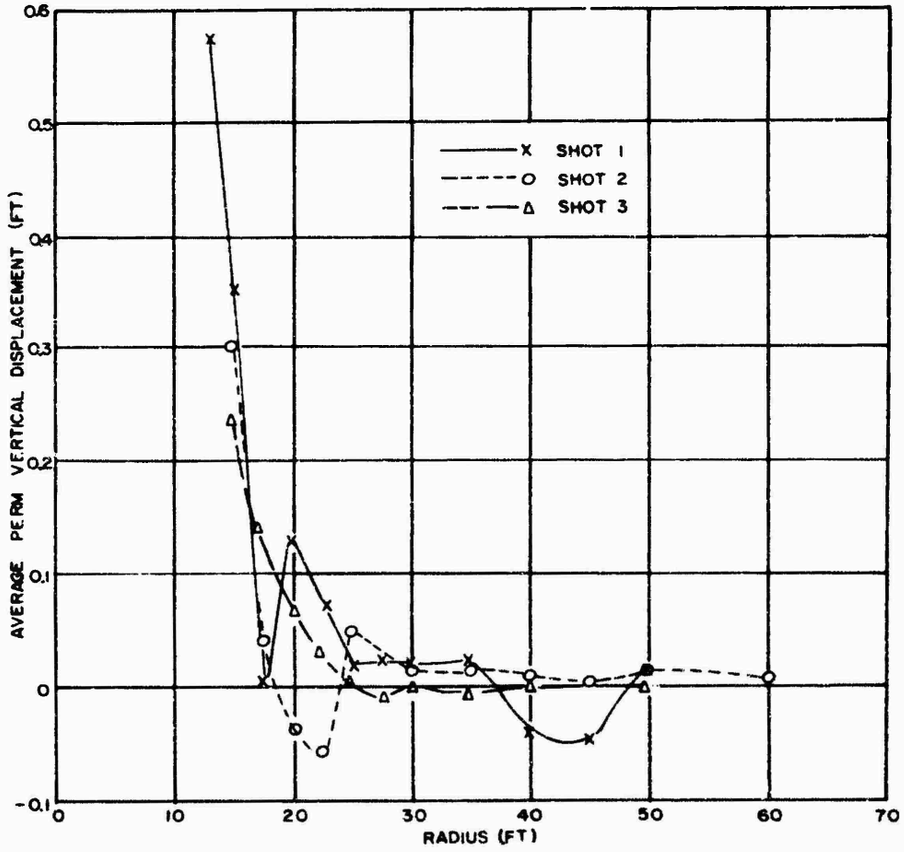

A.12 Permanent vertical displacements.

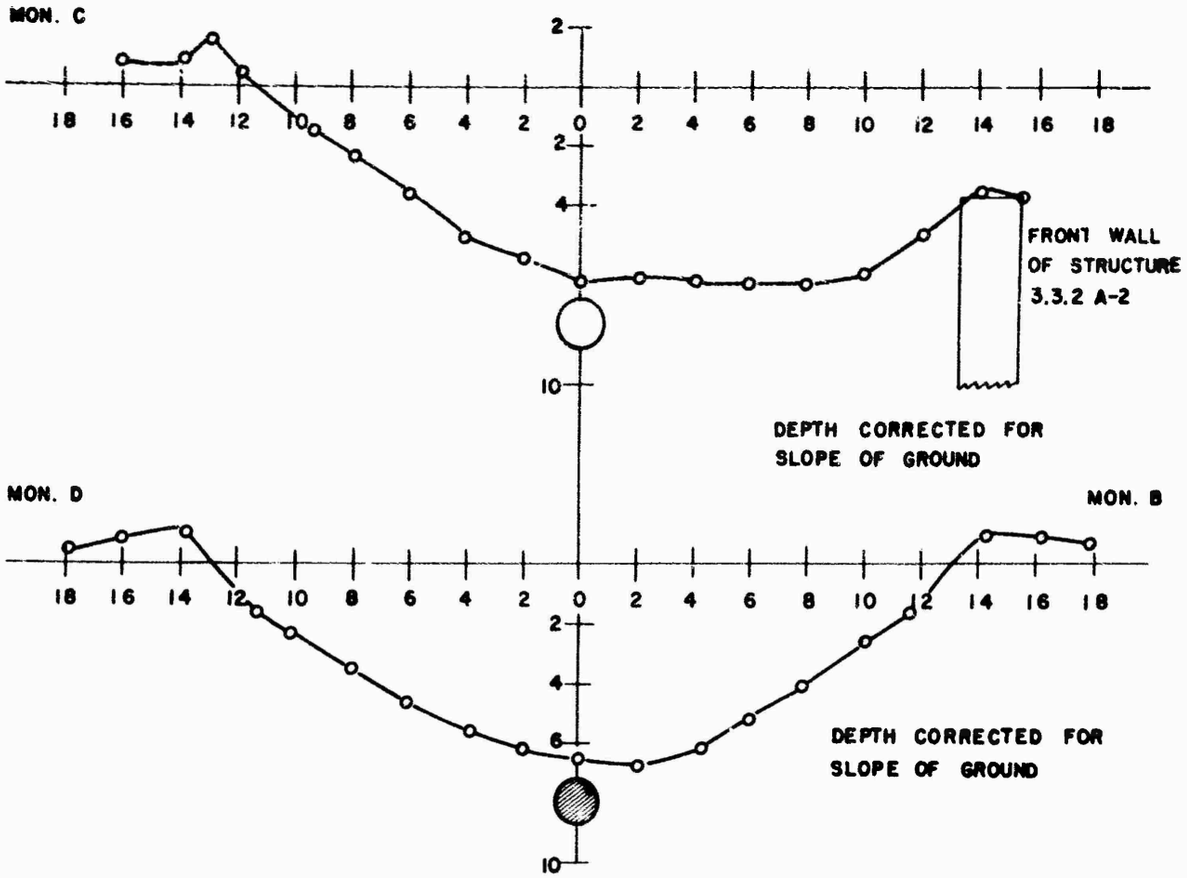

A.13 Crater profiles, Shot 1.

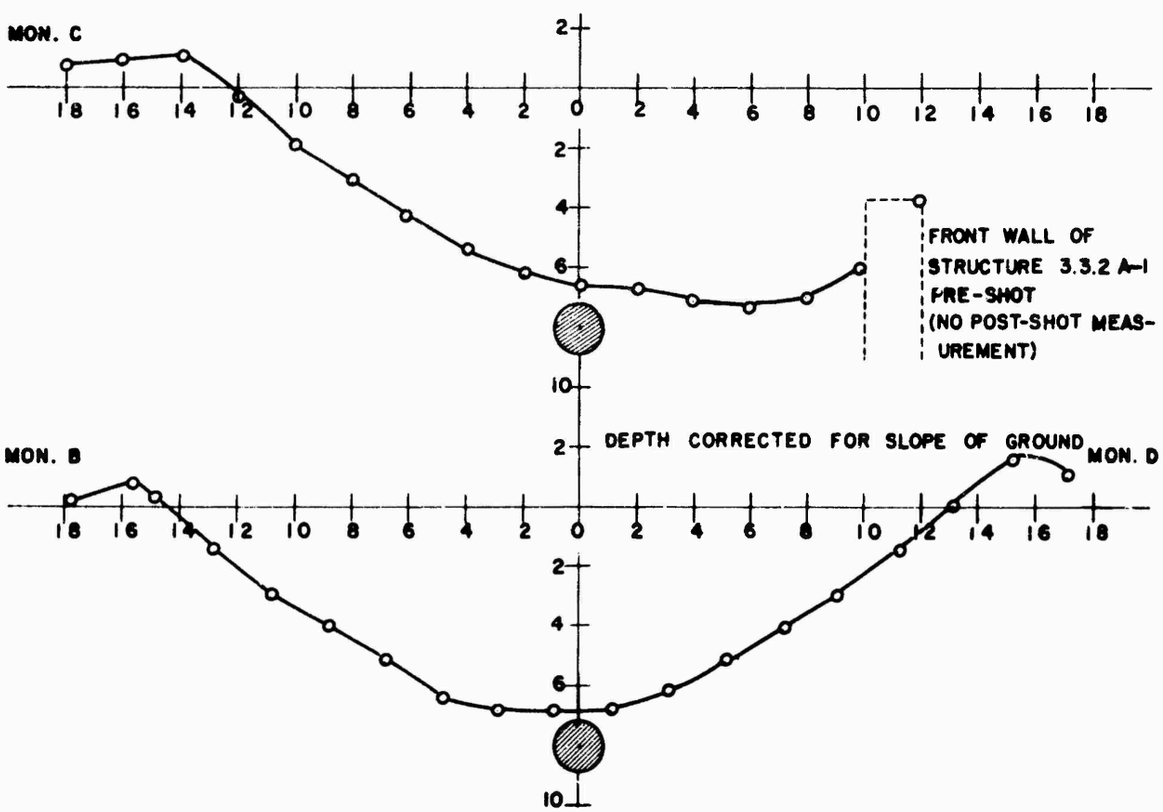

A.14 Crater profiles, Shot 2.

importance were observed at ground ranges greater than 25 feet, beyond which the measurements tended to scatter.

A.7.4 Craters. Data taken on the craters from these shots were limited to the measurement of the apparent craters--no attempt was made to probe for the true crater. As might be expected, the craters were asymmetrical due to the proximity of the structures. This effect is shown in Figures A.13, A.14, and A.15.

The average crater radius (in the symmetrical direction) was 13.15 feet or 2.07λ. An extrapolation of the crater radius curve of Project

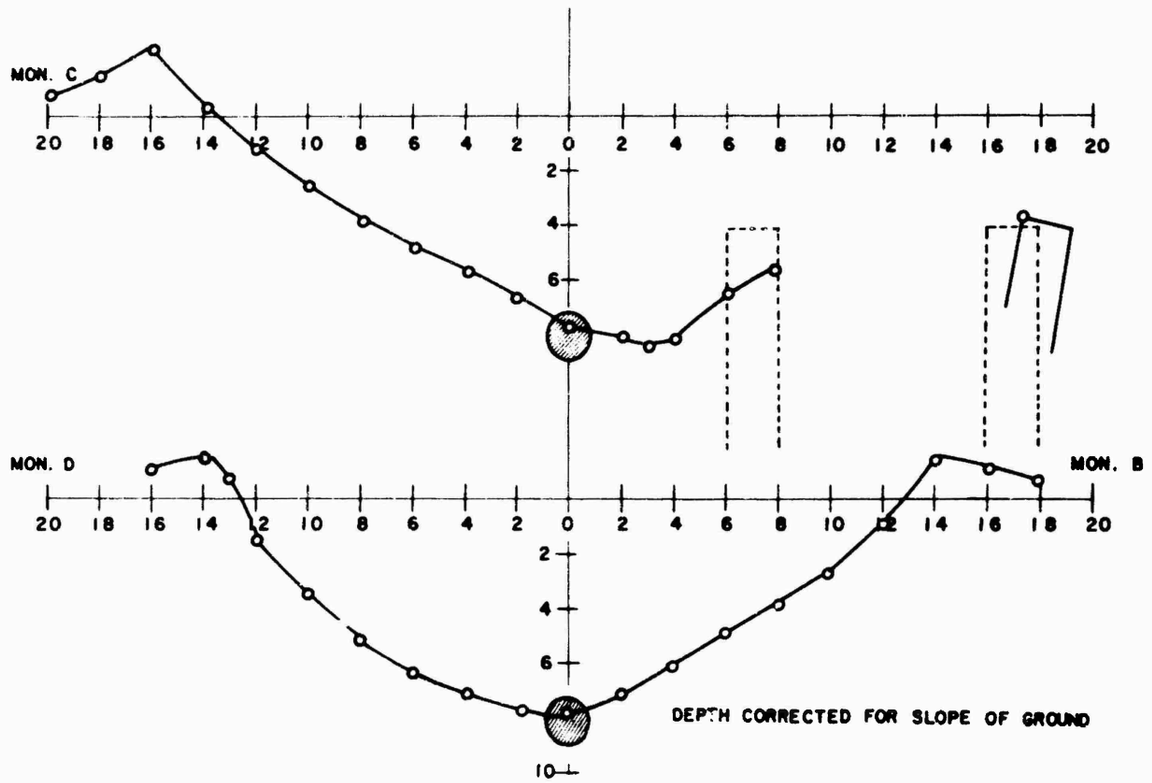

A.15 Crater profiles, Shot 3.

Mole, Phase IIB (Reference 20) to the shot depth used (1.29λ) would lead to a prediction of 2.0λ. This variation from prediction is slight. The results indicate that normal energy release was obtained on each shot of this series.

A.8 CONCLUSIONS

No effort is made in this report to draw any conclusions as to the mechanism of structural loading; such analysis is within the province of Project 3.3.2. The results of these tests do indicate, however, that the pronouncedly low structural loading in comparison with the free-field pressures observed on TEAPOT Shot 7 was not present in these HE tests. This fact indicates that there was no gross error in the performance of the instrumentation or in the placing of the gages on that test and that the deviations noted were apparently a function of the difference in loading mechanisms due to the size of the explosion involved.

REFERENCES

1. Thoenen, J. R. and S. L. Windes, Earth Vibrations Caused by Mine Blasting. Progress Report 2, U. S. Bureau of Mines, Report of Investigations 3407, June 1938. UNCLASSIFIED

2. A Comparison of the Crater Dimensions and Permanent Earth Movements in Clay, Sand, Chalk, and Gravel Soils Due to the Explosion of Buried Bombs, British Ministry of Home Security, Road Research Laboratory, AFSWP-337, March 1941. SECRET

3. Effects of Underground Explosions, Volumes I-IV, Committee on Fortification Design, National Defense Research Committee, Report No. 26, June 1944. CONFIDENTIAL

4. Lampson, C. W., Final Report On Effects of Underground Explosions, National Defense Research Committee, Report A-479, March 1946. UNCLASSIFIED

5. Underground Explosion Test Program, Final Report, Volume I - Soil, Engineering Research Associates, Inc., Armour Research Foundation, Rensselaer Polytechnic Institute, 30 August 1952. CONFIDENTIAL

6. Vaile, R. B., Jr., Final Report Surface Structure Program, Underground Explosion Tests at Dugway, Stanford Research Institute, March 1952. CONFIDENTIAL

7. Doll, E. B. and V. Salmon, Scaled HE Tests, Stanford Research Institute, Operation JANGLE Project 1(9)-1, Final Report, December 1952. SECRET RESTRICTED DATA

8. Summary Report, Weapons Effects Tests, Operation JANGLE, Armed Forces Special Weapons Project, WT-414, November 1952. SECRET RESTRICTED DATA

9. Sachs, D. C. and L. M. Swift, Small Explosion Tests, Project Mole, Stanford Research Institute, AFSWP-291, December 1955. SECRET RESTRICTED DATA

10. Theoretical Studies of the Shock Wave, Office of Naval Research, Operation JANGLE Project 1.9. WT-358. SECRET RESTRICTED DATA

11. Application of the Kirkwood-Brinkley Method to the Theory of Underground Explosions, RAND Corporation, Operation JANGLE Project 1.9-1, WT-328. SECRET RESTRICTED DATA

12. Notes on Surface and Underground Explosions, Armed Forces Special Weapons Project, Operation JANGLE Project 1.9-2, WT-378. SECRET RESTRICTED DATA

13. Salmon, V., Predictions for Underground Test, Stanford Research Institute, Operation JANGLE Project 1.9-3, WT-350, November 27, 1951. SECRET RESTRICTED DATA

14. Pinney, Edmund, Plastic Soil Mechanics Theory, Technical Report No. 2, University of California, Department of Mathematics, July 1953. UNCLASSIFIED

15. Whitman, R. V., et al., The Behavior of Soils under Dynamic Loading; 3, Final Report on Laboratory Studies, Massachusetts Institute of Technology, AFSWP-118, August 1954. UNCLASSIFIED

16. Terzaghi, Karl and Ralph B. Peck, Soil Mechanics in Engineering Practice, John Wiley and Sons, Inc., New York, 1948. UNCLASSIFIED

17. Courant, R. and K. O. Friedrichs, Supersonic Flow and Shock Waves, Interscience Publishers, Inc., New York, 1948. UNCLASSIFIED

18. Salmon, V., Air Pressure vs. Time, Stanford Research Institute, Operation TUMBLER Project 1.2, WT-512, February 1953. SECRET RESTRICTED DATA

19. Doll, E. B., Crater Radius Estimate for TEAPOT ESS, Technical Memorandum TDWET-54-50, Armed Forces Special Weapons Project, October 15, 1954. SECRET

20. Sachs, D. C. and L. M. Swift, Small Explosion Tests: Phase II-B of Project Mole, Stanford Research Institute, Mole Third Interim Report, AFSWP-290, December 1954. SECRET RESTRICTED DATA

21. Dohrenwend, C. O., et al., Flexible Measuring Devices and Inspection of JANGLE Structures, Bureau of Yards and Docks, Operation TEAPOT Project 3.3.1, WT-1125, to be published. CONFIDENTIAL RESTRICTED DATA

22. Newmark, N. M., et al., Behavior of Underground Structures Subjected to an Underground Explosion, Officer Chief of Engineers, Operation TEAPOT Project 3.3.2, WT-1126, to be published. SECRET RESTRICTED DATA

23. Lewis, John E., Crater Measurements, Engineer Research and Development Laboratories, Operation TEAPOT Project 1.6, WT-1105, to be published. SECRET RESTRICTED DATA

24. Brode, Harold L., Numerical Solutions of Spherical Blast Waves, Journal of Applied Physics, Vol. 26, No. 6, June, 1955, pp. 766-775. UNCLASSIFIED

25. Seismic Refraction Survey, Nye County, Nevada, United Geophysical Company, Inc., Operation JANGLE Project 1(8)a-1, WT-327, July 27, 1951. UNCLASSIFIED